Air movement on and around tailings storage facilities on the Highveld of South Africa

DCG Bodenstein

22323422

Dissertation submitted in fulfilment of the requirements for the degree *Magister Scientiae* in Environmental Sciences at the Potchefstroom Campus of the North-West University

Supervisor: Mr PW van Deventer

May 2017

ABSTRACT

Dust from gold tailings storage facilities (TSFs) is problematic in certain areas of the South African Highveld. Many of these localities around TSFs are densely populated, which often result in tailings dust being a nuisance and health hazard. Mines spend large sums of money to mitigate dust from TSFs due to the legal requirements and responsible conduct towards people and the environment. Implementation of these dust suppression measures is often not entirely successful, that may cause financial resource loss and legal liability for mines.

The focus of this study was to acquire data that would contribute towards illuminating the understanding of airflow dynamics over a TSF. By understanding the fundamental concepts of wind movement on and around these facilities, environmental managers can optimise dust management efforts with the limited resources available to them.

A review of literature in this field indicated that very little research has been done on airflow patterns on specifically gold TSFs. This study also revealed that airflow dynamics are inherently complex and difficult to predict. A study site was selected on the South African Highveld that presented suitable conditions for this research. The selected facility was the Chemwest 5 TSF near Klerksdorp in South Africa. In order to investigate airflow over this TSF, twelve wind-monitoring units (WMU) were constructed and placed on the facility for a period of eleven months.

The WMUs were composed of RM Young (model 05103) wind monitors and Campbell Scientific CR200X data loggers. Wind speed and direction data were continuously collected on the facility. The WMUs were placed at different locations on the TSF, which encompassed different levels of wind exposure and elevation differences. The data was analysed for wind speed correlation between TSF WMUs and a reference site, wind velocity profiles at each WMU and the statistical significance of wind direction classes measured during the study period. Data from this study was further used to develop a decision-tree analysis (DTA) system that can be used to predict high wind speed events, before such an event occurs.

Data analysis illustrated that significant wind speed and direction variations occurred for different locations on the Chemwest 5 TSF, relative to a reference wind profile.

Wind roses and wind direction class frequencies of each WMU illustrated that, for much of the research site, there was an over representation (greater frequency that for the reference WMU) of wind from the north. This likely indicates that the geometry of the facility redirects airflow from a range of natural incoming wind directions. Chi-square analyses of the possible 256 wind direction combinations that could take place between a reference site and the TSF indicated that for only eight combination classes, the cause was not associated with the location of the WMU on the TSF.

The Decision Tree Analysis (DTA) software assessed wind speed (mean and maximum), direction, air temperature and relative humidity. The model was tested against a dataset from the research site and found to be able to predict high wind speed events in 63% of cases. The model accuracy is therefore not adequate for implementation. Monitoring of additional atmospheric variables could improve the accuracy of the model.

Susceptibility of the tailings material to wind erosion was also assessed by means of wind tunnel tests. Structureless samples (from three different slopes) with low moisture content were placed in a wind tunnel and exposed to different wind speeds. Mass-loss measurements were made for the samples at different wind speeds and a minimum wind speed threshold velocity (u_t) for the tailings material was calculated. The analysis identified the u_t-value to be 3 $m.s^{-1}$.

Tailings crusts were identified on the Chemwest 5 TSF. Since these structures offer resistance to wind erosion, their compositions were investigated. Genesis processes by which the crusts originated were also investigated by means of a scanning electron microscope (SEM). Results found that three different crusts were present on the site: physical crusts that originated from the settling of fine particles in basins; erosion-induced crusts that originated by the removal of the erodible fraction of the material; and a chemical crust that resulted from the precipitation of secondary minerals.

The structure of these crusts, especially the crust that resulted from the settlement of fines, indicated that the crusts should offer resistance to wind shear.

The study concluded that the geometry of the Chemwest 5 TSF influenced the air movement characteristics on the facility, but that it was not significant enough to ignore the natural wind profile of the area in wind mitigation planning. The study also identified the presence of crust structures on the TSF that could increase surface stability and decrease dust. If these crusts were not present, the u_t–value of the TSF would have been 3 $m.s^{-1}$, as identified by the wind tunnel study. Dust would therefore have been more prevalent, given the frequency with which the wind speed of the study site exceeded the stated threshold value (41.5% of the observations).

Keywords: Wind erosion, tailings storage facility, wind tunnel, soil crusts, gold tailings material, linear regression, correlation, chi-square test, Highveld.

ACKNOWLEDGEMENTS

I, the author, would like to acknowledge the contributions of the following persons/organisations:

- Mr. P.W. van Deventer for his guidance and unwavering commitment to this research project. Also for his initiative in generating this project through his many years of experience and knowledge of market needs.
- Mr. G.J. Bodenstein for his contribution to the statistical analyses found in this dissertation and for his ever-willingness and patience in advising me on the statistical component of the work.
- Mr. T. van der Merwe who endured many a long day and braved the elements to retrieve data from the study site and for his enthusiasm in the construction of the wind tunnel.
- THRIP and Agreenco Environmental Projects for their financial contribution.
- AngloGold Ashanti for access to the study site.
- The South African Weather Service for providing weather data for the study area.
- Professor Harold Annegarn for his recommendations in improving this document.

DECLARATION

This dissertation is original, unpublished and independent work by the author, D.C.G. Bodenstein and a team of dedicated specialists. The literature background and some methodologies were extracted from published work by authors not involved in this research.

The fieldwork was predominantly performed by the following team: the author, Mr. T. van der Merwe and Mr. R. Brummer. The statistical analyses were performed by the author and Mr. G.J. Bodenstein. The author derived the findings of the research, as stated within this dissertation.

CONTENTS

LIST OF FIGURES

LIST OF TABLES

LIST OF EQUATIONS

LIST OF ABBREVIATIONS

µm	Micrometre
cm	Centimetre
E	East
Et al.	*Et alia*
g	Gram
GN	General Notice
km	Kilometre
m	Meter
$m.s^{-1}$	Meters per second
m^2	Square meter
mb	Millibar
mg	milligram
mm	Millimetres
N	North
NEM:AQA	National Environmental Management: Air Quality Act (39 of 2004)
NEMA	National Environmental Management Act (107 of 1998)
^oC	Degrees Celsius
PM	Particulate matter
S	South
SANS	South African National Standards
SEM	Scanning electron microscope
TSF	Tailings storage facility
U_t	Minimum wind speed threshold velocity
W	West
WM	Wind monitor
WMU	Wind monitoring unit

CHAPTER 1: INTRODUCTION

This chapter provides the context of this research and explains what factors justified the work. It also presents the purpose of the study and summarises the procedures followed. This chapter later describes the scope of the work and presents a site description of the study area.

1.1. Conceptualisation

Dust from tailings storage facilities (TSFs) is often problematic and considered both a nuisance and health risk to humans and the environment (Blight, 2008:253; McKenna-Neuman: 2009:520). This is due to the atmospheric loading of TSF particles that, through numerous pathways could negatively affect the environment (Oguntoke, *et al.*, 2013:1).

In South Africa, especially in the Witwatersrand area, dust from TSFs is a common occurrence to which local communities are regularly exposed (Sithole *et al.,* 2000:3). The prospect of jobs from mines tends to draw a large amount of people, many of whom reside in close proximity to the tailings facilities. In the dry, windy months (July – October), dust affects the nearby communities more than during rainy seasons by being a nuisance and health risk (Oguntoke & Annegarn, 2014:19).

The research conducted for this dissertation stems from a first-phase study that was performed in 2013, namely: “Quantifying the wind speed amplification effect on tailings storage facilities”. The aim of the 2013 study was to quantify the possible wind speed amplification on TSFs. The results from that study yielded valuable insight into the amplification of the environmental wind speed (ambient wind speed) by TSF slopes. However, little was known about the wind dynamics that were associated with wind direction seasonality and diurnal cycles on these facilities. In addition, no effort was made to investigate the tailings material and the possible wind susceptibility thereof.

It was of importance to select an appropriate TSF for the purpose of this study. The geographical location and design characteristics of the Chemwest 5 facility presented ideal conditions for the research herein.

A better understanding of the wind dynamics on the Chemwest 5 TSF was achieved by constructing wind-monitoring units (WMUs) and placing them at different locations on the study site. The locations of the WMUs were selected to provide representative data of the wind movement characteristics on the facility. The configuration and the logger programming of the WMUs allowed for concurrent monitoring of the wind dynamics at specific points on the TSF.

In order for wind to be erosive, it must have properties that contribute to this characteristic (discussed in chapter 2.2). The material on which the wind exerts force also contributes to whether the wind is erosive. A formal definition could not be found for a threshold wind speed that is considered “high”. For this reason, it was decided to investigate the wind-speed threshold velocity (u_t) of the tailings material of the Chemwest 5 TSF. This was performed by constructing a wind tunnel that can be used to estimate and test the u_t value of different slopes on the TSF.

The wind tunnel tests were performed for conditions that would be ideal for wind erosion, i.e. loose, dry and unsheltered tailings particles. The conditions on site, however, differed somewhat. The greatest difference, with respect to tailings surface features, was a pedogenic feature found on the tailings surface, namely surface crusts. These crusts could reduce dust formation. It was therefore essential to assess the inherent susceptibility of the material to wind for the purpose of interpreting field and wind tunnel studies.

The physical and chemical features of the tailings crusts were investigated by means of scanning electron microscopy (SEM). These investigations yielded information on the orientation of particles in the crusts and the physical structures that bind the particles.

The author hoped to derive a simple system for environmental managers and dust suppression practitioners to predict, from on-site conditions, whether an erosive wind event was imminent (within 24 hours). This would enable pre-emptive dust suppression action on the TSF, such as irrigation. A decision-tree analysis of on-site data (captured with a control WMU) was performed using SAS software.

1.1.1. Justification of the research

The research conducted for this dissertation is primarily justified by relevant legislative and socio-economic issues. These matters are embodied in degenerative human and environmental health, brought on by wind erosion and deposition of solid mine waste, such as tailings material (Blight, 2008:523). Solid mine waste, such as crystalline silica from gold mines and asbestos from asbestos mines have been associated with silicosis and asbestoses, respectively (Dang, 2013:368; Nelson, 2013:19520). Human populations around TSFs, especially in the Witwatersrand area, often increase despite the associated health risks (Kneen *et al.* 2015:4)

The deposition and liberation of tailings material could contaminate the surrounding environment. This is because the driving force behind the liberation of tailings particles is also a pathway to pollution. Plumlee and Morman (2011:399) and Blight (2008:523) highlighted some of the most relevant routes and pathways. These routes include the inhalation of fine particles (<100 µm) as well as the ingestion of larger particles (<250 µm) (Plumlee and Morman, 2011:400). Atmospheric suspension of tailings dust can lead to the respiration of fine particles, whilst the deposition of dust on crops or crop producing soil, can facilitate ingestion of such particles (Blight, 2008:523). Dust from TSFs can decrease crop quality and yield, pollute soil and water and potentially affect livestock production (Blight, 2008:523). Ingestion of tailings dust containing potentially toxic metals, such as arsenic, cadmium, lead and others, can cause the mobility of these elements to be enhanced in the low pH conditions that are to be found in the digestive tract of humans (Plumlee & Morman, 2011:400). Some studies also suggest that silica could be carcinogenic (Dong *et al*., 1995:70, Hnizdo *et al.,* 1997:274).

The degradation of the environment (soil, water and air resources) due to mining activities exposes a mining company to possible liabilities. A legal burden of required rehabilitation is thus placed upon the mining company. The research conducted for this dissertation will supply information regarding wind erosion events and propose principles by which to better understand the dust nuisance.

Human and environmental health, as threatened by wind erosion of tailings material, is addressed by the Constitution of the Republic of South Africa, Act 108 of 1996. Section 24 of the Constitution of the Republic of South Africa states that,

> "*Everyone has the right (a) to an environment that is not harmful to their health or well-being; and (b) to have the environment protected, for the benefit of present and future generations, through reasonable legislative and other measure that (i) prevent pollution and ecological degradation; (ii) promote conservation; and (iii) secure ecologically sustainable development and use of natural resources while promoting justifiable economic and social development".*

The National Environmental Management: Air Quality Act (no. 39 of 2004) and its amendments regulate air quality standards. Air quality legislation sets national standards to many different air pollutants. This takes the form of the SANS 1929:2011 national standards. These standards refer to, among others, PM10, PM2.5 as well as dustfall rates. The SANS 1929:2011 sets a dustfall limit of 600mg/m^2/day for residential areas and 1200mg/m^2/day, averaged over a 30-day period, for non-residential areas. These standards allow for three exceedances within any year but not in sequential months.

Hence, the acceptance of these standards into law, a number of regulations has also been published. These include:

- GN 1210: The National Ambient Air Quality Standards; from Government Gazette 32816, 24 Dec. 2009.
- GN 486: National Ambient Air Quality Standard for Particulate Matter with Aerodynamic Diameter Less than 2.5 µm (PM2.5); Government Gazette 35463, 29 June 2012.
- GN R827: National Dust Control Regulations; Government Gazette 36974, 1 Nov. 2013.
- GN 893: Listed Activities and Associated Minimum Emission Standards; Government Gazette 37054, 22 Nov. 2013.
- GN 893: List of Activities Which Result in Atmospheric Emissions Which Have or May Have a Significant Detrimental Effect on The Environment, Including Health, Social Conditions, Economic Conditions, Ecological Conditions or Cultural Heritage.

This dissertation is further justified by a small-scale study performed in 2013. Results from the study indicated that wind speed is amplified from the base of a TSF,

along its slope profile to the top crest. Wind speed amplification on a TSF can potentially cause the erosive power of wind to be increased. The amplification of wind speed, in this instance, may very well be due to anthropogenic influences (i.e. the TSF). The wind speed amplification may also be due to the naturally occurring boundary layer or "Law of the Wall" as described by Blight (2008:526), or a combination of both. The research for this dissertation may shed light on the causality of the wind-speed amplification effect.

The findings of this study will increase the knowledge base of air movement over TSFs, which could lead to improved designs for these facilities. These improved designs could inherently affect wind speed, before additional dust mitigation measures need to be employed.

1.2. Purpose

1.2.1. Aims and objectives

The aim of this study is to report on airflow patterns recorded over the Chemwest 5 TSF over a period of one year and to link site and material characteristics, such as height above ground surface, tailings erodibility and tailings crusts to dust risk.

The objectives of the study were as follows:

1) Measure the wind dynamics (speed and direction) over the Chemwest 5 TSF using purpose designed monitoring units for a period of one year;
2) Determine whether a reference site can be used to predict surface wind conditions on selected locations on the Chemwest 5 TSF;
3) Investigate surface crust structures on the Chemwest 5 TSF by means of electron microscopy;
4) Determine the minimum wind speed threshold velocity (u_t) of the gold tailings material of the Chemwest 5 TSF by means of wind-tunnel tests;
5) Determine whether a reference wind-monitoring unit (WMU) can be used to predict erosive wind speed days using a decision-tree analysis.

The first objective of the study was selected to improve the knowledge base and understanding of wind dynamics over a TSF. This would allow for the identification of specific airflow characteristics, such as areas of wind speed amplification or flow separation.

The second objective was selected to determine if a monitoring site could be used to predict wind conditions at specific locations on the TSF. In this section of the research, linear regression, correlation matrices and chi-squared tests were used to determine the relationship between the observed wind speed and direction data. This objective could influence management of dust by enabling dust-suppression practitioners to actively mitigate dust. This can be done by addressing areas that are likely to experience high wind speeds based on the measurements of a reference monitor.

The third objective provides information on the physical structure of the medium that is exposed to wind shear. Understanding the structure of these crusts provides information on how they formed and on the possible resistance that these structures could display against erosion.

The forth objective investigates the inherent erodibility of the tailings material to the force of wind. By knowing the minimum wind speed threshold velocity of the material, additional analyses of the wind data can be made. These analyses include determining what proportion of the time the wind speed measured at the study site could result in erosion. This knowledge also has value to tailings managers, as they can predict dust events from weather forecasts.

The fifth objective investigated whether a high wind speed day can be predicted a day before the event by using a simple diagram with indicators (that can be obtained from a site weather station) to predict the wind event.

1.3. Scope of the research

Air movement patterns over TSFs is of importance since it dictates the areas of highest surface shear and the likely locations of erosion and deposition (Blight, 2008:530). Areas of high wind speed (and associated shear) can be identified by means of measurements.

The research scope is focussed on wind dynamics over a TSF as a function of erosion and landscape development and ultimately how to construct and maintain landscapes. This research investigates the fundamental causes of wind erosion on a TSF and subsequent dust formation. Even though the wind velocity measurements were performed over time, the fundamental outcomes of the wind dynamics

characterisation are independent of periods of time by rather require comparative data of a moment in time. The observations were reported as such. The scope further encompassed the physical and chemical analyses of crust structures that were observed on the research site as well as the statistical analyses of the wind speed and direction relationships between different WMUs. The details of the scope are presented in section 1.2.1.

Although many other physical, social and economic factors, such as health effects of tailings dust, financial and social liability, related to dust and air quality warrant study, it is beyond the fiscal and temporal constraints of this research to investigate and report on them.

Some of these factors are:

- Investigating wind erosion inhibiting factors, such as:
  - Soil moisture and its effects on erosion (Chepil, 1985:15);
  - Tailings-surface roughness characteristics (Tan *et al.,* 2013:67);
  - Soil organic carbon content (Zobeck *et al.*, 2012:43);
  - Particle size distribution (Alfaro, 2008:158);
  - Apparent density and water holding capacity (Chepil, 1951:141);
  - Pedogenic structures (Chepil, 1963:253);
  - Surface cover (Gong *et al.,* 2014:105, Youssef *et al.*, 2012:178).
- Health effects of gold tailings dust to humans and the environment;
- Risks pertaining to the spatial distribution of gold TSFs and sensitive receptors;
- Atmospheric emission modelling of gold TSFs as dust source;
- Time-series analyses of dust events and tailings emissions;
- Dustfall rates and its relevance to current legislation;
- Material loss due to erosion and associated financial loss to the mine.

1.4. Site description

The most relevant characteristics (for this research) of the study location is described in this section, and includes the geographical location of the TSF, the parent material from which the material was derived, the climate of the area, the location of sensitive receptors in the vicinity of the TSF and the nomenclature associated with different areas of the TSF and the associated particle size distribution.

1.4.1. Geographical location

The research was performed on the Chemwes 5 TSF, with coordinates S 26^{o} 46'6.27" and E 26^{o} 46'24.39". The TSF is situated within the North-West province of South Africa and is considered to be on the Highveld plateau. According to Scheifinger and Held (1997:3497) the Highveld is a region in South Africa that refers to the interior plateau of the country and is elevated from approximately 1300 m - 1700m. The Chemwes 5 TSF is situated to the north of Stilfontein, roughly seven kilometres east of Klerksdorp and 32 kilometres west-southwest of Potchefstroom. The geomorphology of the landscape is relatively flat, with a topographic gradient of 30 m / 3500 m (Daniell, 2015:14).

1.4.2. Parent material of the Chemwest 5 TSF

Chemwes 5 TSF is the resultant tailings material from the mining of the Vaal Reef (van Deventer, 2014: personal correspondence). The Vaal Reef is composed of quartz arenite, quartzite and conglomerate (Geological Society of South Africa, 1986:563). Quartz arenite is both auriferous and uraniferous and contains pebbles, whilst the quartzite also exhibits pebbles and is pyritic (Geological Society of South Africa, 1986:563). The Vaal Reef is a member of the Strathmore Formation, which lies within the Johannesburg Subgroup and forms part of the Central Rand Group (Geological Society of South Africa, 1986:555). The Vaal Reef member is at the base of the Strathmore Formation, whilst being superimposed by the remaining members of the formation, namely: Zandpan, Modderfontein argillaceous quartzite and the Pretoriuskraal member, and superimposes the Mapaiskraal member of the Stilfontein Formation (Geological Society of South Africa, 1986:563). The Strathmore Formation is superimposed by the Crystalkop Formation and superimposes the Stilfontein Formation (Geological Society of South Africa, 1986:563). Figure 1 shows the stratigraphic location of the Vaal Reef, from which the milled tailings material of Chemwest 5 originated.

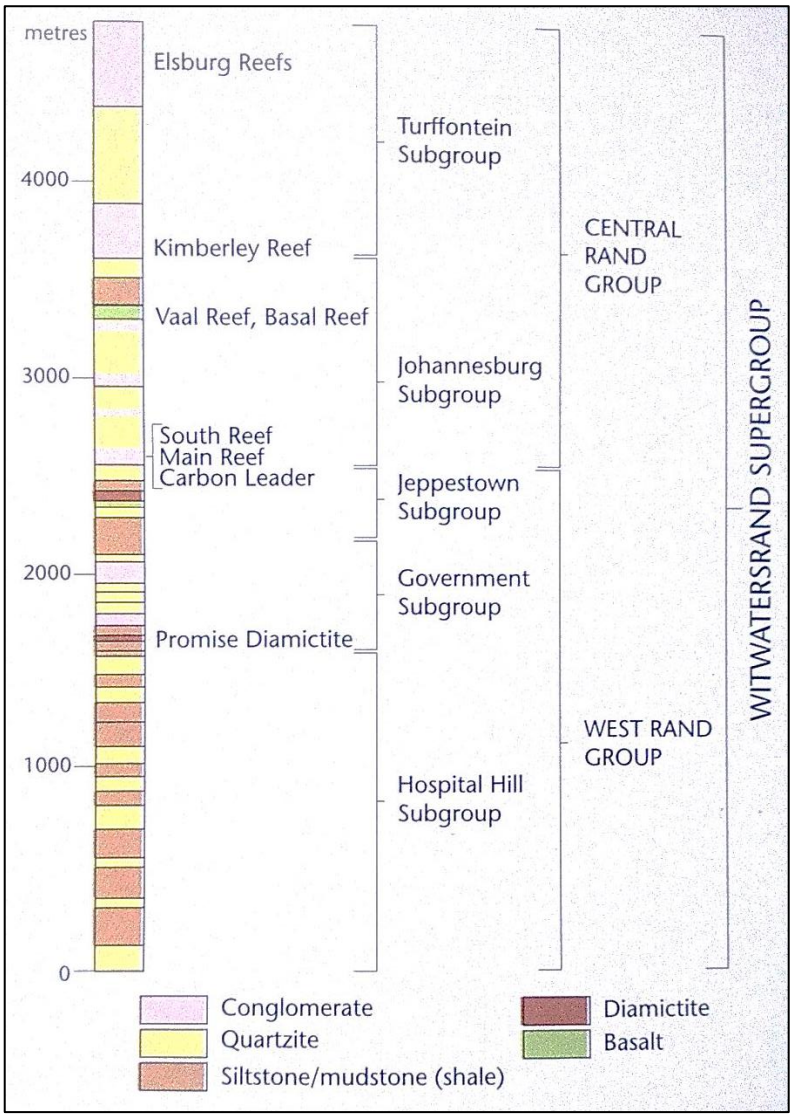

Figure 1: Stratigraphy of the Witwatersrand Supergroup and the stratigraphic location of the Vaal Reef (taken from McCarthy:2005:101).

1.4.3. Climate

The area is characterised by typical Highveld climate, i.e. dry cold winters and warm summers, which is the rain season. Van Wyk and Cilliers (1997:75) reported the average maximum temperature for the area (measured over 49 years) to be 25.6°C and the average minimum to be 9.3°C. Summer maximums can be greater than 30.0°C and the winter minimums can be lower than 0.0°C (van Wyk & Cilliers, 1997:75). Aucamp (2000:3.3) indicated that the A-pan equivalent evaporation for the area exceeds the precipitation rate for any month of the year, indicating that TSFs could be prone to dust formation due to the lack of cohesive forces brought about by inter-particle moisture.

Weather data from January 2003 to July of 2014 was analysed for Klerksdorp as to obtain general weather characteristics for the area. The data was obtained from the South African Weather Service for their Klerksdorp monitoring station (E026.620067; S26.900086). From the interpretation of the data the average annual maximum temperature of the area was found to be 25.6^{o}C, the minimum was 9.8^{o}C, the combined average temperature was 17.7^{o}C. The analysis of the rain data showed an average rainfall of 495 mm/annum and a dominant wind direction ranging from N to NE.

Figure 2 presents the average maximum temperatures for the research area. The data illustrates that the air temperature fluctuated between 24.0°C and 27.2°C. Figure 3 indicates the average minimum temperatures for the research area, during which time the temperature fluctuated between 8.3 C and 10.9°C. Figure 4 illustrates the annual average temperature, which indicates that the average monthly temperatures range between 1.0°C in the winter (minimum) to 30.0°C in the summer (maximum).

Figure 5 displays the rainfall distribution of the site for January 2003 to December 2013. The data shows that rainfall increases from September to January, after which it decreases until August.

Figure 6 illustrates the measured rainfall for Klerksdorp during the research period. The rainfall was erratic, with no rainfall in October 2015. The total annual rainfall for this time was 595 mm.

Figure 7 shows the average monthly wind speed for the study site between January 2003 and December 2013.

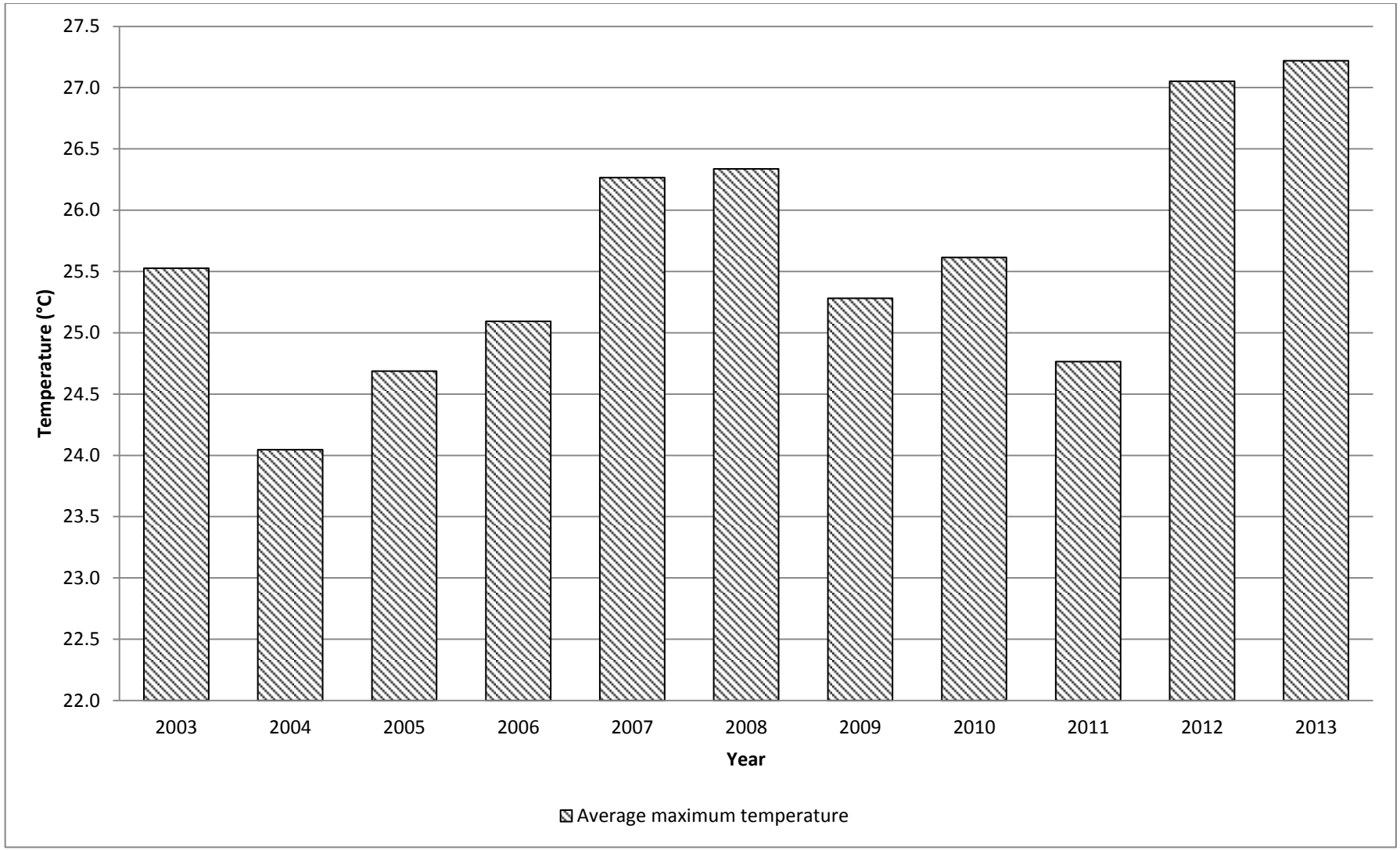

Figure 2: Average annual maximum temperatures for the study site from January 2003 to December 2013.

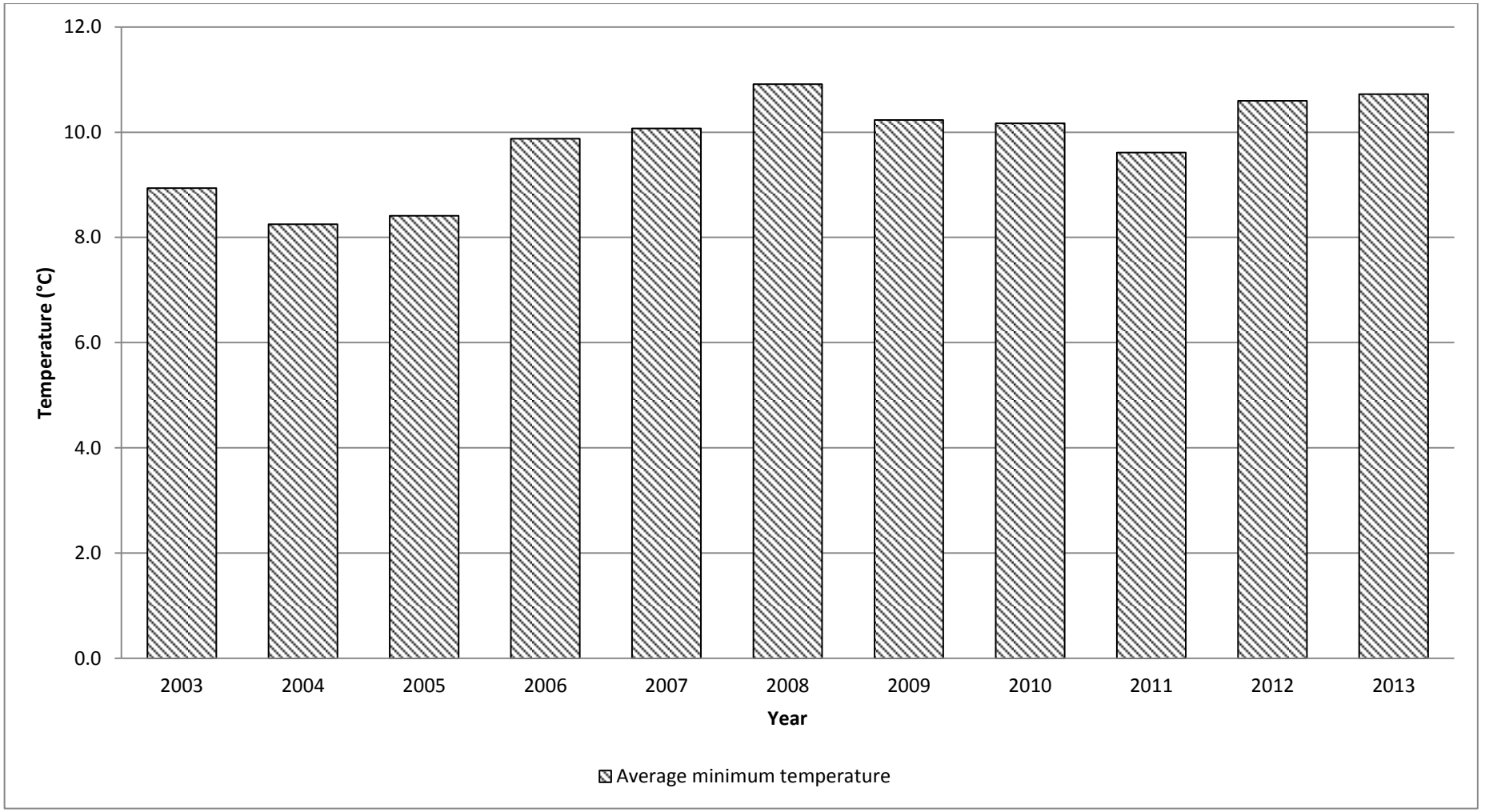

Figure 3: Average annual minimum temperatures for the research site from January 2003 to December 2013.

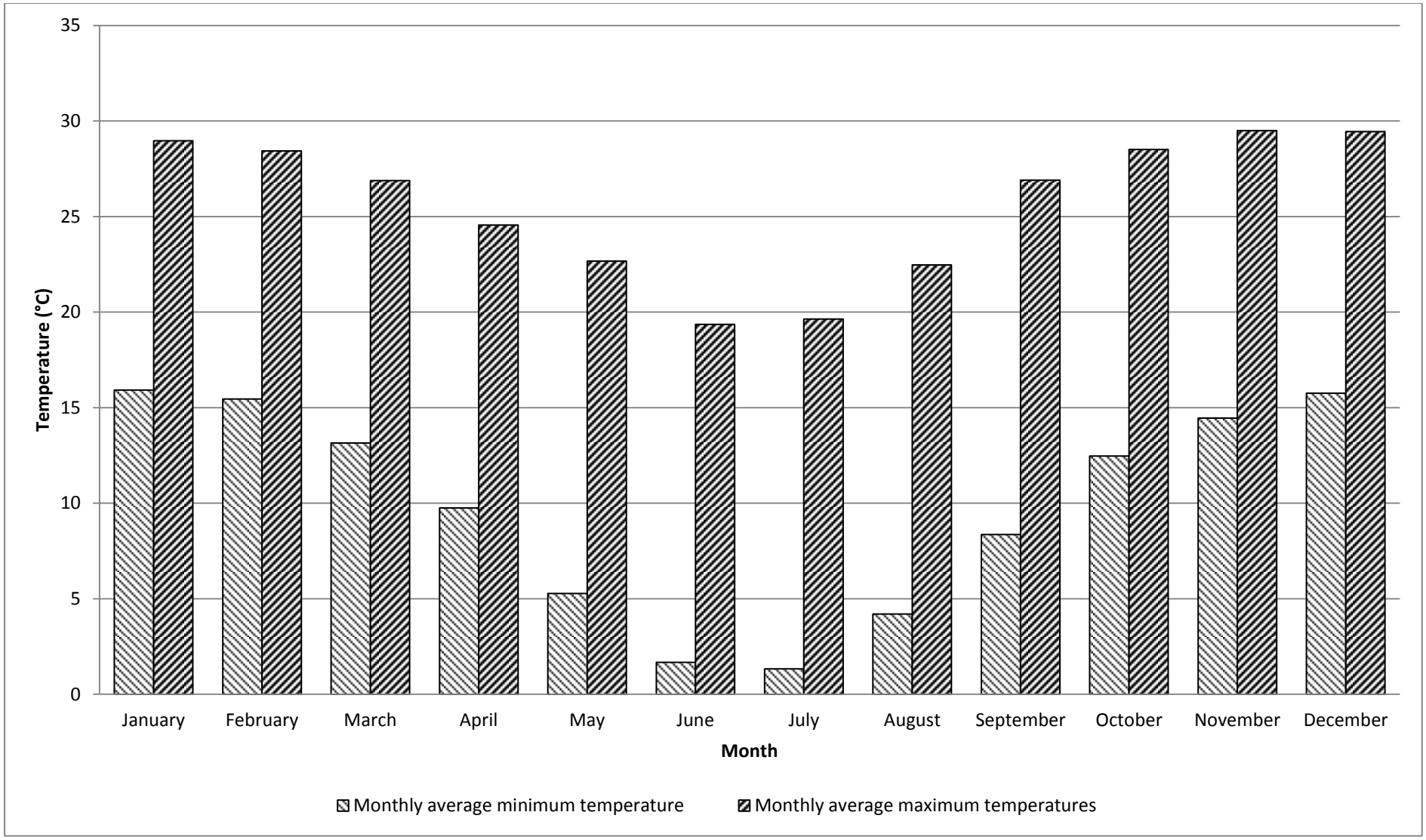

Figure 4: Average monthly temperatures for the research site from January 2003 to December 2013.

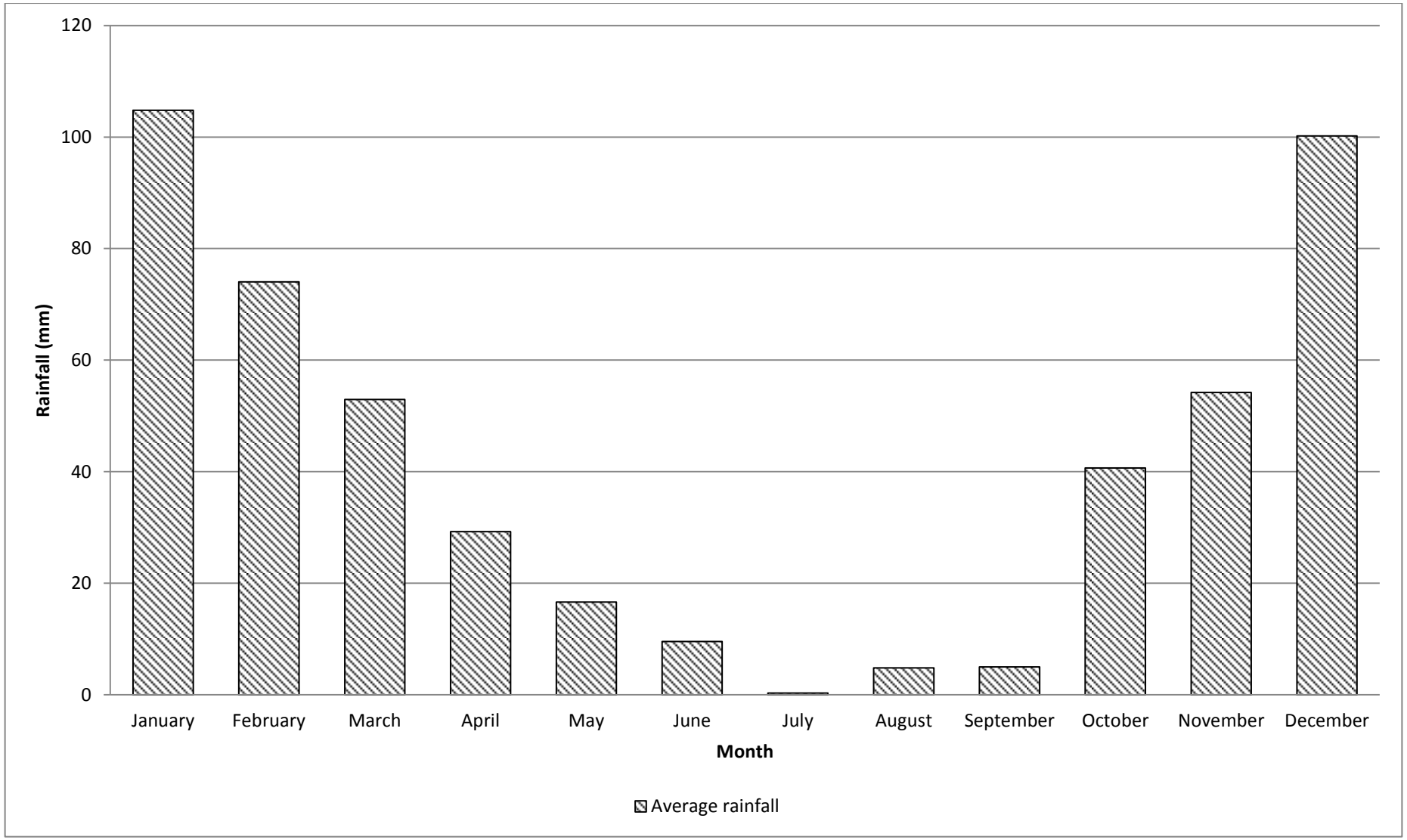

Figure 5: Annual monthly rainfall (total) for the research site from January 2003 to December 2013.

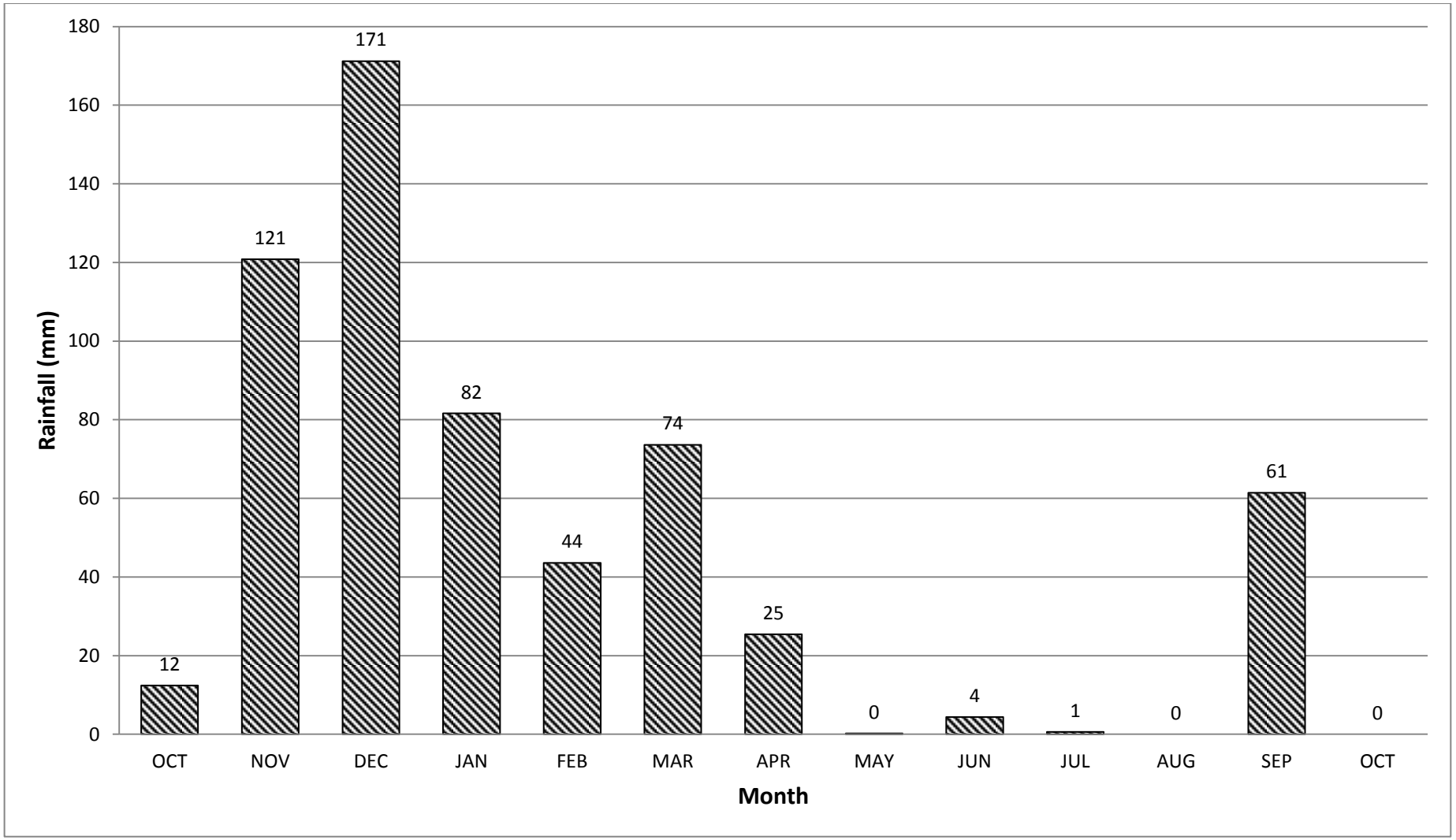

Figure 6: Total monthly rainfall for the period in which the research took place (measured at the Klerksdorp weather station)

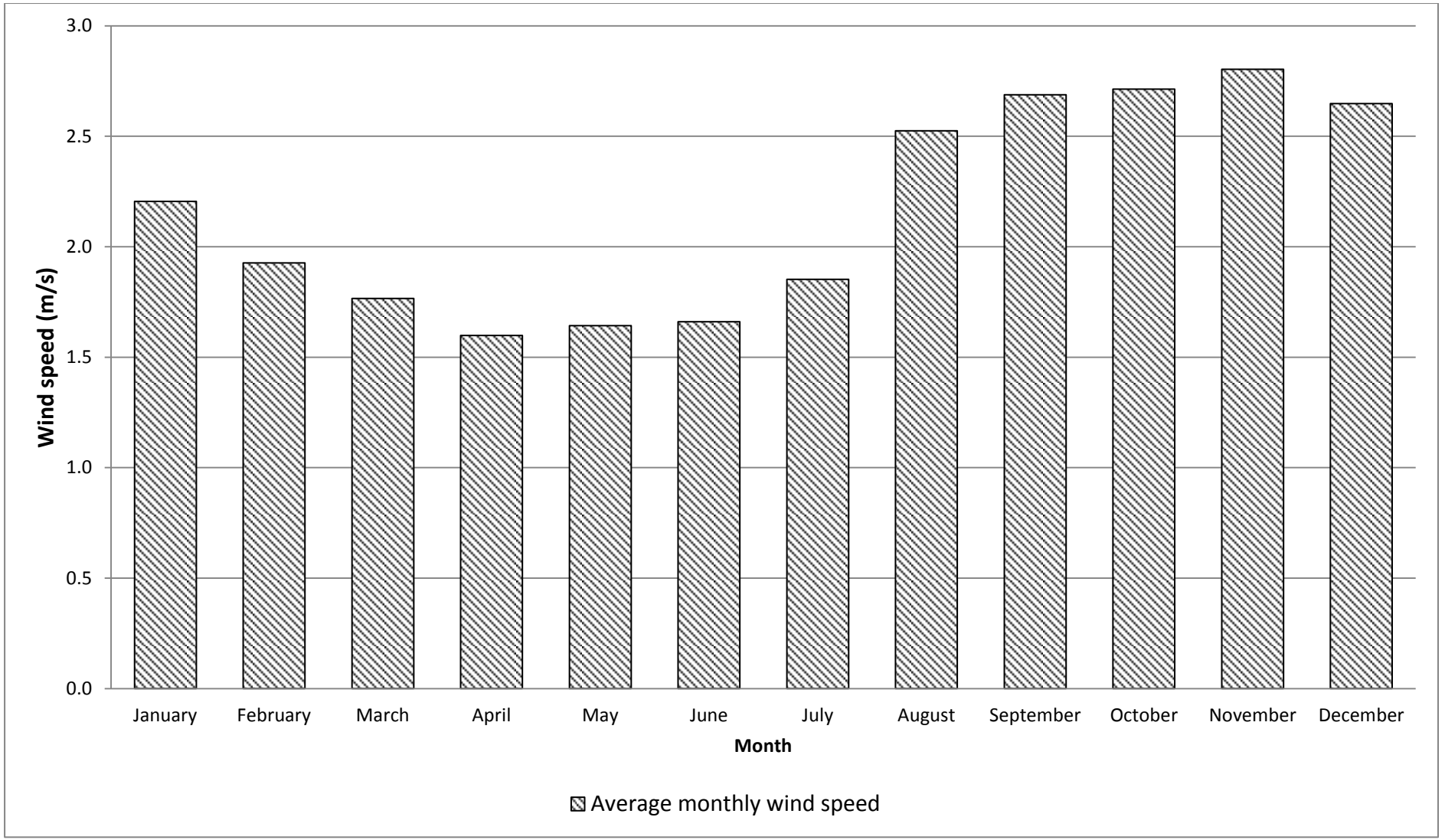

Figure 7: Average monthly wind speed for January 2003 to December 2013 (measured at the Klerksdorp weather station)

In Figure 8, the research area and major concentrations of human dwellings surrounding the TSF are displayed. A wind rose can also be seen in the figure, indicating the major wind direction to be from the north and northeast. The wind data is for the period January 2003 to December 2013. The areas of dense human settlements have also been delineated in the figure. The white angular structures that can be seen in the figure are TSFs.

When taking the major wind directions into account as well as the placement of the TSFs relative to residences and industrial areas, one can see that dust may very well be a hazard in this area.

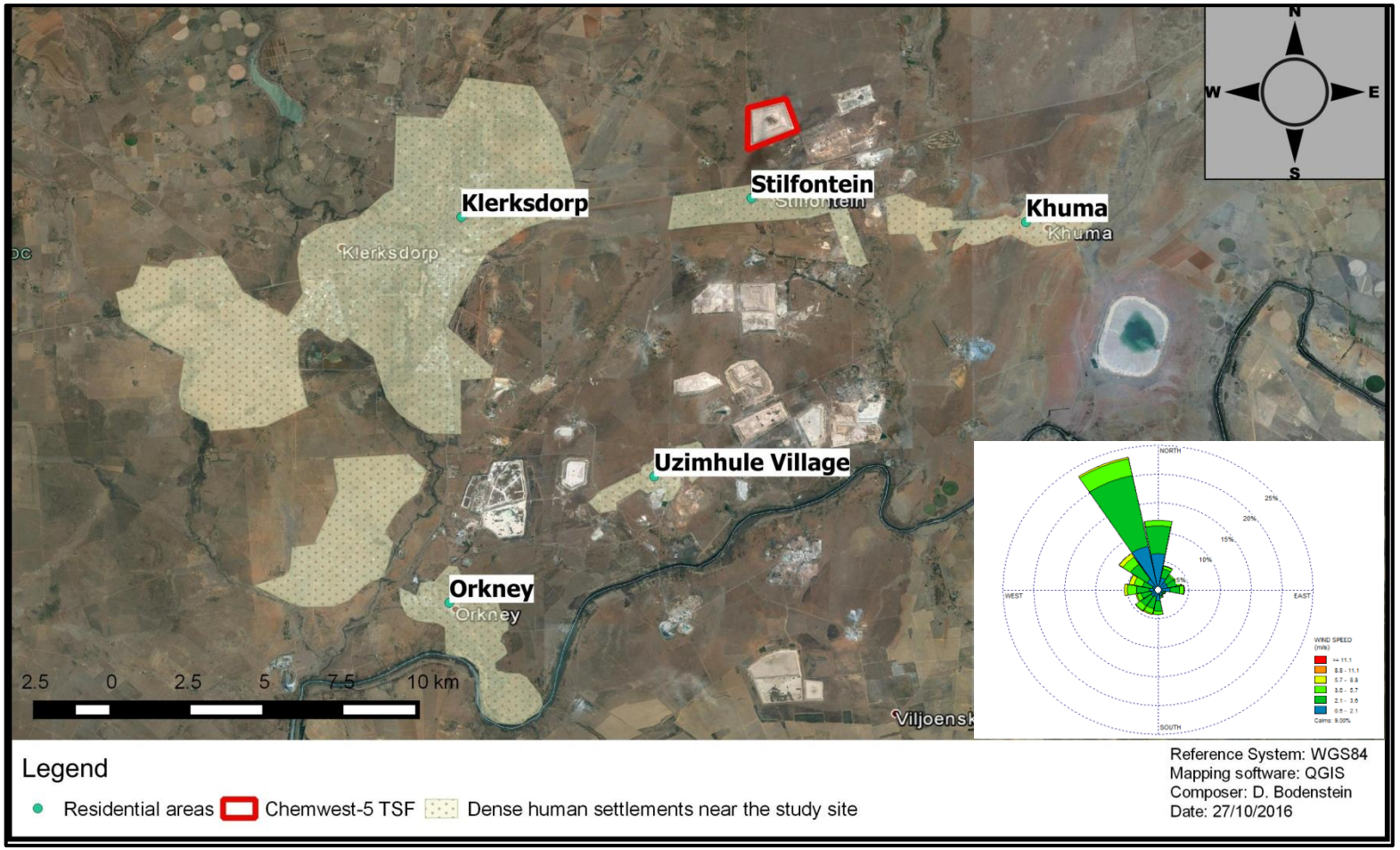

Figure 8: Map of the dense human settlements near the research site (base image Google Earth).

1.4.4. Particle size distribution (PSD)

The Chemwest 5 TSF was constructed with two different methods. The greatest part of the facility (all except the top slope) was constructed using the ring-dyke paddock method. This method entailed the pumping of slurry onto the beach of the facility. The water from the slurry would then transport the finer particle fractions to the pool, whilst the coarser material remained at the crest and outer slopes of the TSF.

The second method, used to construct the top slope, entailed the use of cyclone technology. Cyclones segregated the slurry material into the fines fraction, which was deposited on the beach and pool of the facility. The coarser fractions were deposited on the outer slope of the TSF. Table 1 contains baseline analytical data of the Chemwest 5 PSD information for different locations on the Chemwest 5 TSF.

Table 1: Particle size distribution measured on the Chemwest 5 (CW5) TSF.

Sample no	Very coarse sand 2.0mm	Coarse sand 1.0mm	Medium sand 0.5mm	Fine sand 0.2mm	Very Fine sand 0.1mm	Silt 0.02mm	Clay 0.002mm
	Sand %	Sand %	Sand %	Sand %	Sand %	%	%
CW5 Pool	0.0	0.0	0.1	13.6	58.4	26.1	1.8
CW5 Inner Beach	0.0	0.0	0.3	27.3	50.7	20.0	1.7
CW5 Outer Beach	0.0	0.0	0.1	11.0	39.6	41.9	7.3
CW5 Inner Crest	0.0	0.1	2.2	37.6	38.1	18.0	4.0
CW5 Outer Crest	0.0	0.1	3.6	52.0	30.1	12.6	1.6
CW5 Slope 1	0.0	0.1	3.1	49.5	35.0	10.7	1.7
CW5 Slope Toe 1	0.0	0.1	3.8	44.2	33.2	17.3	1.5
CW5 Slope 2	0.1	0.4	2.7	27.7	38.8	23.7	6.6
CW5 Road	0.0	0.1	2.3	48.8	39.1	8.2	1.6

The difference in PSDs from the different locations causes variation in erosion susceptibility of the facility.

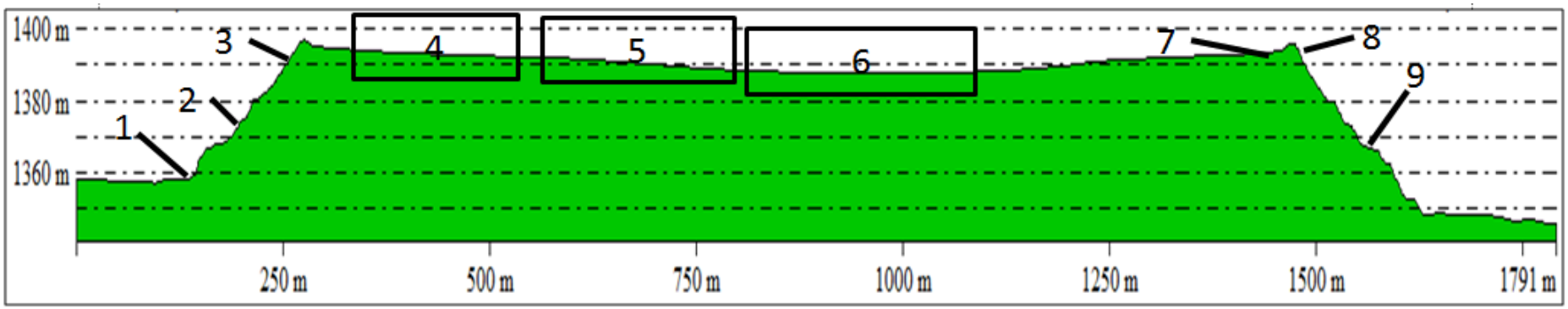

Figure 9: Representation (not to scale) of zones where composite samples were taken on the Chemwest 5 TSF (figure *not according to scale*)

Zone delineation:

1 – CW5 Slope Toe 1

2 – CW5 Slope 2

3 – CW5 Slope 1

4 – CW5 Outer Beach

5 – CW5 Inner Beach

6 – CW5 Pool

7 – CW5 Inner Crest

8 – CW5 Outer Crest

9 – CW5 Road

CHAPTER 2: LITERATURE REVIEW

This chapter consists of a literature review that was required to perform this research. This section investigates airflow phenomena at a range of scales, from thousands of kilometres (synoptic scale circulation) to micro-metres (tailings crust structures). The review provides a brief description of synoptic scale air movement over southern Africa, presents current concepts of boundary layer air movement as well as airflow dynamics over tailings storage facilities and analogue structures.

2.1. Air movement: principles and southern Africa

For dust to form from a TSF on the South African Highveld, a number of different physical processes need to take place. This process starts with solar radiation that heats the earth's surface, driving synoptic scale circulation (Greeley & Iverson, 1985:39; Strahler & Strahler, 2005:188). This in turn affects hemispheric-scale circulation, which results in weather phenomena (such as high wind speed) at local level (Jackson & Tyson, 1971:2; Tyson & Preston-Whyte, 2012:177). In turn, the geometry of the TSF influences how the local weather phenomena influences the tailings material of which it is composed, i.e. by wind speed amplification, flow separation, rainfall runoff, water pooling and mineral precipitation, and so forth (Blight, 2007:103; Lancaster, *et al.,* 1996:55; Sweet & Kocurek, 1990:1027; Walker & Nickling, 2002:52; Zhang, *et al.,*2000:360). The local weather affects the tailings material, which possesses properties that influences its erodibility (Bolt *et al.,* 2011:209, Chepil, 1950a:149, Chepil, 1950b:403, Chepil, 1951:141, Chepil, 1958:1, Hong *et al.*, 2014:76, Langson and McKenna, 2005:40, Lu *et al.,* 2013:16; Zang *et al.*, 2004:53). If the counter-forces that are exerted by the tailings properties are overcome by the local weather phenomena, then dust forms (Bagnold, 1965:85; Greeley & Iverson, 1985:71. This chapter describes this range of factors that eventually causes dust to form.

Near-surface air movement is primarily powered by solar radiation (Blight, 2008:526; Greeley & Iverson, 1985:39; Strahler & Strahler, 2005:188). Air circulation is brought about by means of unequal heating of the Earth's surface (Strahler & Strahler, 2005:174). The pressure gradient that exists between the different points causes air

circulation within a convective loop (Strahler & Strahler, 2005:188). The movement of air masses contributes to the different wind phenomena that are witnessed on Earth (Blight, 2012:98). Although the former explanation is somewhat simplified, it does suffice in being an explanation for air circulation on Earth.

These convective loops are known as Hadley cells (Strahler & Strahler, 2005:181). The Hadley cell principle states that air rises near the intertropical convergence zone (ITCZ), where low pressure systems are created, and moves downwards to the poles, where high pressure systems are created (Strahler & Strahler, 2005:181). Near-surface elements may contribute to the effective heating of the Earth's surface by controlling the effectiveness by which solar radiation is absorbed or reflected back into the atmosphere (Greeley & Iverson, 1985:39). Wind is generally observed to move parallel to isobars whilst the force of the wind relates to the spacing of isobars (Tyson, 1969:2). The direction of air motion does not always conform to the said guideline (Tyson, 1969:2).

Air movement at a specific point on the South African Highveld is the product of climatic and topographic conditions at many different scales. An overview of meso-scale wind is supplied. Local winds and micro-scale turbulence received the most attention. These phenomena are directly involved in the erosion of TSF particles and may appear to function independently of larger scale air circulation (Greeley & Iverson, 1985:39; Tyson & Preston-Whyte, 2012:177), even though they are inextricably linked.

As previously stated, large-scale air circulation is not within the scope of this research. There is however a causal link between upper air circulation and surface air movement, i.e. energy for surface air flow processes, which are ultimately powered by radiation from the sun (Blight, 2012:98). It is for this reason that air circulation of the upper atmosphere will briefly be discussed.

Upper airflow over southern Africa is generally anticyclonic, however upper atmospheric conditions do vary (Jackson & Tyson, 1971:2; Tyson & Preston-Whyte, 2012:177). The anticyclonic circulation generally produces a stratified troposphere of relative stability (Tyson *et al.,* 1996:2218). Conditions in the southern African winter display intensified anticyclonic conditions, where cold, dry westerlies displace moist air brought in by the tropical easterlies (Tyson & Preston-Whyte, 1993:207).

The moist air from the tropical easterlies is displaced equatorward (Tyson & Preston-Whyte, 1993:207). The northward movement of the high-pressure cells of the Atlantic High and Indian Ocean High, together with less heat radiation from the southern African mainland, can often link these high-pressure cells (Hurry & van Heerden, 1983:21). In winter, a high-pressure system often develops over the mainland of southern Africa, causing clear sky conditions (Hurry & van Heerden, 1983:22). Summers in southern Africa display a weak low pressure over the interior (at 850 mb), surrounded by high-pressure systems to the west and east, namely the Atlantic and Indian Ocean High (Tyson, 1987:121). In summer the high-pressure systems that dominated the interior moves south, the Indian Ocean High moves offshore and the Atlantic High moves just offshore of the Western Cape (Hurry & van Heerden, 1983:20). The movement of these cells bring about the circulation of dry air over the south-western part of the country and the inflow of moist air from the south-east, respectively (Hurry & van Heerden, 1983:22).

2.1.1. Fine weather

Tyson (1987:125) and Tyson and Preston-Whyte (2012:185) states that fine weather, heat lows (Taljaard & van Loon, 1963:39) and mildly disturbed conditions are brought about by the presence of anticyclonic settings in the atmosphere and the associated vorticity (von Gogh & Tyson, 1977:4). These systems are predominantly found between 32S in winter, 36S in summer and 34S during the transitional seasons (Taljaard, 1967:986). Weak anticyclones may be found during the months of April to May (autumn) (Taljaard, 1958:32). The high-pressure conditions that are associated with anticyclones are deep layers, illustrated by Tyson and Preston-Whyte (2012:186) as stretching from the 500 hPa level to the near-surface wind field and causing divergence of air near the surface. High-pressure systems are associated with convergence of upper atmospheric levels, i.e. the upper troposphere, and in association with the southern limb of the tropical Hadley cell causes air over southern Africa to descend during anticyclonic conditions (Tyson & Preston-Whyte, 2012:187). Anticyclones are common throughout the year, they are however more persistent during the winter (Tyson & Preston-Whyte, 2012:188).

2.1.2. Tropical disturbances in the easterlies

Easterly waves and lows as well as subtropical lows, as defined by Tyson and Preston-Whyte (2012:194), are mainly a summer phenomenon. Tropical easterly

atmospheric airflow is closely associated with the Intertropical Convergence Zone (ITCZ) and the flow of air between the ITCZ and the subtropical high-pressure belt (Taljaard, 1985:2; Tyson. 1987:127; Tyson & Preston-Whyte, 2012:191). These barotropic atmospheric disquiets are associated with open waves or cool-cored lows (Tyson, 1987:127; Tyson & Preston-Whyte, 2012:191). The easterly atmospheric waves are usually present at the 850 – 700 hPa levels and gradually diminish to the 500 hPa level and are generally not present in the upper troposphere (Tyson, 1987:127; Tyson & Preston-Whyte, 2012:188). A surface trough is usually associated with easterly waves and is the result of the boundary that forms between warm, moist air from the north-east and cool, dry air from the south-west (Tyson, 1987:128; Tyson & Preston-Whyte, 2012:194). Near-surface convergence takes place to the east of the associated surface trough, causing uplift of air and possible rains may develop (Tyson, 1987:127; Tyson & Preston-Whyte, 2012:192). To the west of the trough, clear, hot conditions develop (Tyson & Preston-Whyte, 2012:192).

In the case of easterly lows, strong upliftment takes place to the 500 hPa level to the east of the trough and strong surface divergence to the west of the trough (Tyson & Preston-Whyte, 2012:194). Rains and thunderstorms are associated with the aforementioned phenomenon, in association with northerly winds (Tyson & Preston-Whyte, 2012:194).

Tyson and Preston-Whyte (2012:195) also refers to subtropical lows that may develop in the upper troposphere when anticylonic conditions dominate over the eastern part of southern Africa and westerly waves are not present. Heavy rainfall may accompany these lows (Tyson & Preston-Whyte, 2012:195).

2.1.3. Temperate disturbances in the westerlies

2.1.3.1. Westerly waves

Tyson and Preston-Whyte (2012:195) characterise westerly disturbances as baroclinic Rossby waves. Near the surface, these systems may exhibit closed isobars but may not be present at the 500 kPa level (Tyson, 1987:128). The aforementioned waves may produce clouds and precipitation to the rear of the perturbation, whilst ahead of the wave clear conditions that are associated with subsidence may dominate (Tyson, 1987:129; Tyson & Preston-Whyte, 2012:195).

The rain produced by the wave and accompanying fronts usually does not extend past the South African escarpment and mostly occur during October to April (Tyson, 1987:129; Tyson & Preston-Whyte, 2012:195).

2.1.3.2. Cut-off lows

These westerly troughs are unstable, cold cored, baroclinic systems that are associated with strong convergence near the surface and the associated divergence occurs well above the 500 hPa level (Tyson, 1987:129; Tyson & Preston-Whyte, 2012:197). High-rain events are associated with cut-off lows along its traverse over the mainland as the trough is displaced towards the equator (Tyson & Preston-Whyte, 2012:197). The highest frequency of this type of event occurs between March to May and September to November (Tyson, 1987:129; Tyson & Preston-Whyte, 2012:197).

2.1.3.3. Southerly meridional flow

This atmospheric flow type occurs in a south-north direction and may be driven by a zonal pressure difference between a high to the west and a low to the east, influencing the south coast and eastern Lowveld with cloud formation and rain events (Tyson & Preston-Whyte, 2012:199).

2.1.3.4. Ridging anticyclones

Ridging anticyclones are yet another rain producing system; strong advection of warm, moist air over the Indian Ocean and the east coast of South Africa may bring about precipitation and associated events (Tyson & Preston-Whyte, 2012:200). Precipitation is most prominent in the presence of a westerly wave at the 500hPa level due to the upper-level divergence caused by the wave (Tyson & Preston-Whyte, 2012:200).

In South Africa, the presence of orographic features along the eastern coast also contributes to increasing air pressure gradients and increased advection (Tyson & Preston-Whyte, 2012:200). This system is most prominent during October to May (Tyson & Preston-Whyte, 2012:200).

2.1.3.5. West-coast troughs

In the west-coast trough system, a low pressure, with associated surface level convergence, dominates in the west of the country (Tyson & Preston-Whyte,

2012:200). It is stated by Tyson and Preston-Whyte (2012-200) that the upper air divergence ahead of an upper-tropospheric trough is conducive to rain events in the western, and often central, parts of the country.

2.1.3.6. Cold fronts

Cold fronts are associated with incursions of cold air from the south of the country (Tyson & Preston-Whyte, 2012:202). These systems are usually found in conjunction with other circulation types, especially westerly atmospheric perturbations (Tyson, 1987:131; Tyson & Preston-Whyte, 2012:202). Tyson (1987:131) states that near-surface convergence, and convection, takes place to the rear of a cold front, whilst ahead of the front near-surface divergence and subsidence takes place. The cooling of the atmosphere caused by these systems only tend to last a few days and are most common in winter (Tyson & Preston-Whyte, 2012:202). Summer cold fronts may occur and can result in weather anomalies, such as increased gustiness and wind shear (Tyson, 1987:131; Tyson & Preston-Whyte, 2012:205) and is often the cause of dust on the South African Highveld.

2.1.4. Meso-scale wind

Meso-scale winds, referring to both regional and local wind, are generally characteristic of regional topography (Tyson & Preston-Whyte, 1993:309; Thyson & Preston-Whyte, 2012:271). Temperature gradients between mountains, plains, valleys and ridges cause atmospheric pressure gradients between the different landscape units, giving rise to local and regional wind (Tyson & Preston-Whyte, 1993:309). Large TSF clusters could potentially contribute to this effect, however, additional studies could validate this assumption.

2.2. Boundary layer air movement and the effect thereof on wind erosion

Mean wind speed and turbulent airflow forms the cornerstone of explaining wind erosion rates (Weaver *et al.,* 2011:40). Air turbulence research conducted on dunes indicated that turbulence intensities varied along the windward and leeward faces of the dune (Weaver *et al.*, 2011:40). It is important, however, to consider the effects of the predominant mode of atmospheric motion within the boundary layer, i.e. turbulent flow and the effects thereof on particle erosion. In turn, this necessitates a discussion on the physics of particle erosion as to link two different natural phenomena, i.e.

particle erosion and atmospheric turbulence, to a single natural event on an anthropogenic landscape, like tailings storage facilities.

Before a discussion on airflow within the boundary layer can commence, a brief discussion on analogue models are necessitated. Little work has been done on wind dynamics on TSFs. One of the few researchers in this field was G.E. Blight. Air flow over dunes have been researched to a greater extent by researchers such as Frank and Kocurek, (1996:47), Tsoar *et al.* (1996:171), McKenna *et al.* (2000:211), Qian *et al.* (2009:1109), to name but a few. Due to the knowledge gap in the literature regarding air movement over TSFs, dune analogues will be used where applicable or where concepts can be extrapolated from natural sloping surfaces to tailings facilities. Dune analogues were used by Blight to illustrate similarities between dunes and TSFs (Blight, 2007:99; Blight, 2008:525).

As to better understand the effects of air turbulence on erodible material, the requirements for particle erosion has to be defined. Historically the aforementioned goal was achieved by the research of Ralph A. Bagnold. Bagnold created many papers on erosion and related topic, “The Physics of Blown Sand and Desert Dunes”, which formed the basis of much research that followed. Numerous authors have used his work as reference base in following research, as was the case of Greeley and Iverson in their 1985 book, “Wind as a geological process on Earth, Venus, Mars and Titan”. These books, in conjunction with associated and supporting papers also form the foundation of the literature review regarding air motion as a geological process, presented in this dissertation.

2.2.1. Particle motion

The onset of motion takes place when the forces acting on a particle, lying on a bed of other like grains, are overcome by an external force (Bagnold, 1965:85; Greeley & Iverson, 1985:71). In the case of aeolian transport of particles from TSFs, wind provides the required energy to lift the solid mine waste particulate from the surrounding bed into motion.

Greeley and Iverson (1985:71) identified a single force component that may initiate erosion of tailings grains, namely the lift component brought about by the movement of air over the particle. This is known as the lift force. Gravity brings about a number counter-acting forces, namely weight and moments about the axis of support

(Bagnold, 1965:85; Greeley & Iverson, 1985:71). Physical particle characteristics also play a role in keeping grains stationary, i.e. inter-particle forces and grain geometry (Greeley & Iverson, 1985:71; Shao & Lu, 2000 22440). Shao and Lu (2000:22440) identified van der Waals and electrostatic forces as being a factor affecting the erodibility of particles. The roles that forces fulfil are however complicated to empirically quantify (Greeley & Iverson, 1985:71). Shao and Lu (2000:22440) also admit to this difficulty but recognise that particle forces increase with decreasing particle diameter.

Bagnold (1965:85) illustrated the relationship of forces acting upon a particle exposed to the energy of wind. The downward acting body-force is composed of the grain geometry and density, as well as the moment about the axes of support i.e. the force required to remove the grain from the surrounding bed of grains (Bagnold, 1965:86). Balancing the counter forces exerted by an erodible grain and the fluid force yields the threshold value for particle erosion (Bagnold, 1965:86) and is given as:

$$V * t = A \sqrt{\left(\left(\frac{\sigma - \rho}{\rho}\right) x\ gd\right)} \qquad (1)$$

In this equation, "V*t" is the fluid threshold velocity, "σ" represents grain density, "ρ" represents fluid density, "A" is a general coefficient, "g" is the force exerted by gravity and "d" is the grain diameter (Bagnold, 1965:86). Equation one is, however, confined by the state of atmospheric turbulence (Bagnold, 1965:87).

Greeley & Iverson (1985), as cited by Shao & Lu (2000:22420) determined the following equation for the minimum wind threshold value:

$$U_{*t} = A_1\, G(d)\, F(Re * t) \sqrt{(\sigma p g d)} \qquad (2)$$

"F" is a function of the particle Reynolds number at frictional velocity, "G" is a function of particle diameter, "σ_p" is the particle to air density ration, "g" gravitational acceleration, "d" is the particle diameter and "A_1" is determined from experimental data and is dependent on the $F(Re_{*t})$ value.

Shao and Lu (2000:22441) proposed an alternative equation for wind threshold velocity:

$$U_{*t} = \sqrt{(AN(\sigma pgd + \gamma/\rho d))} \quad (3)$$

In equation (3), "A_N" equals approximately 0.0123 and "γ" is approximately 3 x 10^{-4} $kg.s^{-2}$. "d" is the particle diameter, "ρ" is the air density, "σ_p" is the particle to air density ratio and "g" equals the gravitational force of the Earth (Shao & Lu, 2000:22442). The equation by Shao and Lu differs from the Greeley and Iverson equation by not accommodating the particle friction Reynolds number at the threshold frictional velocity and states that for Earth, the relationship between u_{*t} and Re_{*t} may be omitted (Shao & Lu, 2000:22442).

These equations, as proposed by Bagnold (1965:85), Greeley and Iverson (as cited by Shao and Lu (2000:22420) and Shao and Lu (2000:22441), are aimed at predicting the wind speed threshold velocity over a flat surface, whilst much of the geometry of a tailings dam is not flat, i.e. the slopes, paddock walls and crests. Past research suggests that erosion mainly takes place on the slopes of tailings dams, whilst some fraction is eroded from the top-flat as well (Blight, 2007:103; Blight 2008:530; Blight, 2012:99). Therefore, the wind speed threshold velocity equations will probably not be entirely representative of the wind speed threshold velocity on TSFs. The components of the equations are valid for wind erosion on TSFs, however, the extent to which they influence the U_t – value of the material will likely differ from that provided by the equations. Factors that influence wind erosion on TSFs are also not included in these equations. These factors include organic carbon, secondary mineral precipitation, preferential settlement and particle orientation, crusting, atmospheric moisture and slope angle.

The beach area of tailings storage facilities, if let physically un-ameliorated, can be relatively homogenously flat, with only minor variations in surface topography. These areas can span hundreds of hectares and may very well warrant the validity of wind threshold frictional velocity equations for flat surfaces. A great deal of uncertainty does however exist regarding the wind profile on TSFs. This is mainly due to factors such as the wind speed amplification effect, probably brought about by the slopes of these facilities (Bagnold, 1965:197), as well as probable vortex formations and flow separation (Greeley & Iverson, 1985:207). The relative elevation of the TSF beaches with reverence to the surrounding ground surface

within the atmospheric boundary layer may also bring about a difference in the wind regime on these mine dumps.

2.2.2. Soil/tailings characteristics and cover conditions that influences wind erosion

Tailing materials can differ greatly with respect to mineralogy, particle characteristics and geometry as well as the ways in which they react to environmental stimuli. These differences can be brought about by differences in geology of the parent material, mine processing methods, climate, microbes and time exposed to the different environmental factors (Grondklassifikasiewerkgroep, 1991:226), i.e. general pedogenic processes but with a greater degree of anthropogenic input (Bini and Gaballo, 2006:70; Neels *et al*. 2003:1; Scalenghe and Ferraris, 2008:40). These pedogenic factors will determine the general characteristics of the soil, together with the pedogenic processes that will continuously change the condition of the soil.

Characteristics of soil may influence the wind erodibility thereof (Chepil, 1950a:149). These features are referred to in the work of Bolt *et al.,* 2011:209, Chepil, 1950a:149, Chepil, 1950b:403, Chepil, 1951:141, Chepil, 1958:1, Hong *et al.*, 2014:76, Langson and McKenna, 2005:40, Lu *et al.,* 2013:16; Zang *et al.*, 2004:53, and include the following:

- Soil surface characteristics such as crusts (Belnap and Gillett, 1998:133);
- Soil structure development, surface roughness (Tan *et al.,* 2013:67);
- Apparent density, water capacity (Han *et al.*, 2009:230);
- Soil organic carbon (Zobeck *et al.*, 2012:43);
- Particle size distribution (Alfaro, 2008:158); and
- Surface cover (Gong *et al.,* 2014:105, Youssef *et al.*, 2012:178).

Gold tailings material can undergo a number of pedogenic processes, in some cases in a much shorter timeframe than natural soil. These processes are evident in the redox conditions of the material (Akcil & Koldas, 2006:1139), crust formation (Tutu *et al,* 2008:3669), secondary mineralisation and precipitation (Gieré *et al.*, 2003:1352), oxidation and reduction by means of organisms (Lu and Wang, 2012:119). In the cases where these processes cause structure formation, the tailings material may be less susceptible to wind erosion.

Figure 10 (Iverson & Greeley, 1985:92) shows the wind erodibility of different particle sizes for Earth, Venus, Mars and Titan. Even though only the atmospheric conditions of Earth are of concern, the threshold friction speeds on other planets provide information regarding the effects of air density and gravity in particle displacement. The graph shows that the most erodible fraction on Earth has a particle dimeter of 75 µm, which is the very fine sand and silt fraction of particles.

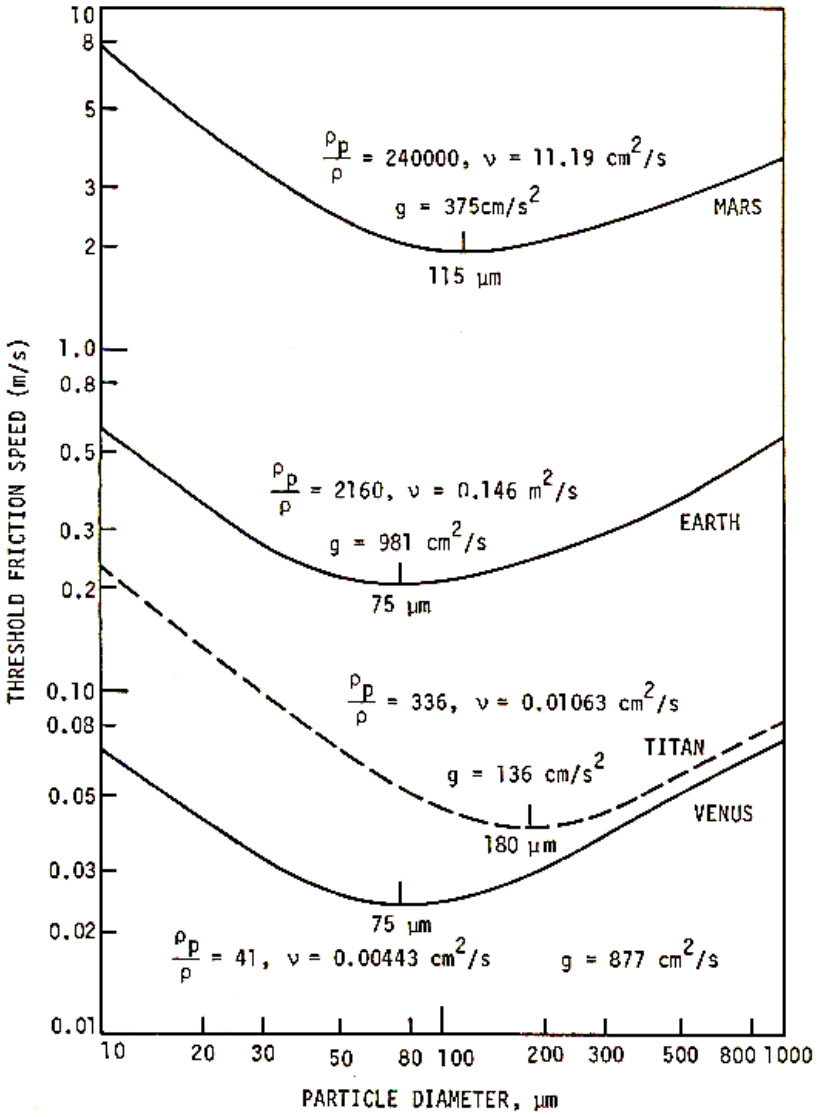

Figure 10: Wind erodibility and particle size distribution (Iverson & Greeley, 1985:92).

2.2.3. Surface crusting

Due to the scarcity of published literature on the topic of crusting and compaction on gold tailings, natural soil will be used as an analogue in the literature review.

Physical soil crusts are often the effects of the action of wind and water on soil particles in areas where the soil/tailings surface is directly exposed wind erosion and raindrop impact (Fang *et al.,* 2007:222; Farres, 1978:243, Gicheru *et al.,* 2004:173). Of these factors, raindrop impact is probably the major cause for crust formation (Ben-Hur *et al.,* 1985:282: Farres, 1980:230). Soil crusts are often formed when soil aggregates are destroyed by the energy of impacting raindrops (Farres, 1980:230,

Onofiok and Singer, 1984:1138) or due to the chemical dispersion of the structural units (Ben-Hur *et al.,* 1985:282: Helalia, 1988: 251).

In the case of gold tailings material, this effect is amplified by the general absence of structure in the form of aggregates. Bloem (1992:8) states that soil aggregates are destroyed when the forces that are exerted on the aggregates are greater than the binding forces. The hydrostatic swelling, brought on by the ingress of water into the aggregate, causes a decrease in the effective binding energies of the Van der Waals and capillary forces, further weakening the structural unit (Agassi *et al.*, 1985:186, Bloem, 1992:8, Farres, 1980:229). Chemical dispersion also contributes to crust formation by weakening the aggregate structure and causing said structure to be more susceptible to raindrop impact (Farres, 1980:230; Gal *et al.*, 1984:872).

Particle sizes in the range of 2 µm and less, can also greatly contribute to the formation of soil crusts by settling into pore spaces after being mobilised by water. The suspended particles are believed to be drawn into the pore spaces of the material due to capillary suction that arises between the water saturated and water unsaturated area within the porous material (Gal *et al.*, 1984:872). This form of crusting causes the compaction of the surface layer and is brought about by hydraulic settling of the particles. This method of compaction is very effective and one of the preferred methods of tailings deposition (van Deventer, 2015: personal interview).

Soil crusting may have a profound effect on the erodibility of a substrate (Eldridge and Leys, 2003:457; Jia *et al.*, 2012:31; Nickling, 1984:111, Zhang *et al.*, 2006:441). The latter is an example of material with a higher density relative to the same material that is without a crust (Roth, 1997:223). The denser material can exert greater downward acting forces on particles and decrease the wind exposure surface, keeping the particles in place and thereby decrease the rate of wind erosion (Chepil, 1951:145; Hupy, 2004:167; Yan *et al.*, 2015:79; Zobeck, 1991:115). Gold tailings materials often exhibit these features and are the product of hydraulic and mechanical compaction as well as drying, structural, depositional, sedimentation, chemical and erosion crusting.

Chemical crusts on gold TSFs are often the result of secondary mineral precipitation (Al *et al.*, 2000:3933). These precipitates regularly contain iron and sulphate, which

is the result of sulphide mineral oxidation (Al *et al.*, 2000: 3934; Roussel *et al.*, 2000:214). These iron precipitate crusts can remain chemically stable in pH conditions of less than 2.5 (Roussel *et al.* 2000:216). Gypsum and magnesium sulphate salts also occur on many gold tailings facilities (Simms *et al.*, 2007:1417). The binding forces of these crusts can increase their resistance to the action of wind, however, the effects of these crusts on wind erosion is yet to be extensively investigated.

It should, however, be noted that whilst soil crusts may decrease the rate of wind erosion, the rate of water erosion is increased. This is due to the decrease in hydraulic conductivity of the substrate brought about by the decrease in porosity. Gold tailings' dry bulk density can increase from 1.4 $g.cm^2$ to 1.7 $g.cm^2$ due to hydraulic compaction, and thereby decrease porosity (Van Deventer, 2015: personal interview).

The effects of biotic crusts were not investigated in this research. This is because few (if any) of these crusts are present on the Chemwest 5 TSF. Biotic crusts do contribute to decreasing wind susceptibility (Belnap and Gillette, 1997:140; Leys, *et al.*, 1998:972; Eldridge and Leys, 2003:463).

2.3. Air movement over tailings storage facilities and like structures

2.3.1. Air movement around objects

Even though fluid flow is complex to define, certain airflow patterns are characteristic of specific geometries (Figure 11). The resultant airflow around these structures have specific properties that influence erosion of particles.

Airflow in the open atmosphere is usually turbulent. As the velocity of airflow increases, the flow becomes increasingly unstable and turbulent flow dominates. The Reynolds number is an indication of air turbulence around structures.

Vortexes develop in zones of fluid separation. Examples of flow separation and the resultant vortexes are displayed in Figure 11. The structures in Figure 11 are characteristic of TSFs, especially the slopes and berms of gold tailings dams. Vortexes can form on both the windward and leeward sides of these facilities. Identifying zones where vortexes could form is important, since vortexes can cause

both deposition and erosion of particles, depending on the intensity of the vortex and associated vorticity.

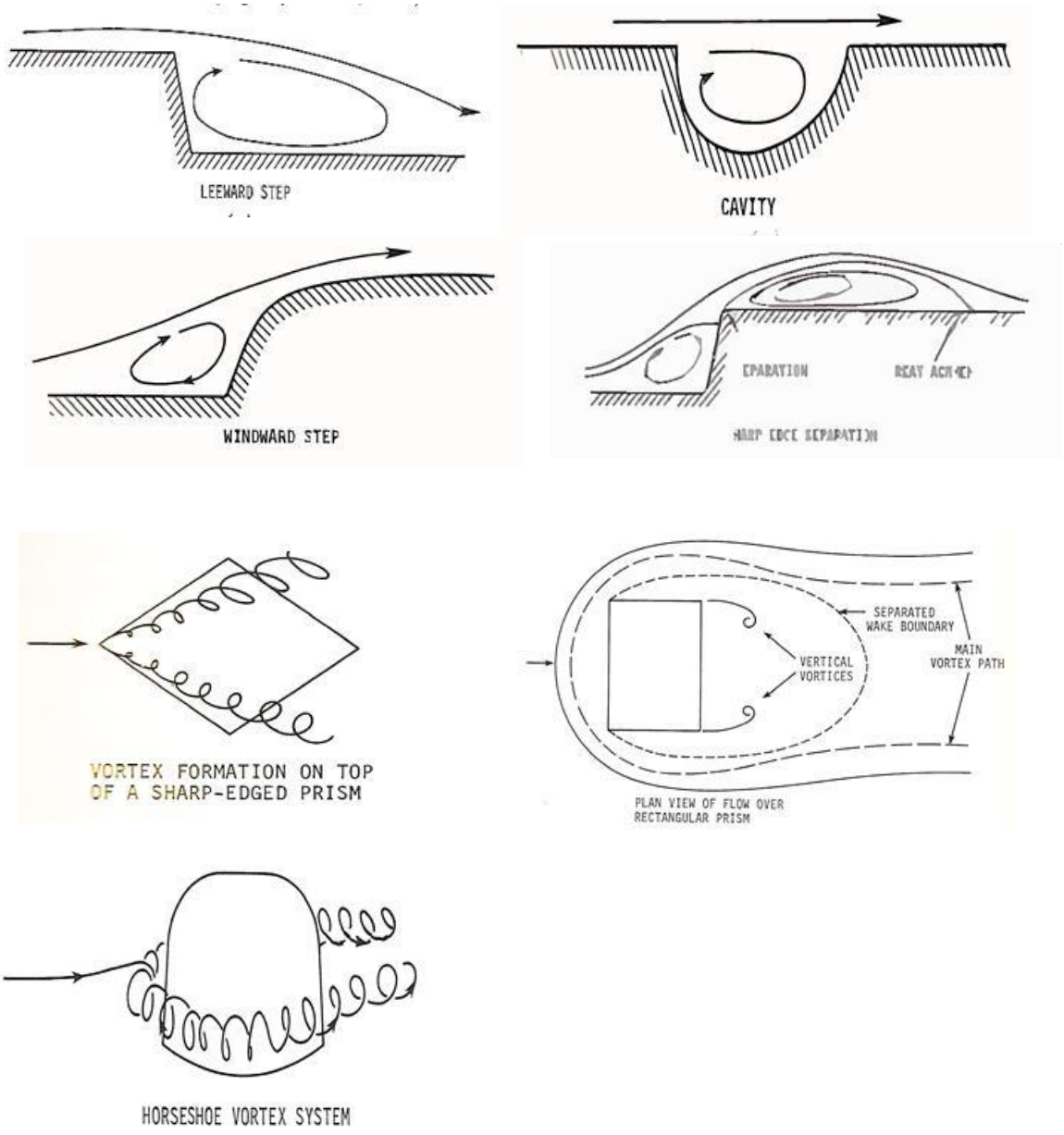

Figure 11: Typical airflow patterns around certain shapes (Greeley and Iverson, 1985: 205 – 209).

2.3.2. The wind speed amplification effect

Numerous studies found that, generally, wind speed increases along the profile of a dune or tailings slope (Blight, 2007:103; Lancaster, *et al.,* 1996:55; Sweet & Kocurek, 1990:1027; Walker & Nickling, 2002:52; Zhang, *et al.,*2000:360). The

amplification effect is due to fluid compression (Walker & Nickling, 2002:53; Weaver, 2011:32) as the air is forced around the TSF. Figure 12 illustrates the wind speed amplification effect for a dune and tailings facility. The figure shows that a dune is a possible analogue for a conventional tailings storage facility with reference to wind speed amplification.

Even though not explicitly stated in the text by Blight (2012:97), Figure 12 depicts that the wind speed for the upwind slope of dunes and tailings facilities is influenced by the slope angle and surface uniformity. In (a) of Figure 12, the illustration shows how the wind speed amplification factor increases with absolute elevation and along the dune surface. The amplification factor reaches its maximum just before the dune crest, where after it drastically decreases. Zhang, *et al.* (2000:360) reported similar results for a pyramid dune, where airflow is amplified from the base to the crest of the dune. Amplification of the wind speed also took place in a study by Sweet & Kocurek (1990:1027) from the base to the crest of a dune.

In (b) of Figure 12, the illustration shows that the wind speed is amplified with elevation and over the dune surface, until the air mass reaches the first inter-bench area of the TSF. Over this part of the TSF, the wind speed amplification decreases drastically, but not to the extent of nullifying the amplification effect completely. Zhang, *et al.* (2000:360) also reported an area of decreased wind speed on the leeward side of a pyramid dune crest. It is at the crest of the facility that the wind speed reaches its maximum. The crest (as a disturbance in the slope profile) causes the wind speed to decrease significantly over the beach and pool area of the TSF, however, the wind speed is still greater than at the base of the TSF. A study of wind speed on the lee of a dune by Sweet and Kocurek (1990:1027) also showed how wind speed decreases until it reaches the base of the dune. The wind speed then increases as the air moves away from the dune.

Figure 13 presents another approximation of airflow patterns over a portion of a TSF by Blight (2012:97). The image depicts the wind speed amplification factors iso-lines for the slope and beach section of a TSF, in relation to vertical and horizontal distance ratios. The iso-lines depict an increase in the amplification factors from the base of the TSF to the crest. The airflow behind the area of possible flow separation (crest) has lower amplification factors than that witnessed at the crest. In some

cases, the airflow over the beach area has a lower speed than at the base of the facility (0.8 in relation to 1.0).

The wind speed decrease that Blight (2012:97) witnessed is not unexpected, since Figure 11 (a) and (b) show how flow separation takes place around structures that are akin to that of Blight (2007:103) in Figure 12. Tsoar, *et al.,* (2004:294) reported that flow separation takes place between the crest and lee of a dune slope. Flow separation takes place because the compressed fluid reaches an area of low pressure and a component of the flow vector is drawn into this low-pressure zone. The resultant airflow often exhibits vorticity, and is classified as a vortex.

Flow separation and the resultant low wind speed measured in the lee of a crest is important because most TSFs have a crest that surrounds the beach and pool area. Airflow characteristics in the zones between the crest and outer beach are likely to be akin to the same zone of certain dunes. Results from numerous studies show that the lee of a dune exhibit much lower wind speed than the crest and that negative wind speed amplification can occur (Walker, 1999:437; Wiggs, *et al.*, 1996:43). Particle deposition (eroded fraction from the slope) takes place in these areas of low wind speed (Blight, 2007:103; 2008:530). Identifying the areas of deposition, in this authors opinion, is nearly as important as identifying the areas of erosion. This is because the deposition areas have relatively high volumes of wind erodible particles that are no longer protected by the effects of chemical and physical crusting or vegetation. A change in wind direction can cause this highly erodible material to be subjected to the force of wind, whereby copious amounts of dust is generated.

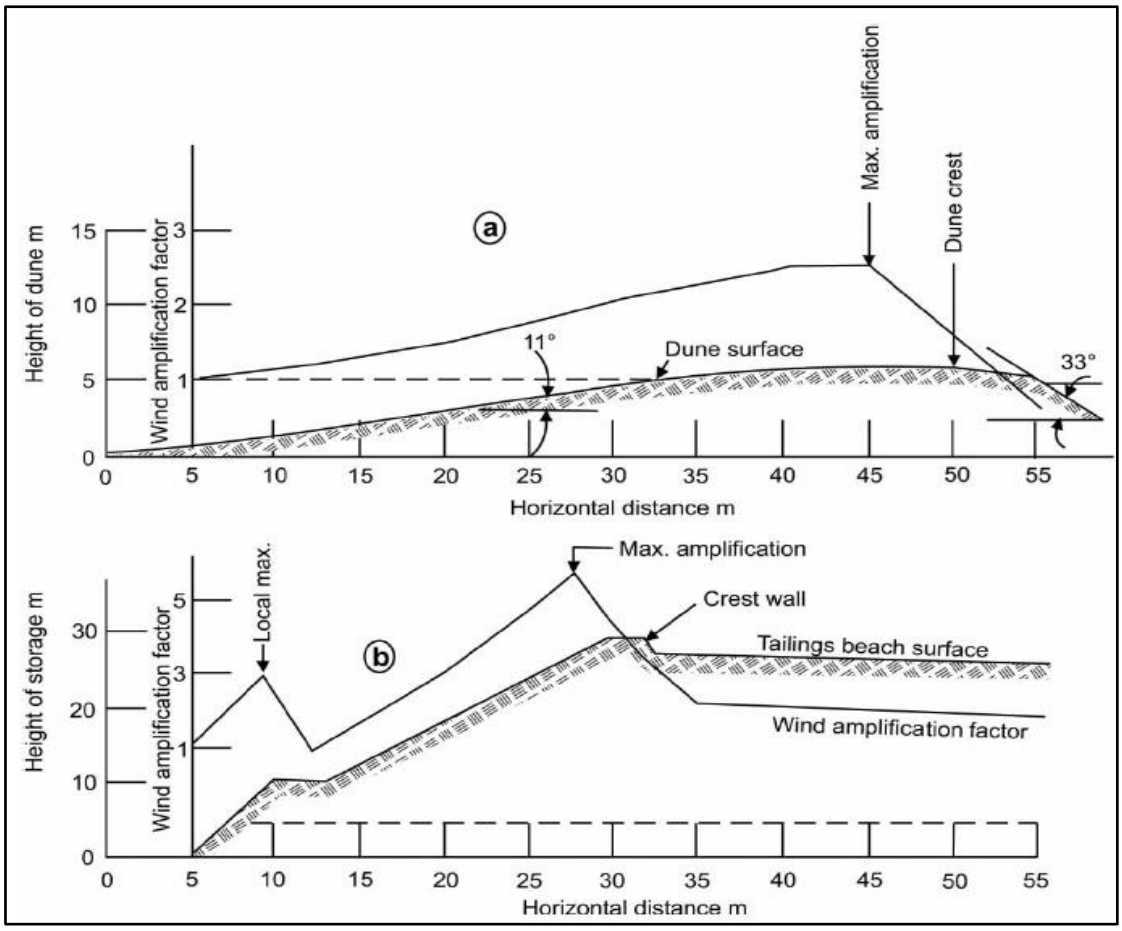

Figure 12: Wind speed amplification illustration for a dune and tailings facility (Blight, 2012:97).

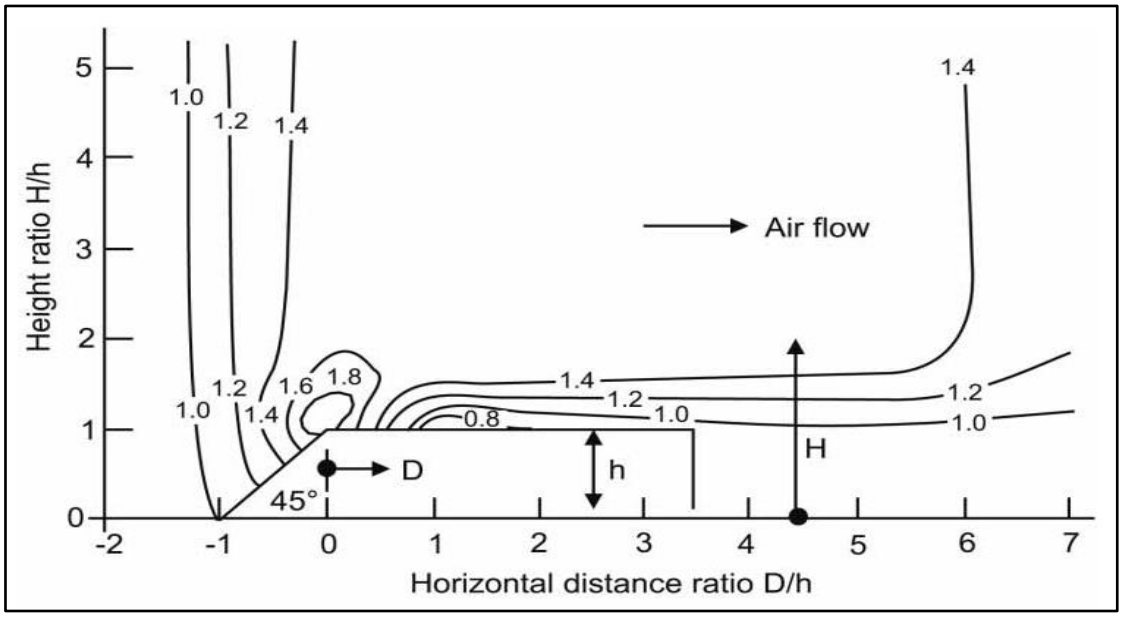

Figure 13: Airflow vectors over a portion of a TSF (Blight, 2008:526).

CHAPTER 3: MATERIALS AND METHODS

This chapter details the data acquisition process of the research. It highlights the materials used as well as the methods by which they were utilised. The first section of this chapter deals with the crust collection and analyses by means of Scanning Electron Microscopy. The second section explains the placement and data collection intervals of the wind monitoring units on the Chemwest 5 TSF. The final section of this chapter describes the wind-tunnel tests that were conducted to obtain the minimum wind-speed threshold velocity (u_t) of the tailings material.

3.1. Scanning Electron Microscope (SEM) analyses

The SEM was used to obtain images of the particles that constitute the different crusts that were found on the TSF. XRD analyses of the crust matrix and mineral intergrowths were performed during the SEM investigation.

3.1.1. Sample collection and preparation

Samples were collected from the Chemwest 5 TSF. The samples included drying crusts (sampled at two locations), an erosional crust and a chemical crust. These were all sampled at different locations on the TSF in areas where the relevant crusts were present. Figure 14 illustrates the traverse line (along which crust types were identified) on the TSF as well as the crust sampling locations.

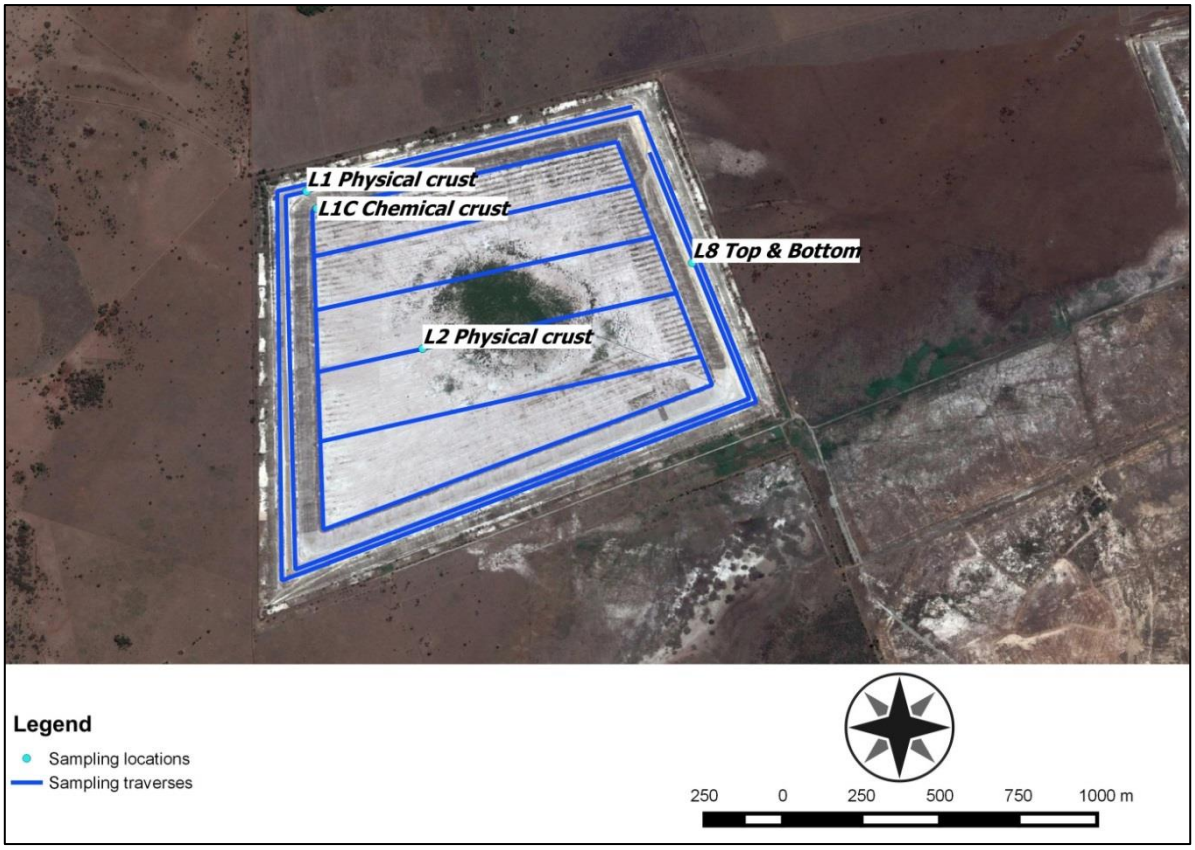

Figure 14: Sampling locations of the TSF crusts.

The drying crusts were found in small basins on the TSF, usually where the road used to be. The chemical crust was found on the outer-beach area of the facility as a slightly elevated precipitate. The material was loose from the TSF surface and appeared to have a lower density than the underlying material. As the water evaporates, gypsum starts to precipitate and acquires a less dense state. Gypsum is hydroscopic and will naturally accumulate water as it becomes available, thereby decreasing the surfaces' susceptibility to wind erosion (van Deventer, 2015: personal interview). The erosion crust was sampled on the northwestern crest. The aforementioned crust was the thickest of the three types sampled and was approximately 7-10 mm thick.

The samples were removed as intact crust pieces of approximately 50 mm x 50 mm and placed in plastic bags. The samples were moved from the site to the SEM-lab in a protective case as to minimise physical damage to the structure.

3.2. SEM visual and chemical analyses

The North-West University's SEM was used for the crust investigation. The analyses were performed the personnel from the SEM laboratory.

The SEM that was used was a Quanta FEG SEM with an integrated Oxford INCA X-Max EDS system. Different vacuum intensities were used during the analysis and photos. The machine was automatically calibrated by the accompanying software.

The energy dispersive x-ray spectroscopy (EDS) analysis was performed at 15 kV. The working distance (WD) was set to 10 mm – 11 mm in high vacuum mode. Each sample was analysed for 100 live seconds.

The SEM images were obtained using 10 kV potential. In the analysis, a LFD detector was used that was set to SE mode. The working distance (WD) was 10 mm – 11 mm. A low vacuum was used, with vacuum pressure of 33.67 Pa. The spot size of the analysis was 4.5. In order to prevent excessive scattering and to obtain better quality imagery, the samples were coated with palladium-gold ions.

For the analysis in the SEM, the crusts were reduced in size to approximately 10mm x 10mm pieces. These pieces were then placed on double-sided carbon tape.

The chemical analysis was done on the samples by performing numerous analyses that were performed in a zigzag transverse of the sample over the period of 100 seconds. The imagery was obtained by coating the crust samples with palladium-gold ions as to homogenise and optimise the electrical conductivity over the sample and to obtain higher quality imagery.

The photographic and XRD analyses of the crusts can be summarised as follows:

- The Chemwest 5 TSF was traversed on pre-defined lines to identify different types of crusts that were present of the facility;
- Representative samples of the crust was carefully removed (approximately 7 mm - 10 mm);
- The samples were placed in plastic sampling bags, which were in turn placed in protective casings that minimized damage to the crusts during travel;

- The EDS analysis of the samples were performed with a pre-calibrated detector at a working distance of 10 mm – 11 mm. The potential at which the tests were carried out was 15 kV;
- The EDS analysis was performed over 100 live seconds;
- The SEM images were obtained by first coating the samples with palladium-gold ions to obtain a homogeneous reflective surface for electrons;
- The working distance was set to 10 mm – 11 mm;
- A low vacuum of 33.67 Pa was used for this analysis;
- Standard reference images were obtained for a 100 µm scale.

3.1. Wind tunnel materials and methods

A wind tunnel was used to analyse the minimum wind speed threshold velocity of tailings material that were sampled from the Chemwest 5 TSF.

3.1.1. Sample collection and preparation

The Chemwest 5 TSF was constructed in three stages, using two different techniques. The lower sections of the TSF were constructed as a ring-dyke dam, using a “day-walling” technique. The top slope was constructed using cyclone technology, in which the finer material is segregated from the coarse material and deposited on the beach and pool section of the TSF. The coarse fraction of the material was deposited on the outside of the slopes. Due to the differences in particle size distribution of these deposition methods, different wind erodibility is possible. These distributions can be seen in Table 1.

Composite samples were collected to a depth of 100 mm on the second, third and fourth slope from the bottom on the east of the facility. The locations where the samples were extracted are shown in Figure 15.

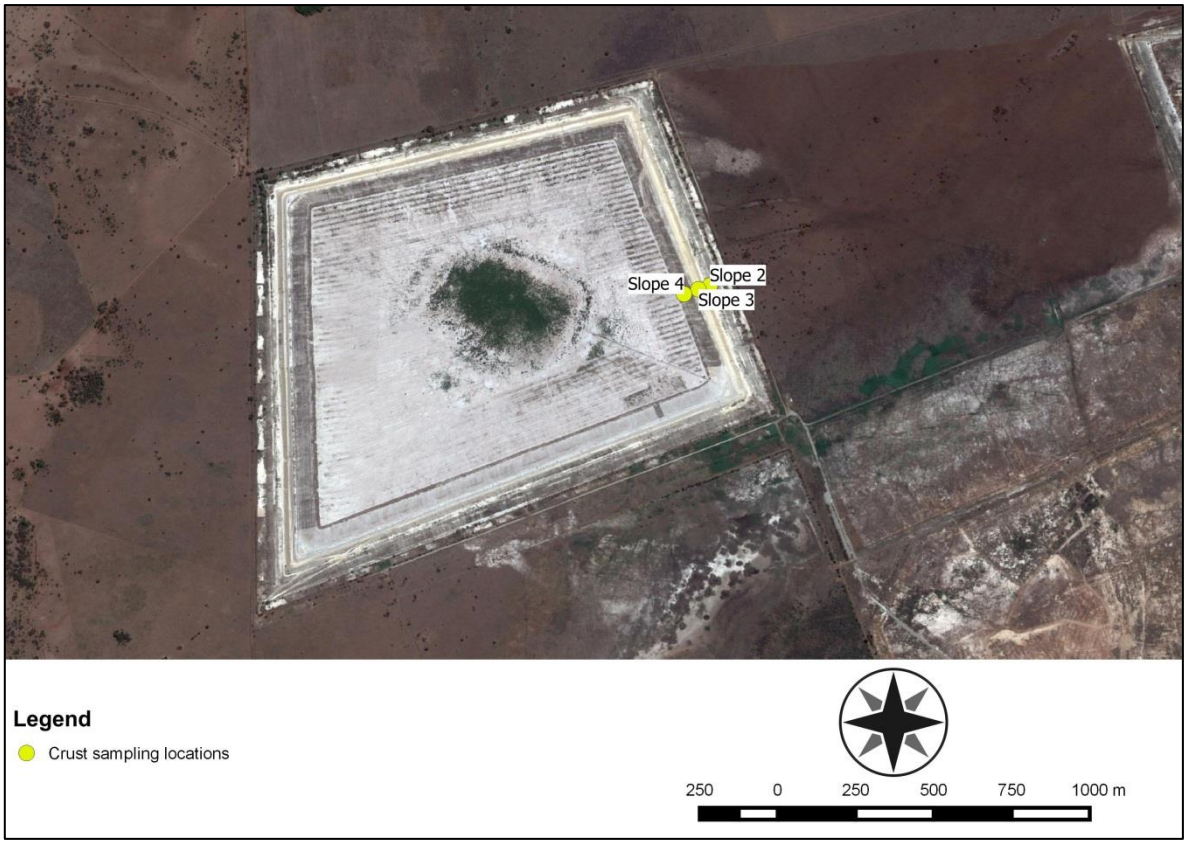

Figure 15: Locations of composite tailings sampling in the Chemwest 5 TSF.

The goal was to identify the $\underline{u_t}$-value for the scenario than is likely to produce dust on the TSF, which is dry, loose, un-consolidated and structureless tailings material. These conditions were obtained by crushing the samples with a mortar and pestle. The fine material was sieved through a 2 mm sieve and dried at 50°C for 24 hours.

For an average of the u_t-value, five replicas per sample were analysed in the wind tunnel. Each replica had to be the same mass and had to occupy the same amount of space with as similar geometry as possible. To that end, a metal stand was used to place the sample on and a frame of approximately 100 mm x 50 mm x 10 mm was used to mould the sample. The sample stand was located in the centre of the test chamber to minimise the effect of the "Law of the Wall". The frame was then removed before the test to expose the entire surface area to the wind. Once the frame was removed, the sample (under the influence of gravity force) assumed its natural angle of repose.

3.1.2. Wind tunnel test methodology

The wind tunnel that was used was composed out of three components, namely a bell-mouth, test chamber and diffuser. The bell-mouth measured 500 mm x 500 mm at the intake and 300 mm x 300 mm at the outflow. The test chamber dimensions were 300 mm x 300 mm x 300 mm. The diffuser measured 300 mm x 300 mm at the intake and 500 mm x 500 mm at the outflow. The airflow was controlled by a three-phase fan, the revolution frequency of which was regulated by a frequency regulating drive.

The airflow speed of the tunnel was calibrated by placing an anemometer inside the test chamber, in the same location as where the samples were to be placed. The wind speed calibration was performed in the centre of the test chamber as to decrease airflow speed variability that could have been brought on by friction of the test chamber walls (Law of the Wall). This enabled the accurate prediction of wind speed at specific motor revolutions. The minimum accuracy of the tunnel was 0.5 $m.s^{-1}$. Turbulence was decreased by the three rows of air-stabilising mesh that was located in the bell-mouth of the wind-tunnel.

The samples were placed in the wind tunnel and exposed to different wind speeds. Each time a new wind speed was selected, a new sample was prepared. This was done in order to maintain the original erodibility of the sample. Before and after each test the mass of the sample was measured. This was done as to record any loss of the sample mass due to wind erosion. The tests began with a wind speed of 2.5m/s and, due to the accuracy of the tunnel, wind speed was increased in increments of 0.5$m.s^{-1}$. This procedure was followed until a fraction was recorded as being eroded.

The following is a stepwise layout of the procedure that was followed to determine the mass loss of each sample:

- Composite samples were removed from the research site to a depth of 100 mm. Five samples of approximately the same mass was extracted to form the composite samples;
- The samples were dried at 50°C for 24 hours;

- The samples were crushed with mortar and pestle and sieved through a 2 mm sieve as soon as they were removed from the ovens. This reduced the amount of atmospheric moisture that could have accumulated in the samples;
- The samples were left for 30 minutes to cool to room temperature, it is believed that this reduced the amount of convection that could have been present over hot samples, thereby increasing the accuracy of the tests;
- A metal stand was used to place the sample on in the wind tunnel. The stand had a low aerodynamic profile, with the purpose of reducing any possible turbulence, vortices and eddies that could have compromised the results;
- Five replicates of each composite sample was placed in the wind tunnel and individually tested;
- The samples occupied approximately the same space as all the samples were placed in a 20 mm x 20 mm mold, which was removed before each test;
- The mass of the samples were determined before and after each test and recorded;
- The tray was removed after each test, as the incorporation of a scale into the wind tunnel was not possible due to the decrease in pressure that resulted in the wind tunnel during the tests;
- New samples of the same material was used for each wind speed, as the highly erodible fraction was removed during the low-speed test. Using the same sample would have resulted in a lower mass loss than what was actually measured;
- The wind speed that was required to erode 0.1% of the sample was determined by interpolating between the measured mass loss values;
- In all cases, a linear relation was assumed for instantaneous particle liberation. This was because of two reasons, namely:
    - The length of the sample was not sufficient to have caused particle liberation by means of saltation, as the trajectory of eroded particles are nearly vertical, thereby removing it from the particle bed before impacting on other particles. Assuming an exponential relationship would therefore have been erroneous;
    - The data points were close enough together to assume a linear relationship.

3.1.3. Calculating the u_t value of the sample

The u_t value was calculated by using the wind speed at which the first mass loss was recorded and the wind speed at which >0.1% of the sample was eroded. By interpolating the mass loss results from the these wind speeds, the theoretical wind speed value at which 0.1% mass loss took place could be calculated.

The sample mass loss values are presented in Table 11. The u_t – value for the different slopes are presented in Table 12.

3.2. Wind dynamic monitoring

Figure 16 shows the spatial distribution of wind monitoring units (WMU) on the Chemwest 5 TSF. WMU 1, WMU 2, WMU 4 and WMU 6 were placed on the top crest of the facility, as can be seen in Figure 16. WMU 3, WMU 11, WMU 8 and WMU 6 were placed on benches of the N, E, S and W slopes (see Figure 16 for location and Table 2 for altitude).

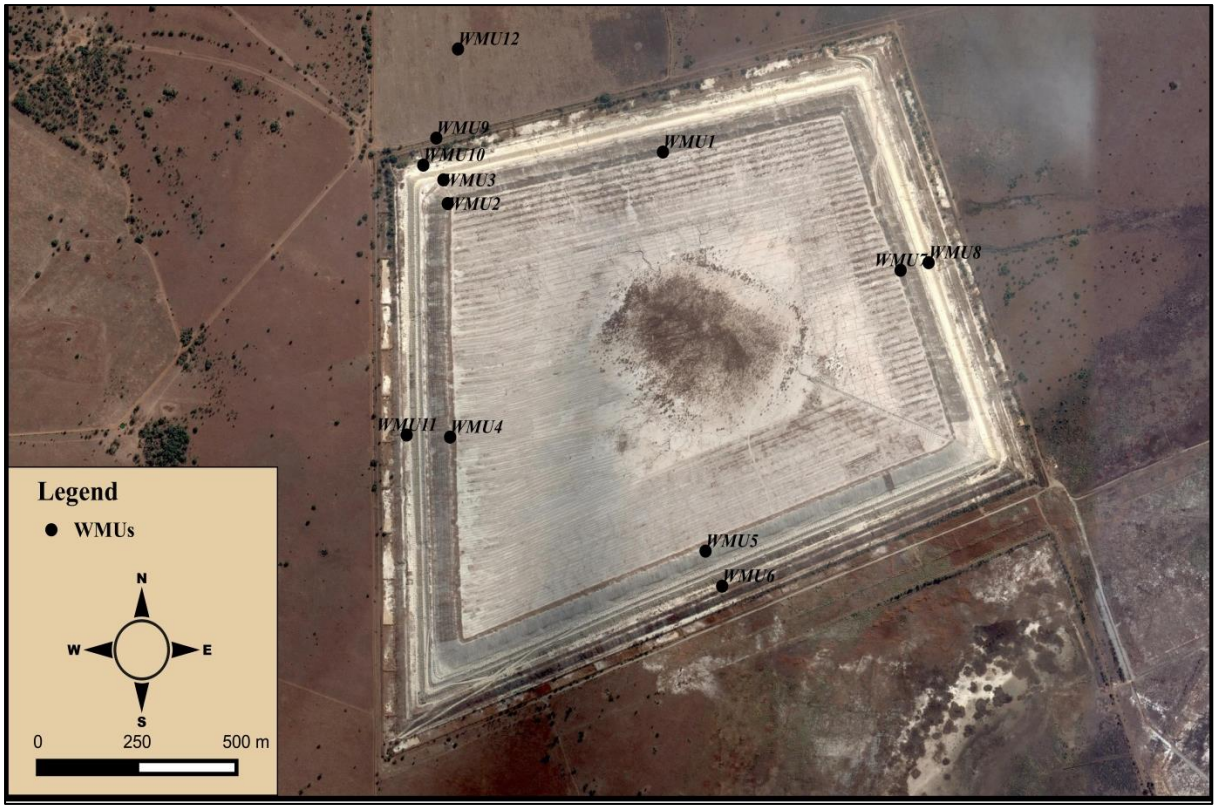

Figure 16: Placement of the WMU on the Chemwest 5 TSF

Since the dominant wind direction is from the north, more WMUs were placed on the northern side of the TSF. This was done in order to assure detailed data for the major wind direction.

The WMUs were placed at the edge of the slopes. This was done to minimise any possible sheltering effect that may have arose due to topographic influences. The WMUs were placed at different elevations above mean sea level. This was performed in order to acquire a better understanding of the wind speed dynamics that are found with height on the TSF.

The WMU were placed clear of possible obstructions to airflow that could cause misrepresentations of wind direction or wind speed. The monitors were installed with 0°/360° facing true north. True north was determined using a Garmin eTrex GPS.

Table 2 shows the co-ordinates and altitude of the WMUs that were placed on the Chemwest 5 TSF.

Table 2: Co-ordinates and altitude of the different WMUs on the Chemwest 5 TSF during the research period.

WMU no.	S	E	Alt (m)
1	26.81365	026.77250	1399
2	26.81487	026.76705	1397
3	26.81431	026.76694	1379
4	26.82040	026.76711	1398
5	26.82310	026.77358	1396
6	26.82393	026.77400	1365
7	26.81645	026.77852	1399
8	26.81627	026.77923	1375
9	26.81332	026.76676	1361
10	26.81396	026.76643	1367
11	26.82035	026.76601	1364
12	26.81121	026.76731	1365

The data gathering on the TSF was performed using wind-monitoring units. Each unit was equipped with, at least, a R.M. Young Wind Monitor and a Campbell Scientific data logger (CR200X) and was 2.2 m tall. The following figure depicts the wind-monitoring unit:

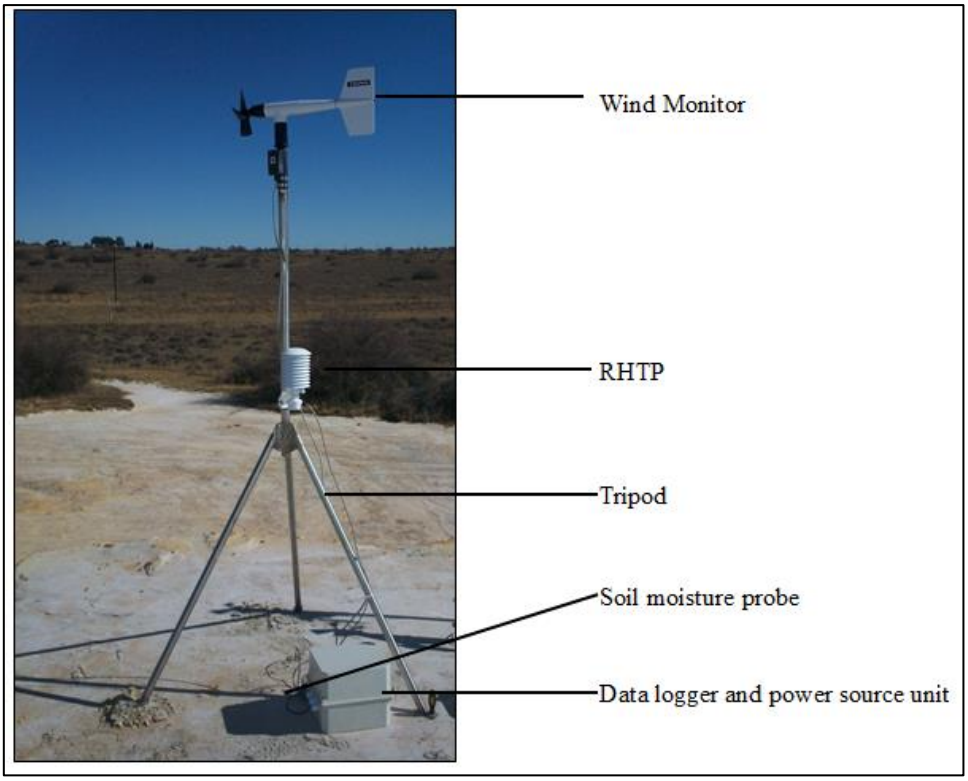

Figure 17: R.M. Young Wind Monitor Model 05103 (R.M. Young Company, 2012).

The R.M. Young Wind Monitor (WM) was used to measure horizontal air movement in terms of both speed and direction. The WM was capable of measuring wind speed in the range of 0- 100 $m.s^{-1}$ with a 1.0 $m.s^{-1}$ threshold sensitivity. The wind speed is derived from the AC sine wave produced by the six-pole magnet within the device, three complete sine waves represents one blade rotation of the WM.

Furthermore, the WM was used to monitor the wind direction. The device was capable of a 360 degree mechanical rotation and a 355 degree electrical rotation. The wind direction threshold sensitivity for the device was 1.1$m.s^{-1}$ with a 10° displacement. The vane position was transmitted by a 10 kOhm potentiometer that was subjected to a constant excitement voltage of which the analogue voltage is directly proportional to the angle of the wind direction.

3.2.1. R.M. Young Relative Humidity/Temperature Probe (RHTP) Model 41382VC (R.M. Young Company, 2011)

The RHTP was used to measure the relative humidity as well as the air temperature. The probe was able to determine the relative humidity ranging from 0-100% with a

1% precision sensitivity. The device's relative humidity readings remained stable to a 1% precision through the entire year.

The device can measure temperatures between -50 and +50 with a 0.3°C accuracy. The probe was installed in a well-ventilated radiation shield. The device was connected to a Campbell Scientific data logger.

3.2.2. Campbell Scientific CR200X data logger (Campbell Scientific, 2011a)

This device was used to store and interpret the information sent by the aforementioned electronic equipment. The CR200X data logger was powered by an external power source. The data was stored on the device and after the measurements were taken, the data was moved to a computer for statistical analysis.

3.2.3. The wind-monitoring unit

The wind-monitoring unit consists of a two-meter high tripod, capable of mounting the relative humidity and temperature probe with radiation shield and the wind monitor.

3.3. Data analyses techniques

This section provides information of how the different analyses were performed. The calculations that underlie the different statistical concepts are not discussed in detail, but rather the reason for using specific statistical methods.

3.3.1. Arithmetic mean

Describes the mean conditions found on site and was useful for data comparisons over time and space for wind speed, temperature and rainfall (Thompson, 2006:119).

3.3.2. Standard deviation (σ)

A measure of the dispersion of data in a dataset, i.e. the manner in which the data distribution is spread (Thompson, 2006:119).

3.3.3. Variance (σ^2)

A measure of the way in which data is distributed and is the standard deviation squared (Thompson, 2006:119).

3.3.4. Range

A numerical value of the difference between the smallest and largest value in a dataset (Thompson, 2006:118). The range supplies the extent of variation that was identified in the study site.

3.3.5. Pearson's product-moment correlation coefficient (r)

This analysis provides the linear correlation between two datasets (Thompson, 2006:120). It was used extensively in analysing correlations in wind speed between positions on the TSF and the reference site.

3.3.6. Pearson's Chi-squared test

The assessment of the goodness of fit between observed and expected values in a dataset. This analysis allows for determining the statistical significance of a relationship between two variables (Greenwood & Nikulin, 1996: vii).

CHAPTER 4: RESULTS AND DISCUSSION

This chapter contains, 1) the results of the SEM analyses of the crust materials, which highlights the physical orientation of the crust particles, inter-particle crystal growth and the chemical composition of the material, 2) the minimum wind speed threshold velocity of the tailings material, which was established by the wind tunnel study, 3) the results of the wind dynamic research on the TSF are also discussed in this chapter.

4.1. Results and discussion of the SEM analyses on the TSF crusts

SEM was utilised to qualitatively assess the physical characteristics of the crusts that formed on the Chemwest 5 TSF. It was also used to quantitatively identify the chemical elements of which the crusts were composed.

Physical characteristics of the crust allows for the possible identification of the mechanisms that could have led to the formation of crusts on the TSF. The particle shape and orientation as well as crust composition can give an indication of the environment that led to its formation (Langston & McKenna Neuman, 2005:41; Pagliai *et al.,* 2004:38). This principle was applied in the SEM crust analyses.

Chemical characteristics of the crusts were assessed in order to identify a possible binding agent that may have been present between the particles that could form larger cohesive units. These units may then also be less susceptible to wind erosion due to their mass and shape (Langston & Mckenna Neuman, 2005:40).

4.1.1. Drying physical crust (L1)

Two drying crusts were analysed in the research site, namely L1 and L8. The purpose of the SEM imagery was to identify the bonding agents that form the crust structure.

The SEM image in Figure 18 and Figure 25 shows a fine-grained matrix with larger silicate grains. The grains are connected by fine silicate particles and gypsum crystals. These crystals were mainly found on silicate particles. This is likely due to a nucleation surface provided by the silicate particles and the subsequent precipitation of gypsum. Annexure 1 shows additional images of these crusts in Figure 74 and Figure 75.

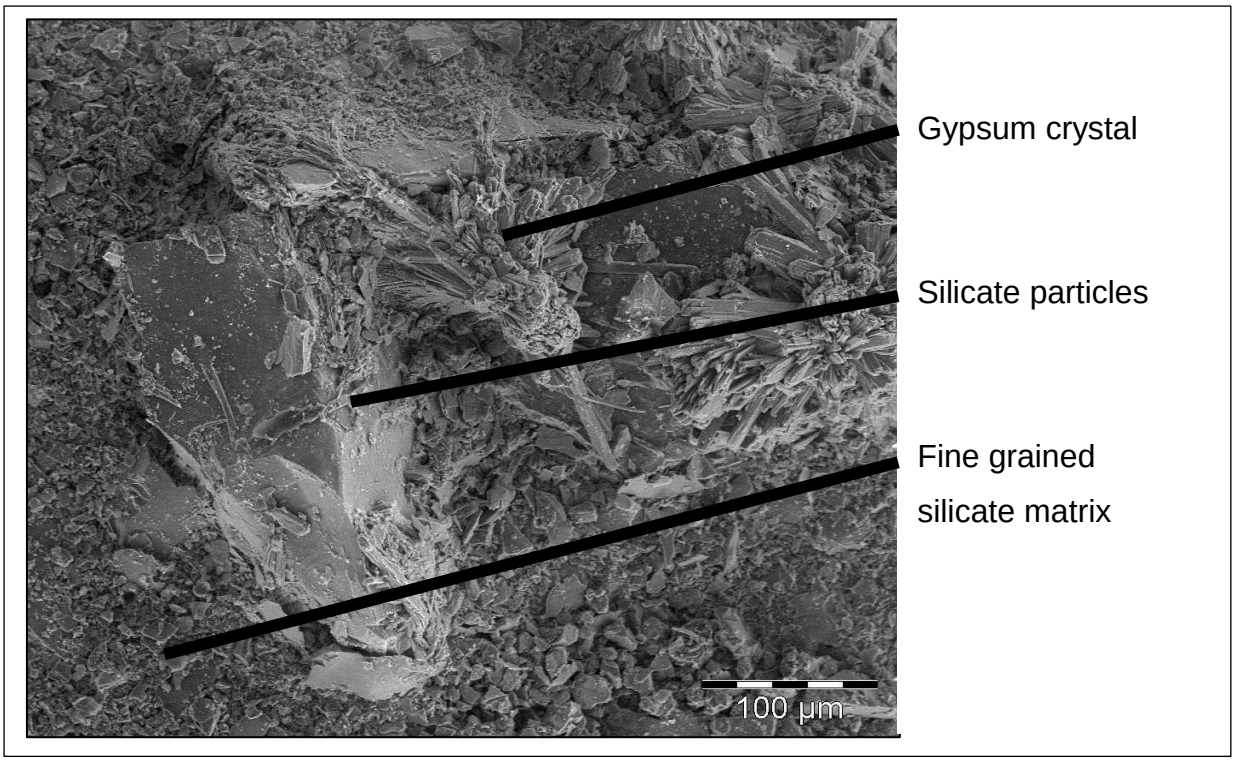

Figure 18: SEM image of the drying crust L1

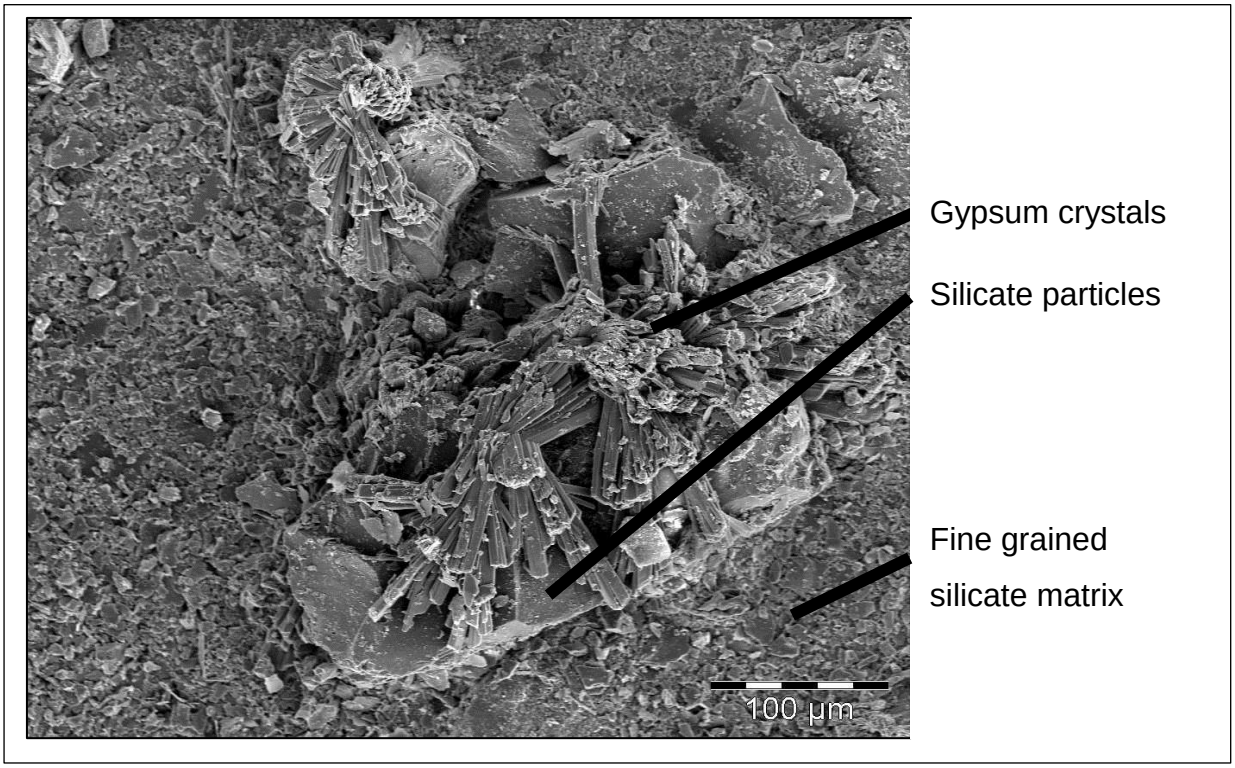

Figure 19: SEM image of the drying crust L1 and inter-particle minerals

The sampling locations coincided with the expected location where these type of crusts would form, namely in low-lying areas. On the Chemwest 5 TSF, the berms and paddocks provided these locations. This environment could have allowed for settling of fine particles and the precipitation of gypsum crystals. After the water drained away, a tailings crust was left behind that was less susceptible to wind erosion due to the horizontal orientation of particles and the inter-particle gypsum bonds (Langston & Mckenna Neuman, 2005:40) and the hydroscopic nature of the material, due to the gypsum content (van Deventer, 2015: personal correspondence).

Table 3: Spectral analysis of the crystals in the sample crust of L1 physical crust (results in weight %)

Spectrum	C	Mg	Al	Si	S	K	Ca	Fe	O	Total
Spectrum L1 (crystal)	7.1		0.7		18.3		19.4		54.6	100

Table 4: Spectral analysis for the sample matrix of the physical crust L1 (results in weight %)

Spectrum	C	Na	Mg	Al	Si	S	Cl	K	Ca	Ti	Mn	Fe	O	Total
L1 Physical crust	3.6	0.4	0.5	7.5	21.2	5.1		2.4	2.9	0.2		4.7	51.6	100

The crystals in the image were chemically analysed using the SEM. The minerals were relatively abundant in Ca, S, C and O, as can be seen in Figure 20. This information indicates that the mineral seen in the crystals is likely gypsum. The mineralogical composition of gypsum is $CaSO_4 \cdot xH_2O$. The following information (Table 3 and Table 4) was obtained regarding the sample matrix and the gypsum crystals (Spectrum L1).

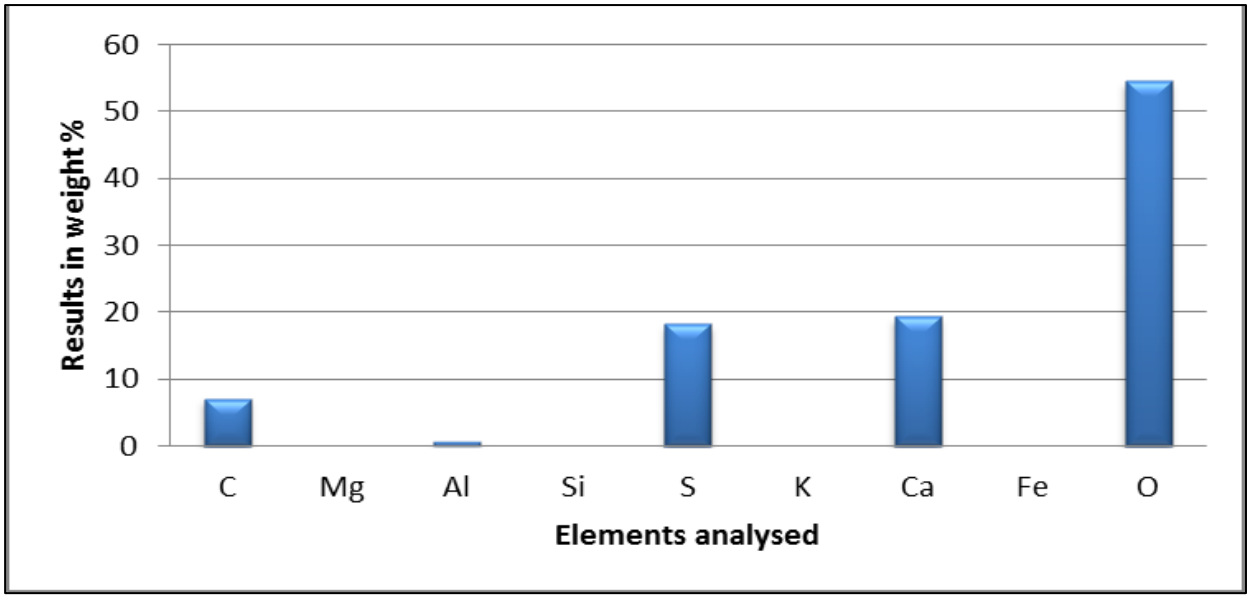

Figure 20: Spectral analysis of minerals found between silicate particles of drying crust L1

4.1.2. Drying physical crust L8 (upper crust)

The second drying crust was investigated in two parts, the first was the top crust and can be seen in Figure 22 and Figure 23 (approximately upper 1 mm) and the second was the underlying material of the crust and can be seen in Figure 25 and Figure 76 and Figure 77 (Annexure 1).

In Figure 21 to Figure 24, it can be seen that the crust is composed of finer material relative to the particles in the physical, drying crust - L1. Gypsum crystals can once again be seen binding larger particles together. The crust matrix is primarily composed of silicate minerals, presumably quartz (see Table 5 and Figure 24).

The horizontal orientation of the fine grain matrix particles are noteworthy since it corresponds well with the description of the so-called “washed-in”/ illuviation layer that is associated with soil crusts.

Table 5: Spectral analysis of the crystals in the sample crust (results in weight %)

Spectrum	C	Mg	Al	Si	S	K	Ca	Fe	O	Total
Spectrum L8 (inter-grown crystal)	5.7		2.7	7.5	14.1	0.4	14	2.1	53.5	100

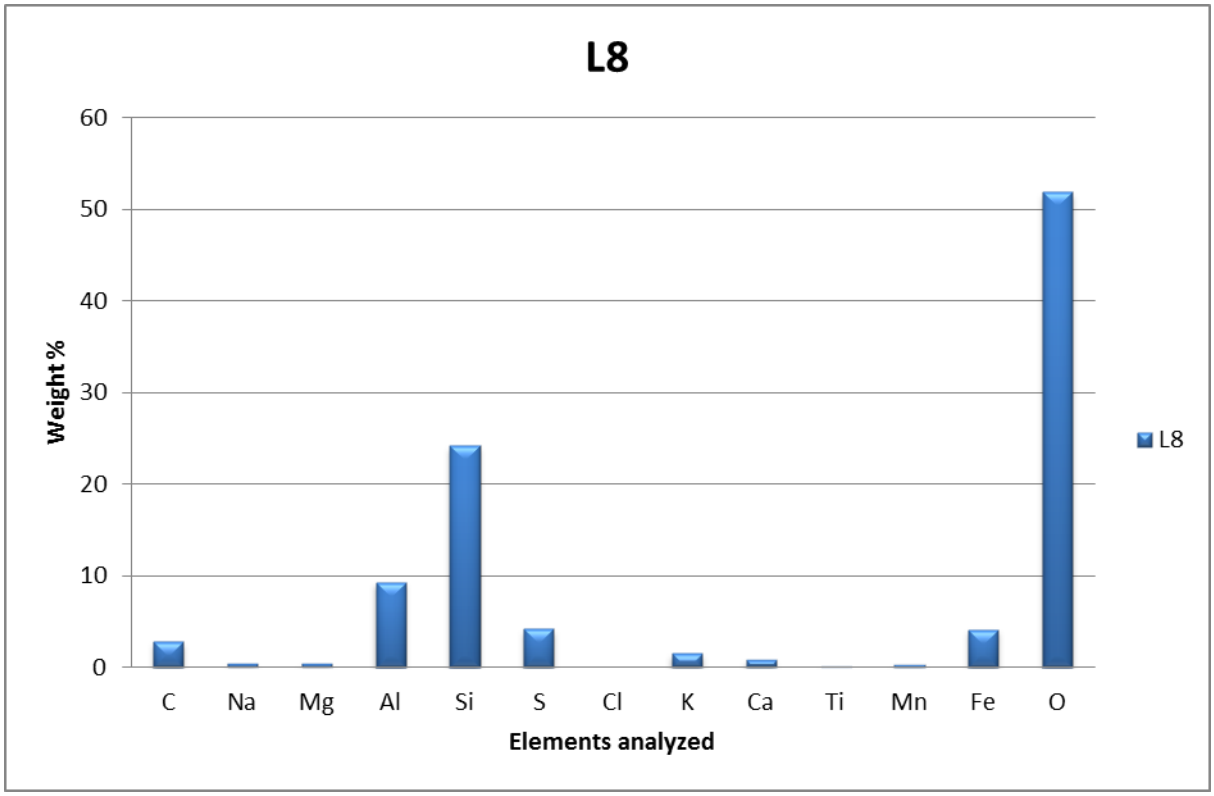

Figure 21: SEM analysis of the L8 drying crust top.

Table 6: Spectral analysis of the matrix material in the sample (results in weight %)

Spectrum	C	Na	Mg	Al	Si	S	K	Ca	Ti	Mn	Fe	O	Total
L8 – Physical crust (top)	2.8	0.4	0.4	9.3	24.2	4.2	1.5	0.8	0.1	0.3	4.1	51.9	100

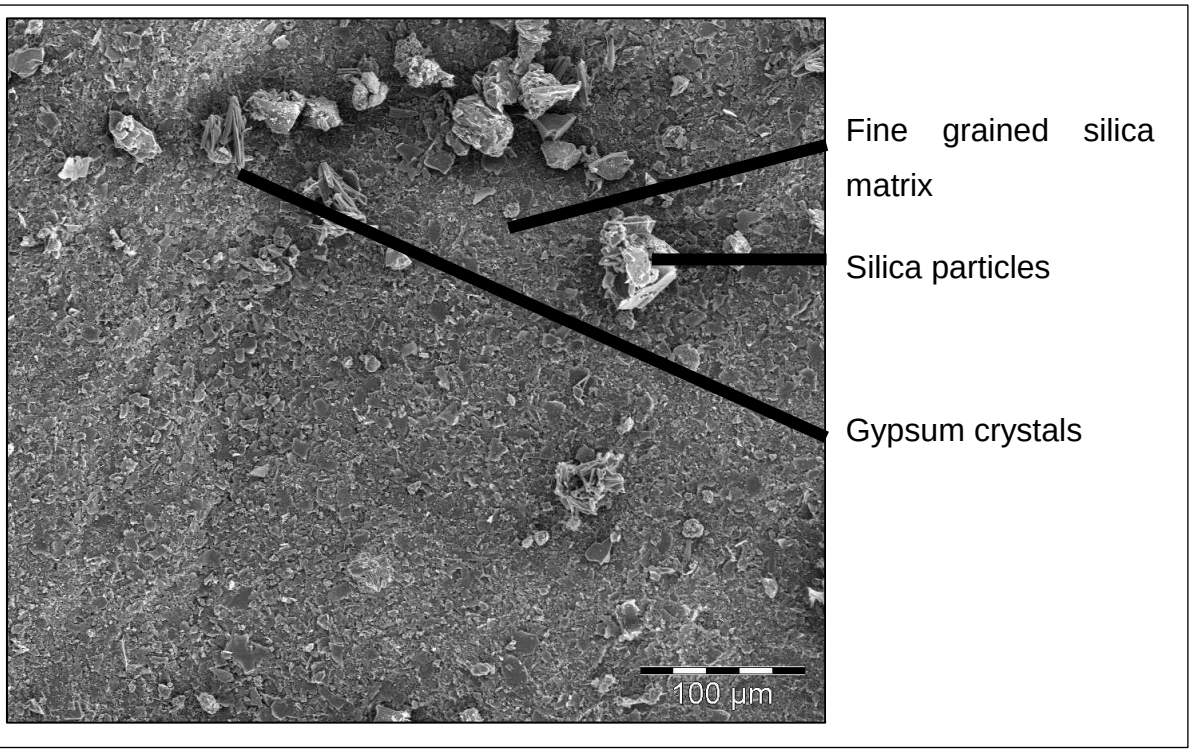

Figure 22: SEM of the drying crust L8 Top (100 µm)

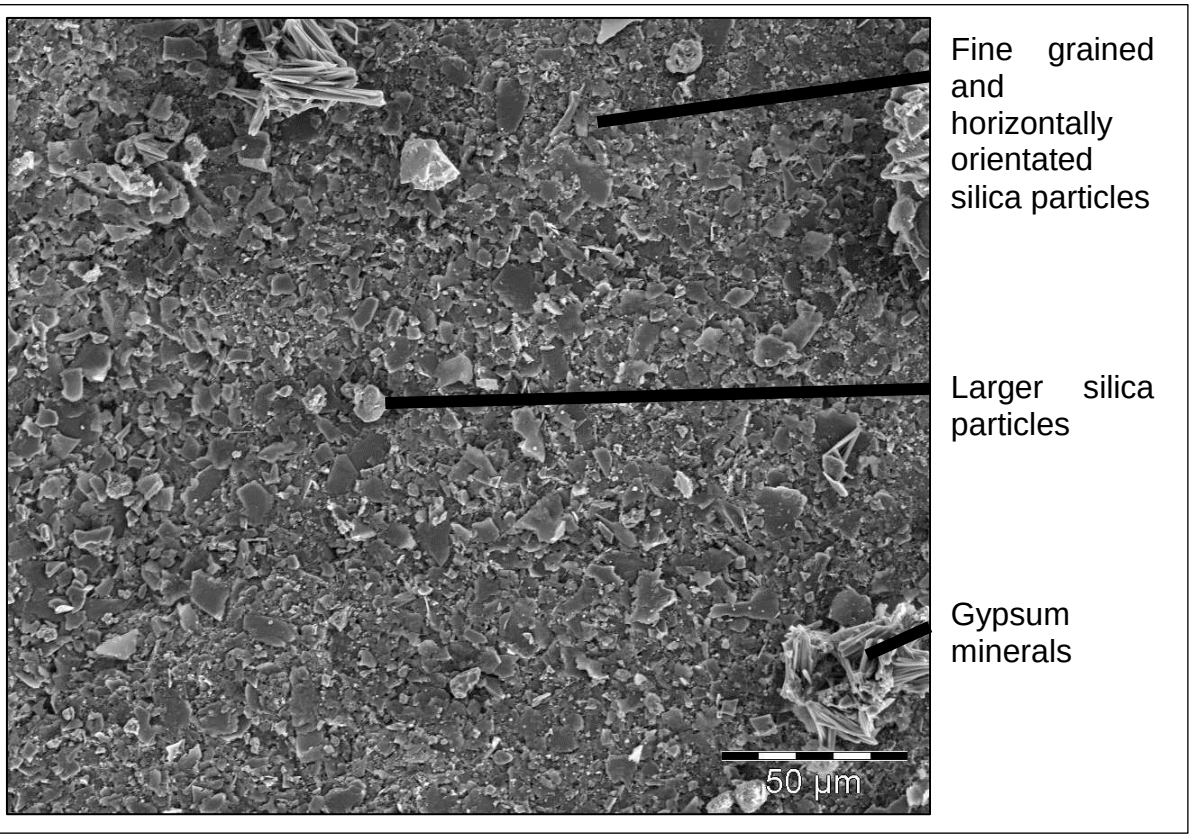

Figure 23: SEM of the drying crust L8 Top (50 µm)

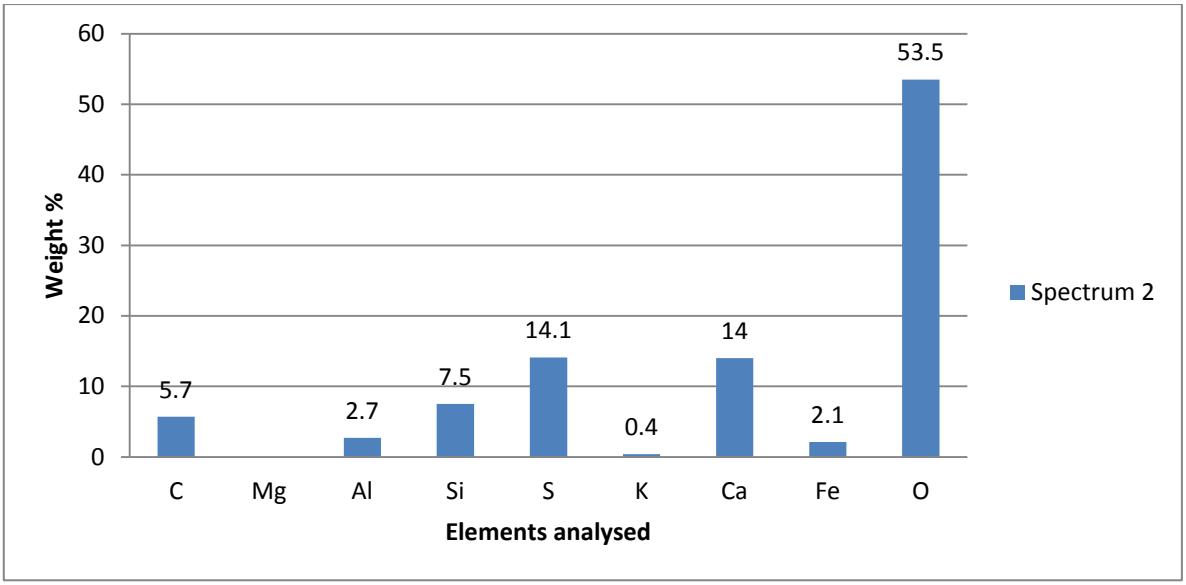

Figure 24: SEM analysis of the crystal chemistry of L8 drying crust.

4.1.3. Drying crust L8 (lower crust)

The L8 Bottom crust was sampled directly below the L8 Top crust. The sampling depth was approximately 1 mm – 2 mm from the surface. From Figure 25 it is evident that the matrix material differs from the top 1 mm of the crust (L8 Top) sample with reference to the particle size and orientation. When comparing Figure 22 and Figure 25, both are 100 µm images, a difference can be seen in the particles that comprise the structures. The lower section of the crust did not appear to have a distinct preferred orientation, as many of the sharp edges of the particles can be seen in the image (which was taken perpendicular to the crust surface).

Table 7: Spectral analysis of the matrix material of the L8 drying crust in the sample (results in weight %)

Spectrum	C	Na	Mg	Al	Si	S	K	Ca	Ti	Mn	Fe	O	Total
L8i – Physical crust (bottom)	1.1	0.1	0.1	3.5	37.5	1.3	0.6	0.5	0.2	0.1	2.7	52.1	100

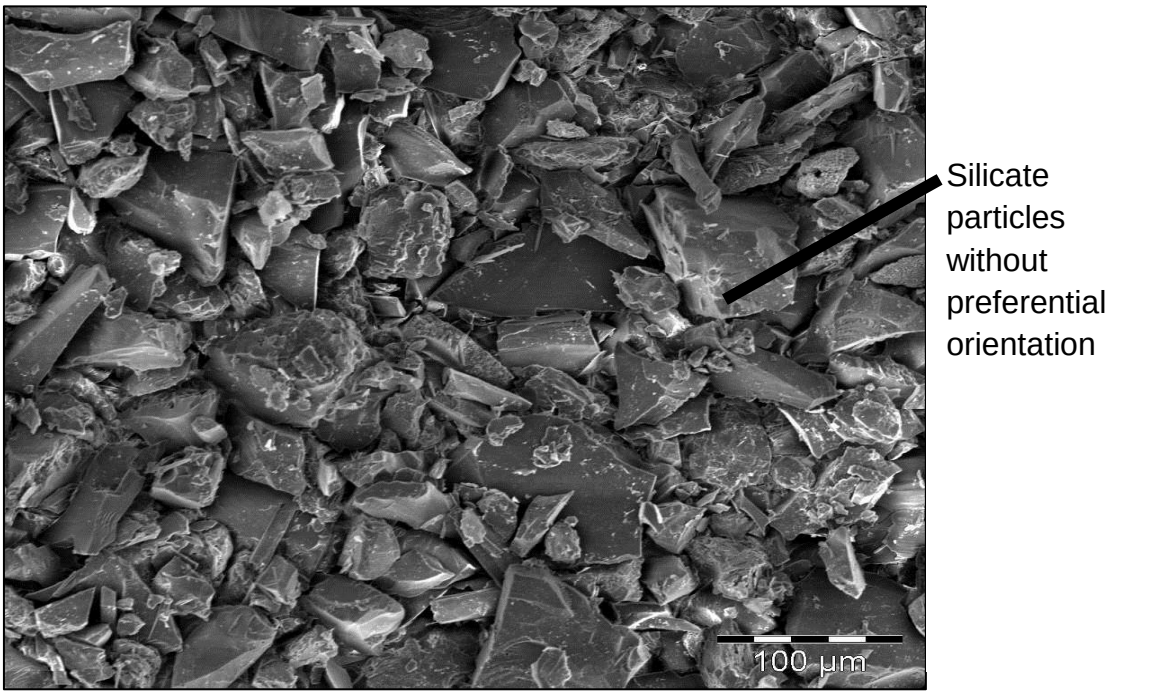

Figure 25: SEM of the drying crust L8 Bottom

4.1.4. Chemical crust (L1C)

Chemical precipitated crust was, as with the other samples, dominated by Si and O (Table 8 and Figure 26). When taking the ore from which the tailings material originated into consideration, one may assume the mineral to be crushed conglomerate, which is dominated by quartzite pebbles in a quarzitic matrix. No clear crystals were observed, as was the case with the drying crusts.

The SEM image shows many different particle sizes present in the crust. No clear orientation preferences of the particles were observed either, as can be seen in Figure 27 and Figure 28. Due to the lack of a binding agent in the form of a precipitated salt, e.g. gypsum, the apparent greater porosity of the sample (with reference to the drying crusts) and the presence of a greater sand fraction, it may be assumed that the chemical crust may be more susceptible to wind erosion.

Table 8: Spectral analysis for the sample matrix of the L1C chemical crust (results in weight %)

Spectrum	Na	Mg	Al	Si	S	Cl	K	Ca	Ti	Mn	Fe	O	Total
L1C – Chemical crust	1	1.6	4.9	32.6	3.7	0.5	1.8	0.2	0.2	1	2.6	50	100

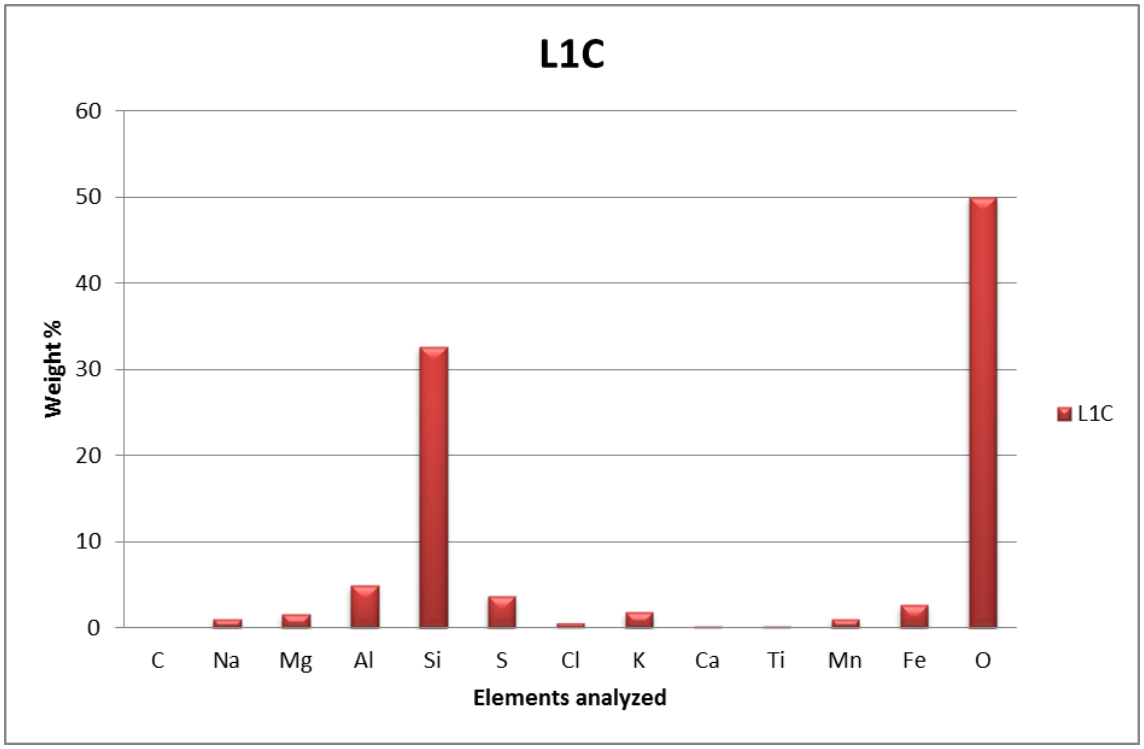

Figure 26: Spectral analysis of the chemical crust.

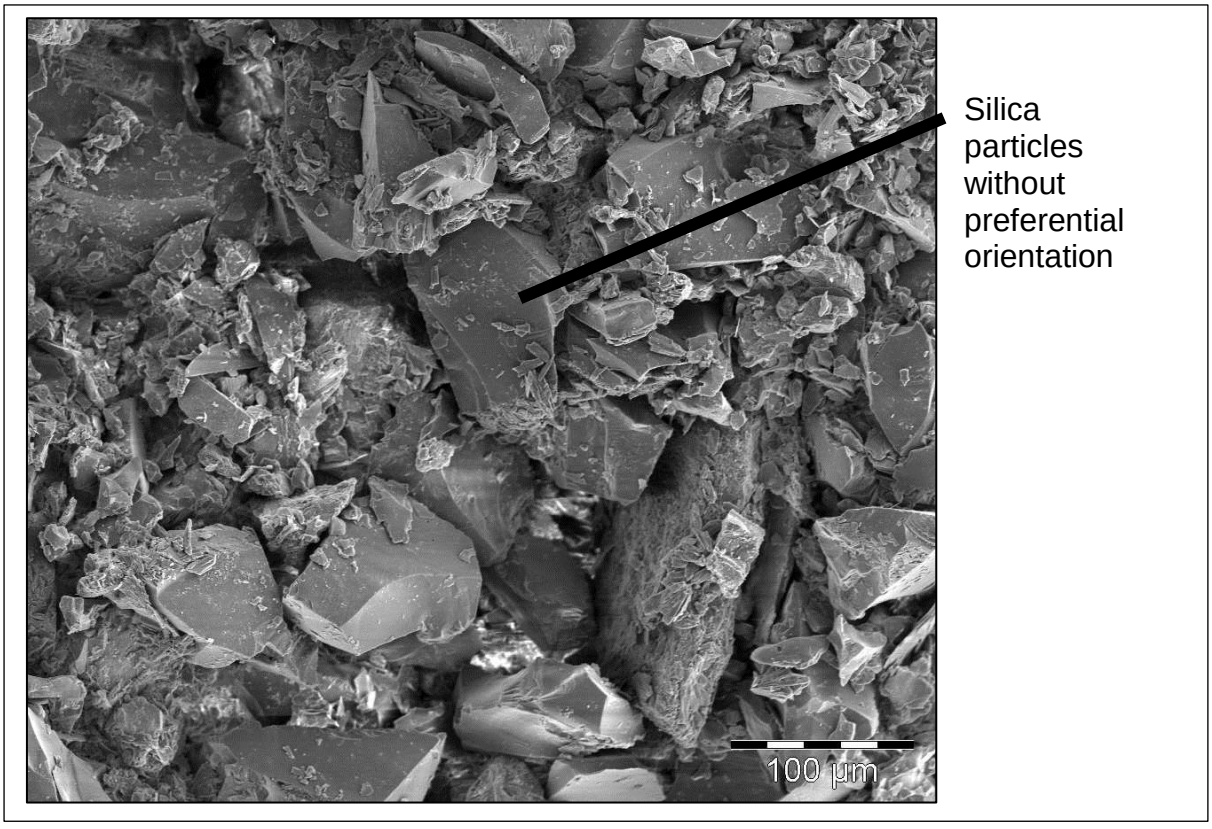

Figure 27: SEM of the chemical crust L1C

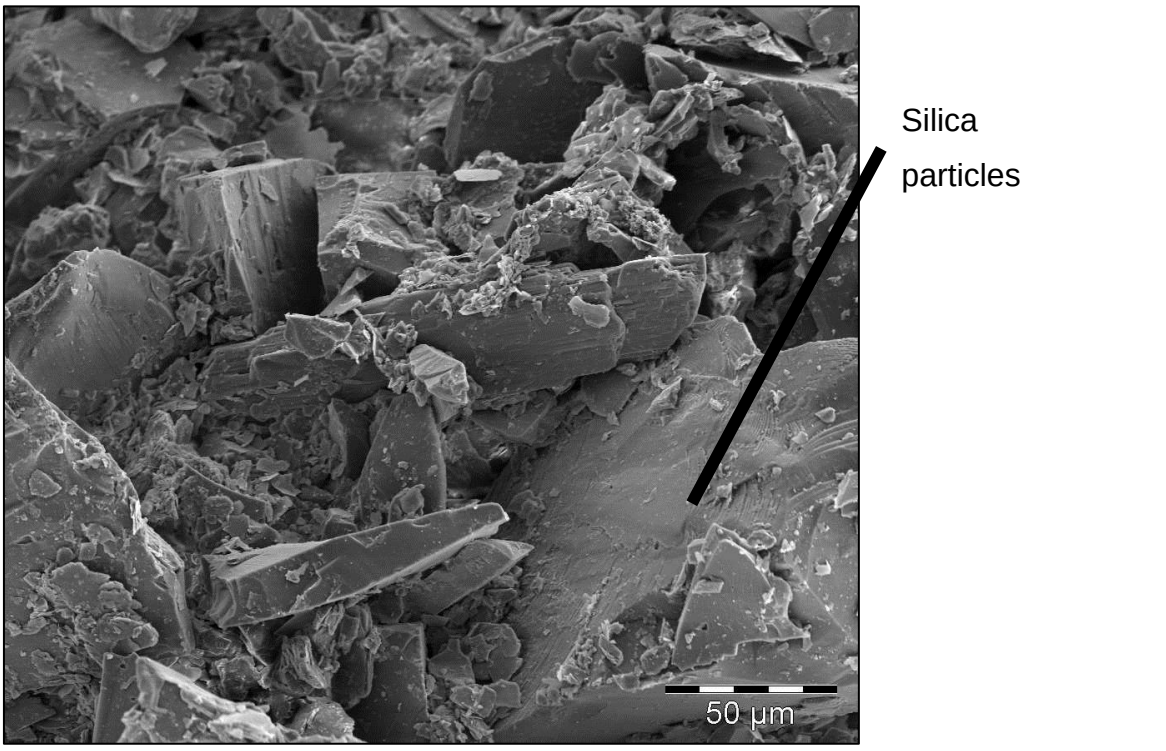

Figure 28: SEM of the chemical crust L1C

4.1.5. SEM of the physical erosion crust (L2)

The erosion crust was sampled on a crest of the top slope, on the north-east corner of the TSF (see Figure 14). The area was exposed to the wind and rain as there was no grass or other surface cover. From the SEM image (Figure 29 and Figure 30) it can be seen that the fine fraction serves as matrix to the larger particles that form the crust. In contrast to the drying crusts, the finer particles have no preferred orientation. This contradicts the possibility of a washed-in/illuviation layer that formed the specific crust. The illuviation was also more prominent in the basins and not on the crests. Additional images of this crust structure are displayed in Annexure 1 in Figure 81, Figure 82 and Figure 85.

The SEM analysis Table 9 and Table 10 of the elements present shows Si and O as being the most abundant. Figure 31 displays the spectral analysis of the matric material of the crust. This may once again point to quartz as being the major mineral element of which the erosion crust is composed.

Table 9: Spectral analysis of the crystal structures found in the physical/erosion crust (L2).

Spectrum	C	Mg	Al	Si	S	K	Ca	Fe	O	Total
Spectrum L2 (crystal)		0.3	3	40.7	1.5	0.7		1.7	52.1	100

Table 10: Spectral analysis for the sample matrix of the L2 physical crust (results in weight %)

Spectrum	C	Na	Mg	Al	Si	S	K	Ca	Ti	Fe	O	Total
L2 Physical crust	1	0.2	0.4	6.5	33.3	0.7	2.5	0.8	0.1	4.2	50.1	100

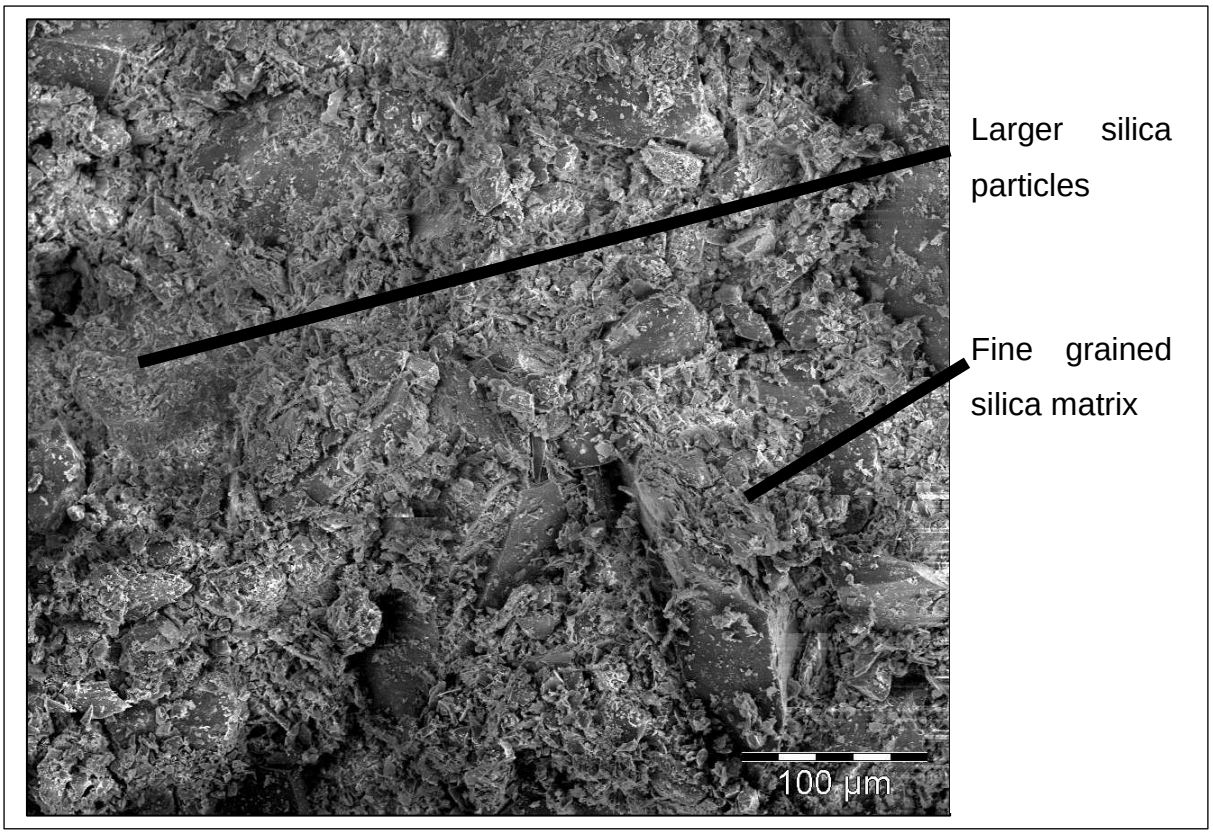

Figure 29: SEM of the erosion crust L2

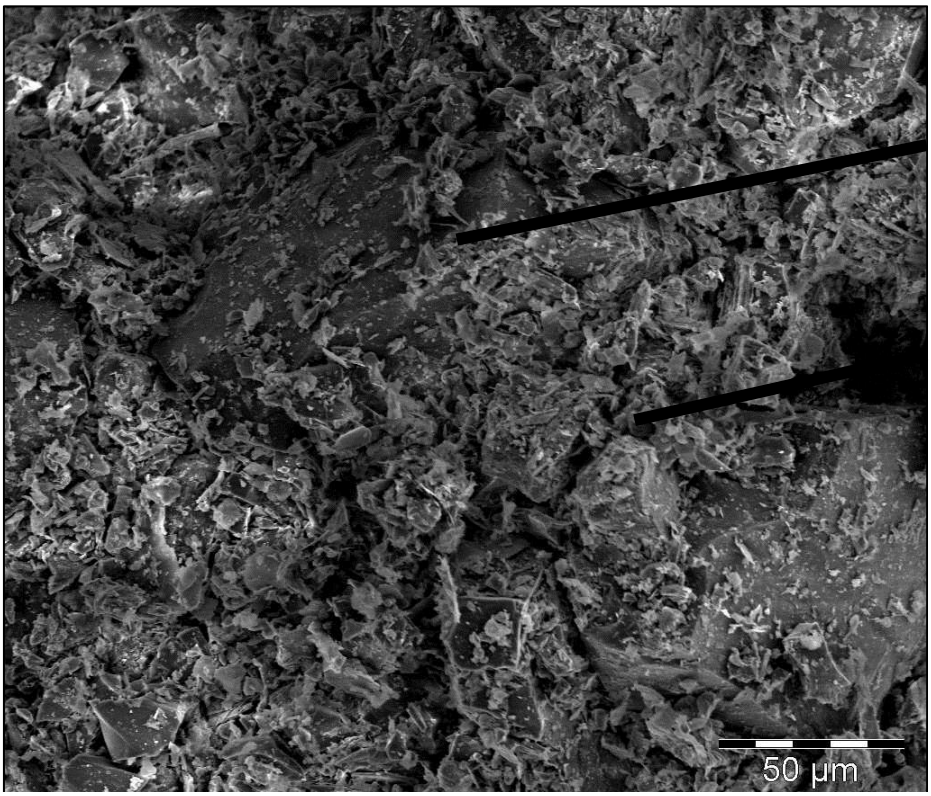

Figure 30: SEM of the erosion crust L2

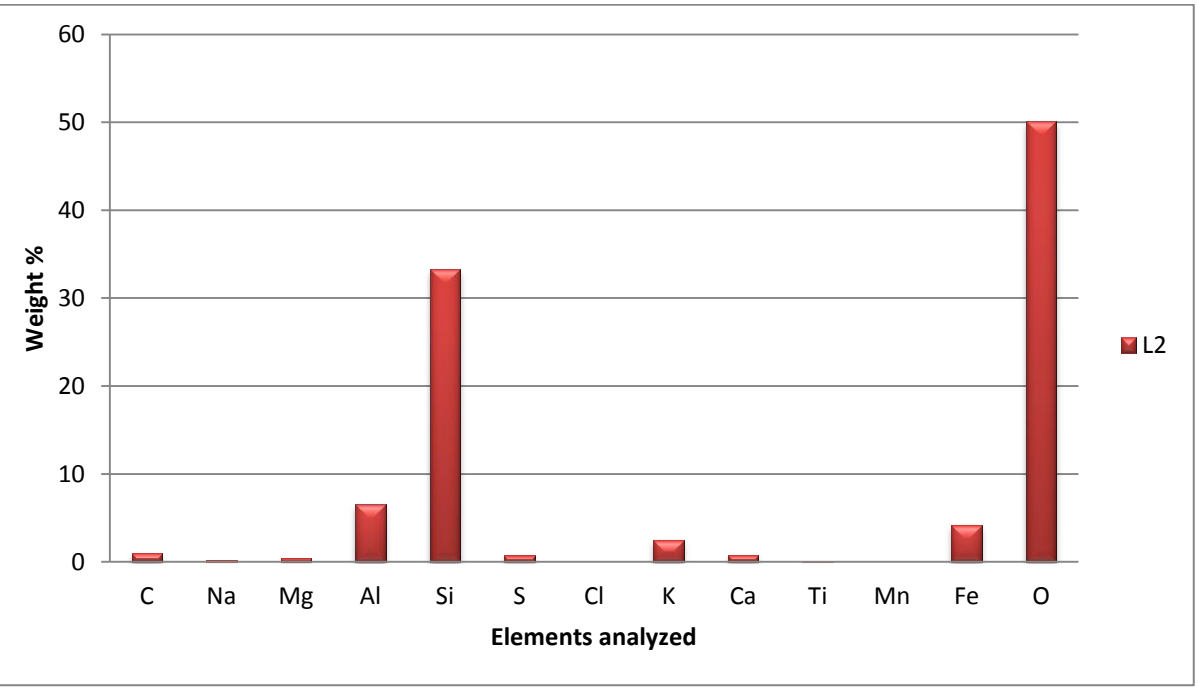

Figure 31: SEM analysis of the erosion crust (L2) chemical composition.

4.1.6. SEM of loose dune sand

The SEM image shown in Figure 32 illustrates the particles from dune sand sampled from a location approximately 20 km from Port Nolloth. The sandy dune was un-crusted and shows contrast to the crusted material that was shown in L1, L8, L1C and L2. The dune sand provides a standard from which to estimate wind erodibility of the material, as dune sand is known to be susceptible to wind erosion, whilst the crusts are expected to offer significant resistance to the action of wind.

In Figure 32 there is an absence of a sharp angled matrix material (as was evident in all the crust material analysed). There is also a lack of visible binding agents (gypsum intergrowths and interlocking particles), as was seen in the drying crusts, erosional crust and chemical crusts.

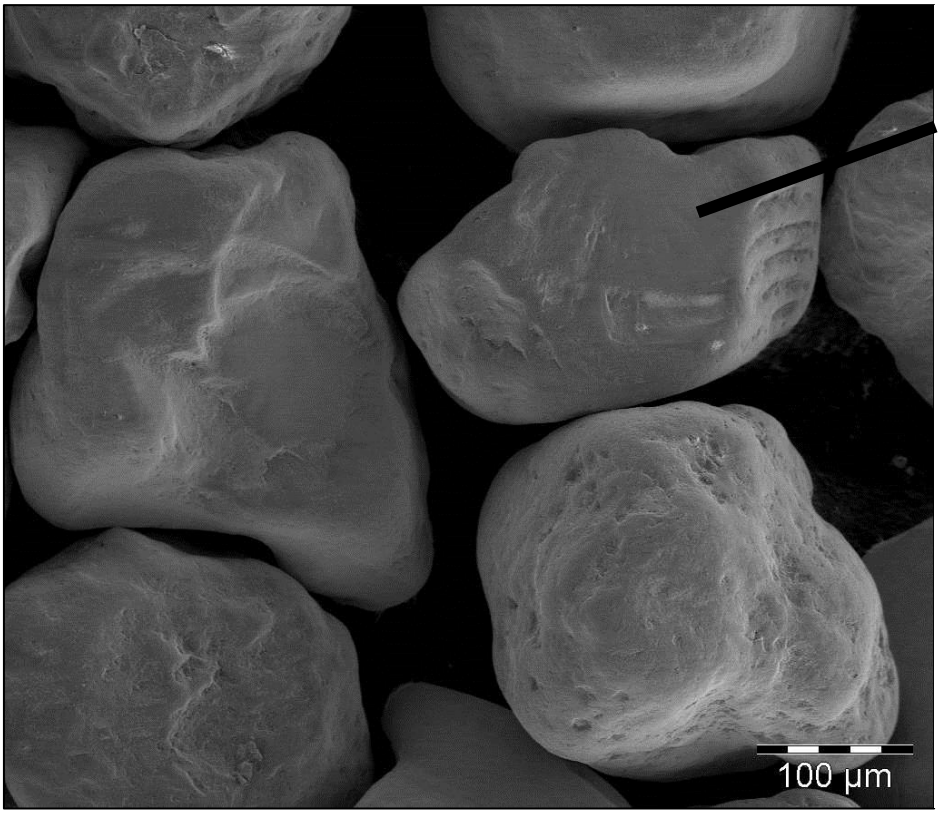

Figure 32: SEM image of loose dune sand.

4.1.7. Conclusion on the SEM analyses of the different crust structures found on the Chemwest 5 TSF.

This section of the research investigated the different types of crusts that were identified on the Chemwest 5 TSF by means of SEM analysis. The matrix material was investigated for distinct particle orientation, interlocking particles, inter-particle minerals that bind the material and the elemental composition of the crust material.

Three different types of crusts were identified, namely a physical drying crust, a chemical crust and a crust believed to have originated from the action of wind and water.

These results found that the matrix material was dominated by quartz (which corresponds to the mined conglomerate reef from which the material originated). A difference between the particle orientations was observed between the different types of crusts. The drying crusts (L1 and L8 Top) had a horizontal orientation (along the long axis), whilst the chemical and erosion induced crusts did not exhibit preferential orientation. This likely indicates that the particles interlock, which should increase the resistance of the crust to abrasion by wind. Future studies could confirm this hypothesis but was beyond the scope of this research to quantify.

Drying crusts also exhibited a feature that was largely absent from the other crusts, which is well-developed gypsum crystals (Figure 25). Since these crusts were observed in low-lying areas, it is likely that water accumulation in those areas resulted in the precipitation of gypsum and the resultant crystal growth. It is therefore possible that the gypsum precipitate contributes to stabilising the crust and increasing resistance to wind shear. During wet conditions the gypsum could go into solution and leach from the system, leaving the crust vulnerable when dry. This assumption could also be validated in future studies.

4.2. Wind tunnel results

The following sub-section provides the data obtained from the wind tunnel study as well as the interpretation of the data.

4.2.1. Results and discussion of the minimum wind speed threshold velocity (u_t) tests

Wind tunnel tests were performed in order to understand the relative susceptibility of different zones on the TSF to wind erosion. The data was also used to identify days on which the wind speed could potentially have cause TSF particles to become liberated from the particle bed.

This wind speed value was calculated by using erosion data from a wind tunnel. Three samples were taken for this research from the slopes of the TSF. One sample was extracted on each of the slopes 2, 3 and 4 on the eastern side of the facility. Each sample was extracted to a depth of approximately 200 mm.

Table 11 summarises the results from the wind tunnel test for the different samples and wind speeds.

Table 11: Wind tunnel data (u_t) for Chemwest 5 slopes

Chemwest slope 2						
WS	Percent mass loss					
(m/s)	S 1	S 2	S 3	S 4	S5	$\bar{x}$
3	0.12	0.08	0.08	0.12	0.04	0.09
3.5	0.25	0.28	0.28	0.25	0.27	0.27
Chemwest slope 3						
WS	Percent mass loss					
(m/s)	S 1	S 2	S 3	S 4	S5	$\bar{x}$
3	0.05	0.1	0.07	0.13	0.1	0.09
3.5	0.18	0.22	0.2	0.13	0.2	0.19
Chemwest slope 4						
WS	Percent mass loss					
(m/s)	S 1	S 2	S 3	S 4	S5	$\bar{x}$
3	0.1	0.06	0.06	0.05	0.03	0.06
3.5	0.24	0.18	0.2	0.21	0.23	0.21

Note: WS – Wind speed
S – Sample

Table 12: Minimum wind speed threshold velocity (u_t)– Value for the different slopes.

Slope	u_t – Value
2	3.0 $m.s^{-1}$
3	3.0 $m.s^{-1}$
4	3.1 $m.s^{-1}$
Average	**3.0 $m.s^{-1}$**

Results represented in Table 12 are the measured wind speed that was required to erode 0.1% of the sample in the wind tunnel. Since the experiment was designed to measure the u_t – value at dry, un-crusted and laminar flow conditions, the measured mass loss cannot be extrapolated to all TSFs. However, the mass loss measured is believed to be small enough to be representative of the wind speed threshold values, since the extrapolated mass loss represented one-thousandth of the sample mass.

Minimum wind speed threshold velocity values should be considered a minimum value. This is due to the ideal conditions for wind erosion that were created in the

wind tunnel. In reality, as was illustrated in Section 4.1, some of the TSF surface was covered in different types crusts. This would probably decrease the erodibility of the tailings substrate, but must be confirmed in future studies.

4.2.2. Conclusion on the wind tunnel study to determine the u_t value of the Chemwest 5 slope tailings material

Results found that for dry, structureless and unconsolidated tailings material, the minimum wind speed threshold velocity ranges between 3.0 $m.s^{-1}$ and 3.1 $m.s^{-1}$. Figure 33 illustrates the percentage of the time (during 18 October 2014 to 18 October 2015) the wind speed exceeded the estimated wind speed threshold velocity of the tailings material. Potential erosive events therefore took place 41.5% of the time during the research period.

The implication of the results is therefore that wind erosion of the Chemwest 5 tailings material can initiate from wind speeds as low as 3.0 $m.s^{-1}$. With the onset of particle motion, more particles can become eroded due to the saltation process, causing dust to form.

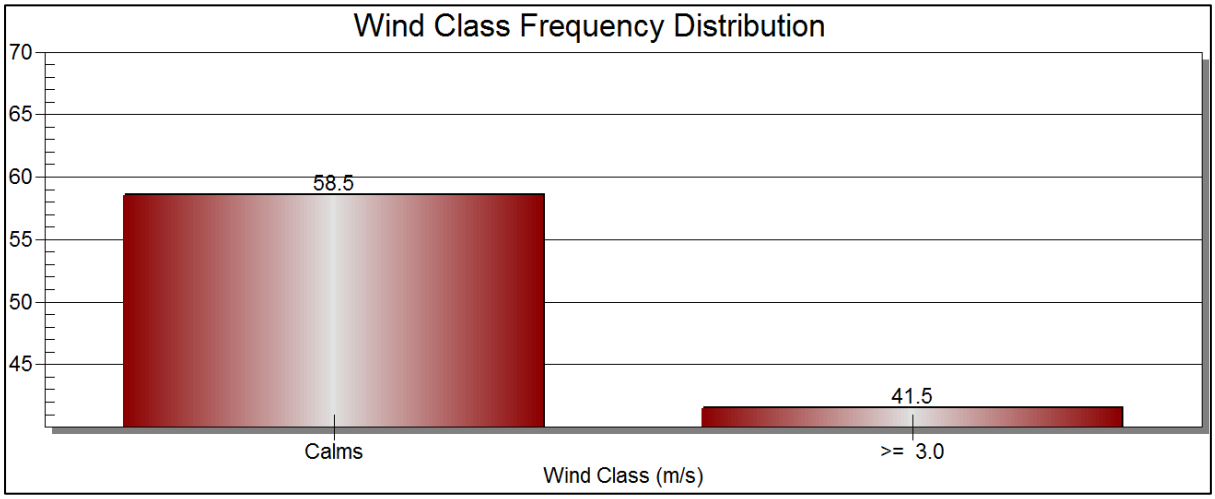

Figure 33: Percentage of time the average wind speed of the reference WMU exceeded the average u_t – value of the tailings material.

When the results of the wind tunnel study are applied to the concept of wind speed amplification on TSFs and like structures, then the critical elevation on the TSF can be calculated where erosion could take place from a wind speed that would have not have been erosive.

Calculating the actual u_t – value of the tailings material will require additional variables in the wind tunnel experiments. Isolating and measuring the effects of grain density, fluid (air) density and grain diameter, particle to air density ration, Reynolds Number, crust structures, organic carbon, surface roughness, surface moisture variability and surface cover, could yield the actual u_t – value of the tailings material. Individual contribution of each factor could also be determined and used for emission modelling (quantifying these factors are beyond the scope of this research project).

4.3. Results of the wind dynamics monitoring on the TSF

In order to quantify the wind movement over the Chemwest 5 TSF, 12 wind-monitoring stations were erected on the facility. Wind monitoring units were placed at representative locations around the TSF. Locations of these units are shown in Figure 16 and is repeated on the following page in Figure 34.

Datasets were obtained for the period of 18 October 2014 to 18 August 2015. During this period of time the average and maximum wind speed, wind direction, relative humidity and air temperature were monitored for each of the stations. The data were logged every 15 minutes and is the result of the average and maximum values of five-second scans. It must be noted that during this time some of the WMUs were damaged by wildlife, lighting and theft. Very little wind data was lost but with some of the WMUs the air temperature and relative humidity measurements were lost. Due to the number of data points (approximately 3,888,000 data entries), the raw data is not presented in this report, but rather summarised in figures and tables.

A summary of conditions encountered at each of the WMUs are given in Table 18 to Table 29. WMU 12 was used as the control. This station was mounted on a 10 m high mast and away from local wind disturbances (Figure 16). The conditions varied between the control point and the other monitoring stations. The highest wind speed was at WMU 5 and was measured at 34.6 $m.s^{-1}$ or 124.6 $km.h^{-1}$, whilst the maximum wind speed of the control was only 24.4 $m.s^{-1}$ or 87.8 $km.h^{-1}$. Additional descriptive statistics for the different WMUs can be found in Annexure 2 in Table 18 to Table 29.

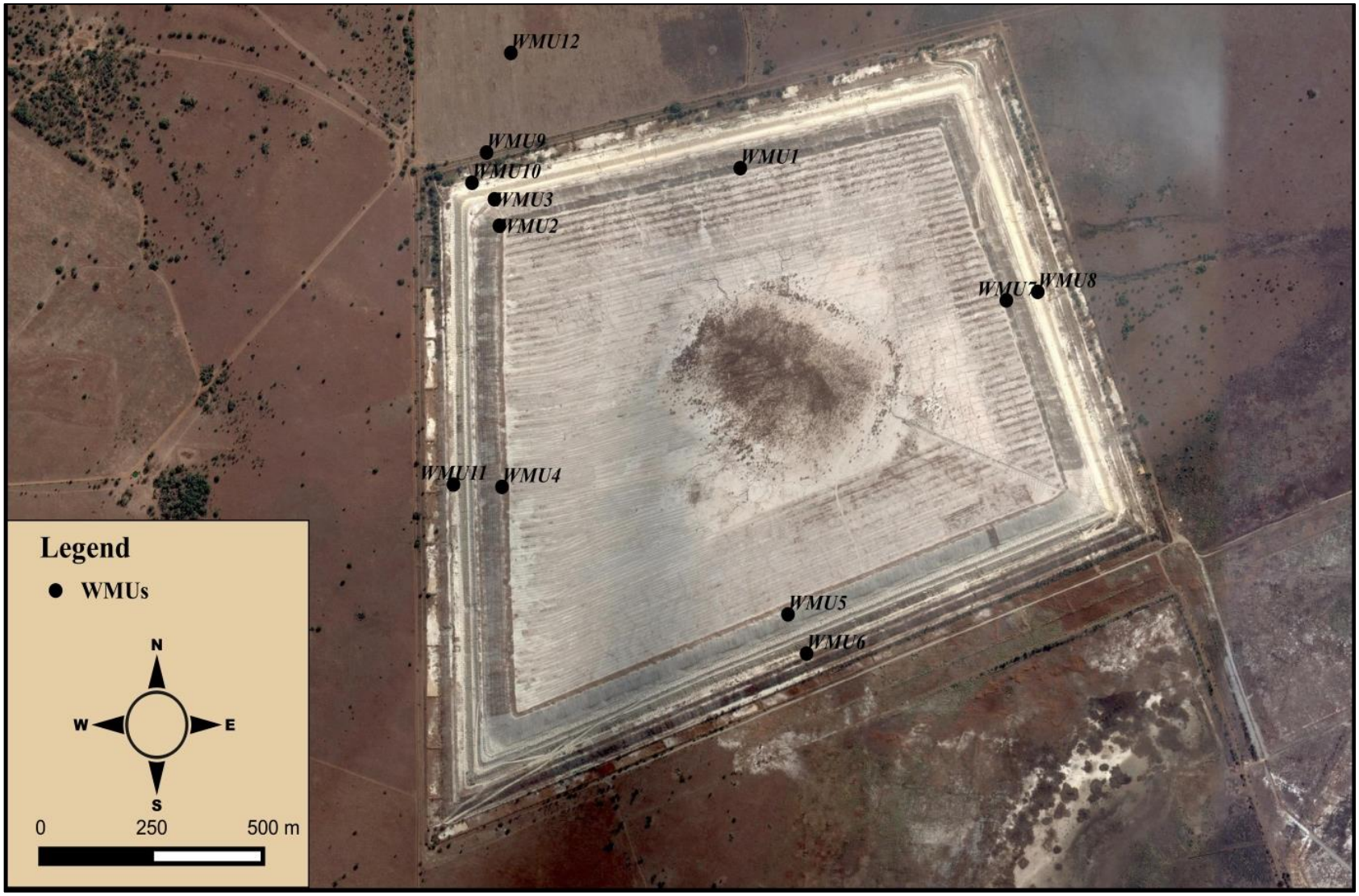

Figure 34: Placement of the WMUs on the Chemwest 5 TSF

4.3.1. Wind profile for WMU 12 (reference site)

Figure 35 illustrates the wind rose for WMU 12, which was also the reference site. The data from the monitoring unit indicated that the dominant wind direction was from the N, with a secondary component ranging from northeast to east.

Wind speed at this station was measured at an average value of 2.9 $m.s^{-1}$ and experienced a maximum wind speed of 14.2 $m.s^{-1}$. Wind speeds that could possibly be erosive were recorded 41.5% of the time during the research period (Figure 33).

This figure indicates that primarily the N slope, followed by the E and W slopes, was likely to experience the greatest amount of wind erosion.

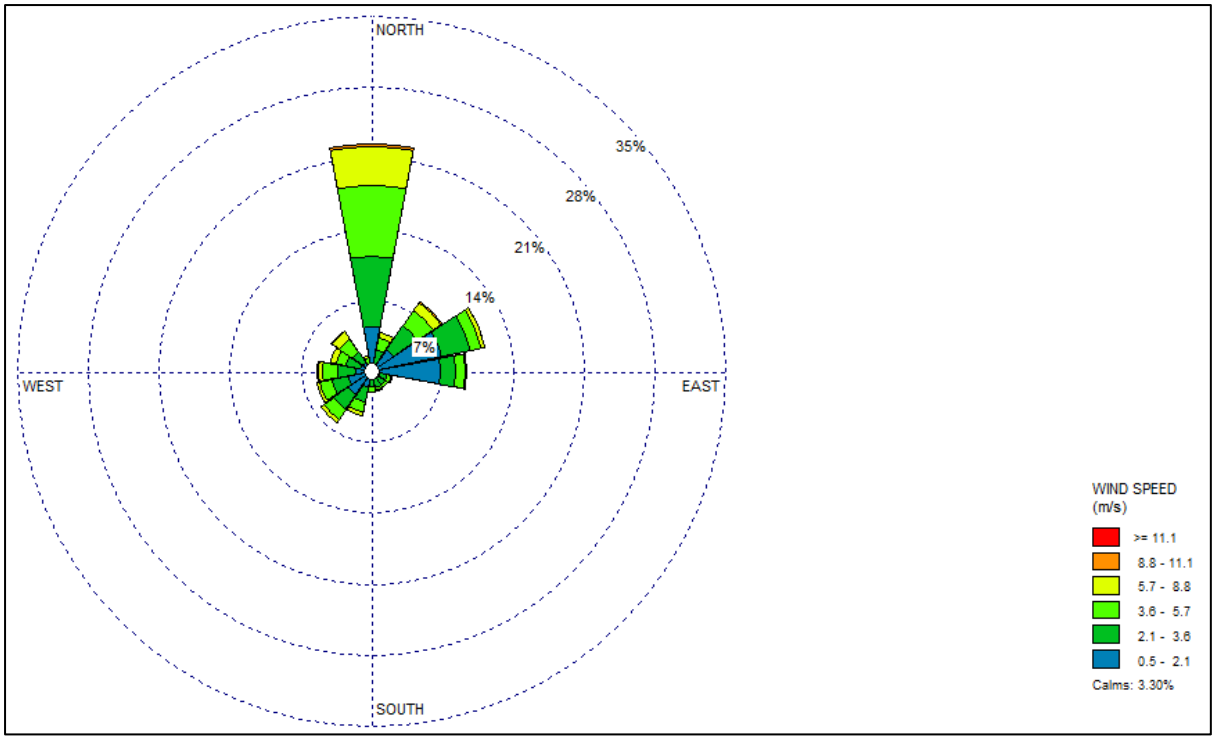

Figure 35: Wind rose for WMU 12 for the period 18 October 2014 to 18 August 2015.

4.3.2. Wind profile for WMU 1

Figure 36 is a wind rose of the measured wind velocity profile that was measured by WMU 1 during the research period. This WMU was located on the north facing crest of the facility at an elevation of 1399 m above mean sea level or 35 m above the ground surface.

The wind direction of this monitoring station was dominantly from the north, with subordinate directions from the north-northeast, northwest and south. These wind directions all exhibited speeds in excess of 3 $m.s^{-1}$, which would have resulted in wind erosion taking place.

Figure 37 illustrates that the frequency with which the u_t – value of the tailings material was exceeded. The graph shows that the value was exceeded 61.7% of the time during the research period (Figure 37). This value is greater than that of the reference WMU and indicates that the area in which this WMU is located is a higher risk zone for wind erosion.

The average wind speed measured at WMU 1 was 3.5 $m.s^{-1}$, as opposed to 2.9 $m.s^{-1}$ measured at WMU 12. The average wind speed amplification factor was therefore 1.2, with a 25 m elevation difference between these WMUs.

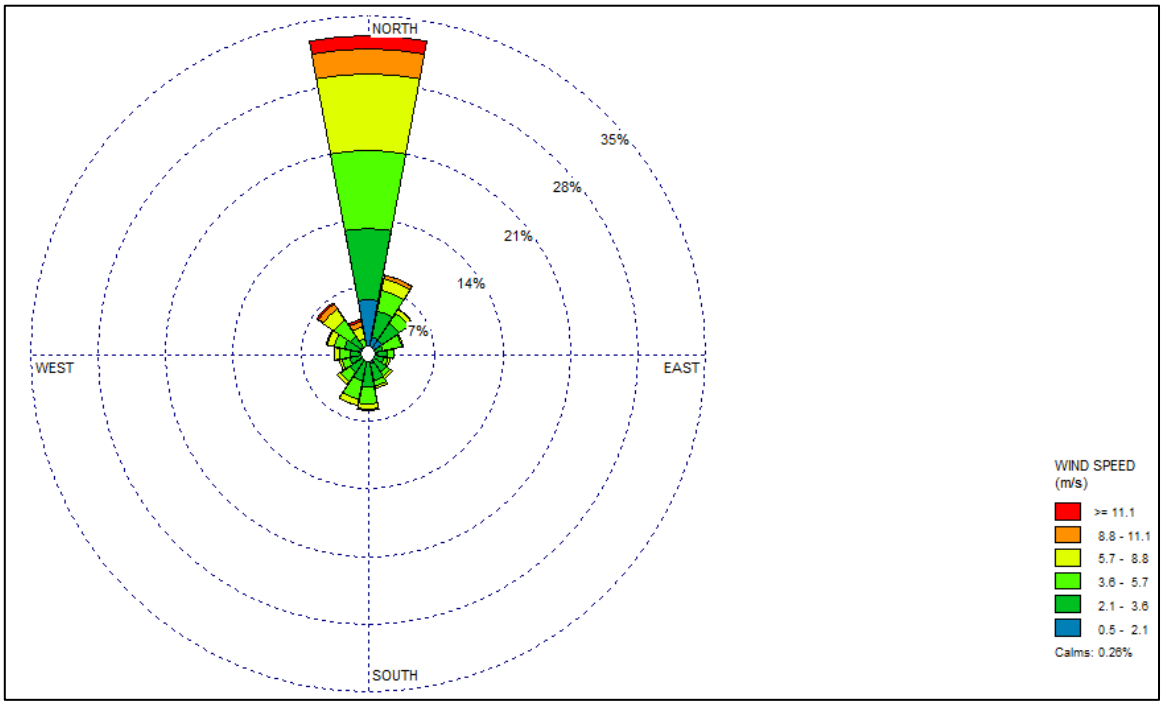

Figure 36: Wind rose for WMU 1 for the period 18 October 2014 to 18 August 2015.

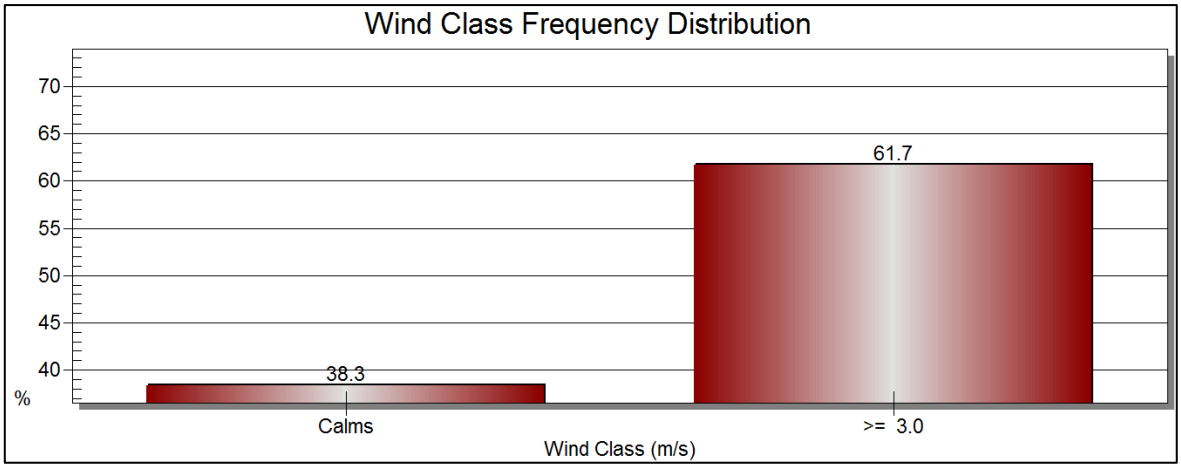

Figure 37: Frequency with which the average wind speed exceeded the tailings material's u_t value for WMU 1.

4.3.3. Wind profile for WMU 2

Figure 38 is a wind rose of the measured wind velocity profile that was measured by WMU 2 during the research period. This WMU was located on the corner of the NW crest of the facility at an elevation of 1397 m above mean sea level or 32 m above the ground surface.

The wind direction of this monitoring station was dominantly from the east-northeast, with the greatest component of the wind direction from the north to east quadrant. These wind directions all exhibited speeds in excess of 3 $m.s^{-1}$, which would have resulted in wind erosion taking place. The wind directions measured for this WMU did not exhibit a distinct wind direction profile, as with WMU 1. A possible cause for this is that the corner on which WMU 2 was located caused redirection of the incoming air, resulting in the abnormal direction distribution.

Figure 39 illustrates the frequency with which the u_t – value of the tailings material was exceeded. The graph shows that the value was exceeded 69.7% of the time during the research period (Figure 39). This value is greater than that of the reference WMU and indicates that the area in which this WMU is located is a higher risk zone for wind erosion.

The average wind speed measured at WMU 2 was 4.3 $m.s^{-1}$, as opposed to 2.9 $m.s^{-1}$ measured at WMU 12. The average wind speed amplification factor was therefore 1.5, with a 22 m elevation difference between these WMUs

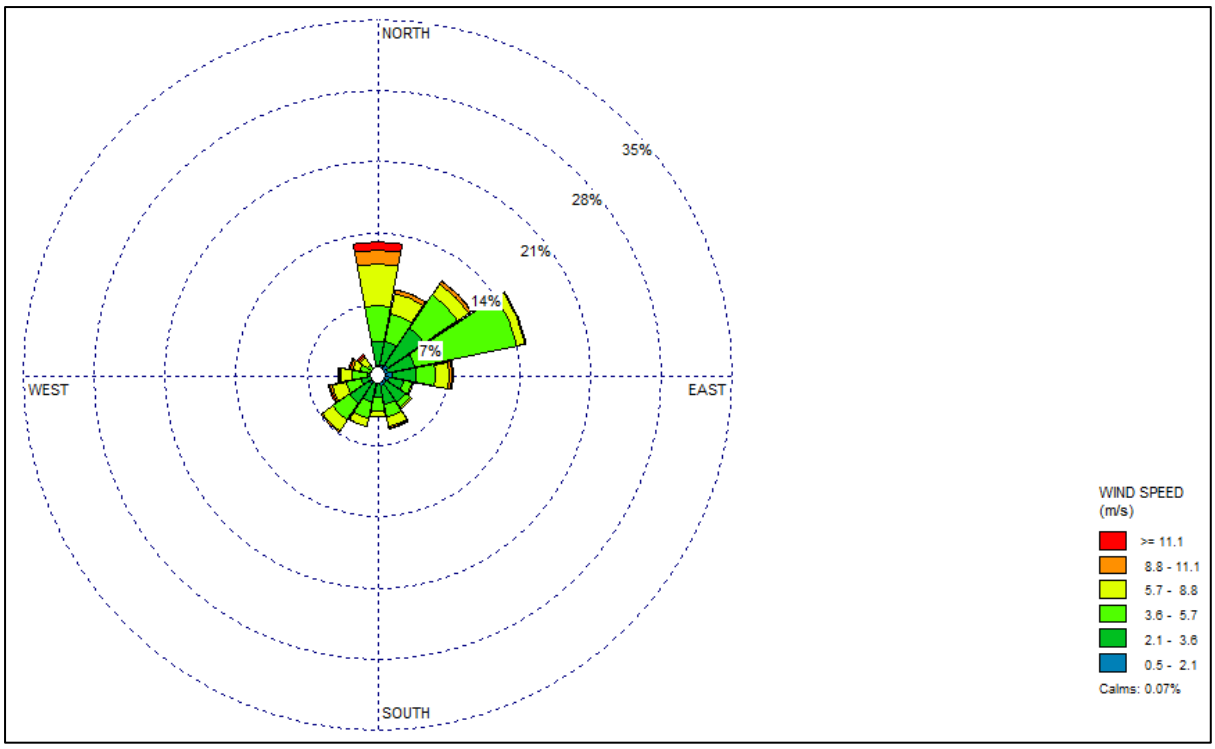

Figure 38: Wind rose for WMU 2 for the period 18 October 2014 to 18 August 2015.

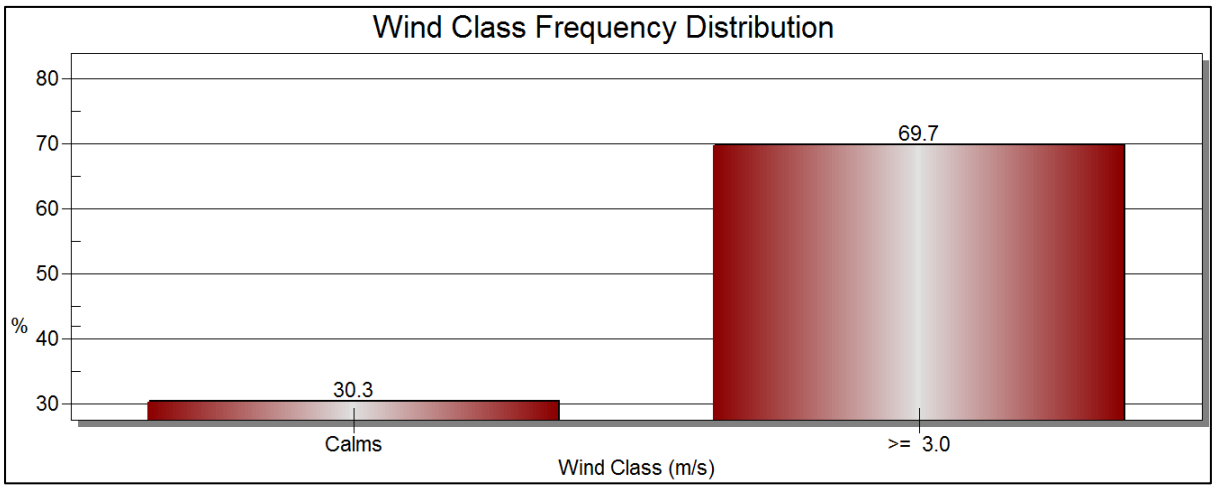

Figure 39: Frequency with which the average wind speed exceeded the tailings material's u_t value for WMU 2.

4.3.4. Wind profile for WMU 3

Figure 40 is a wind rose of the measured wind velocity profile that was measured by WMU 3 during the research period. This WMU was located near the northwest corner of the second bench from the bottom of the facility at an elevation of 1379 m above mean sea level or 14 m above the ground surface.

The wind direction of this monitoring station was dominantly from the east-northeast, with the greatest component of the wind direction from the north to east quadrant. These wind directions all exhibited speeds in excess of 3 m.s^{-1}, which would have resulted in wind erosion taking place. The wind directions measured for this WMU did not exhibit a distinct wind direction profile, as with WMU 1. A possible cause for this is that the corner on which WMU 2 was located caused redirection of the incoming air, resulting in the abnormal direction distribution.

Figure 41 illustrates the frequency with which the u_t – value of the tailings material was exceeded. The graph shows that the value was exceeded 43.3% of the time during the research period (Figure 41). This value is less than that of the reference WMU 12 and indicates that the area in which this WMU is located is a lower risk zone for wind erosion.

The average wind speed measured at WMU 3 was 3.0 m.s^{-1}, as opposed to 2.9 m.s^{-1} measured at WMU 12. The average wind speed amplification factor was therefore 1.0, with a 4 m elevation difference between these WMUs

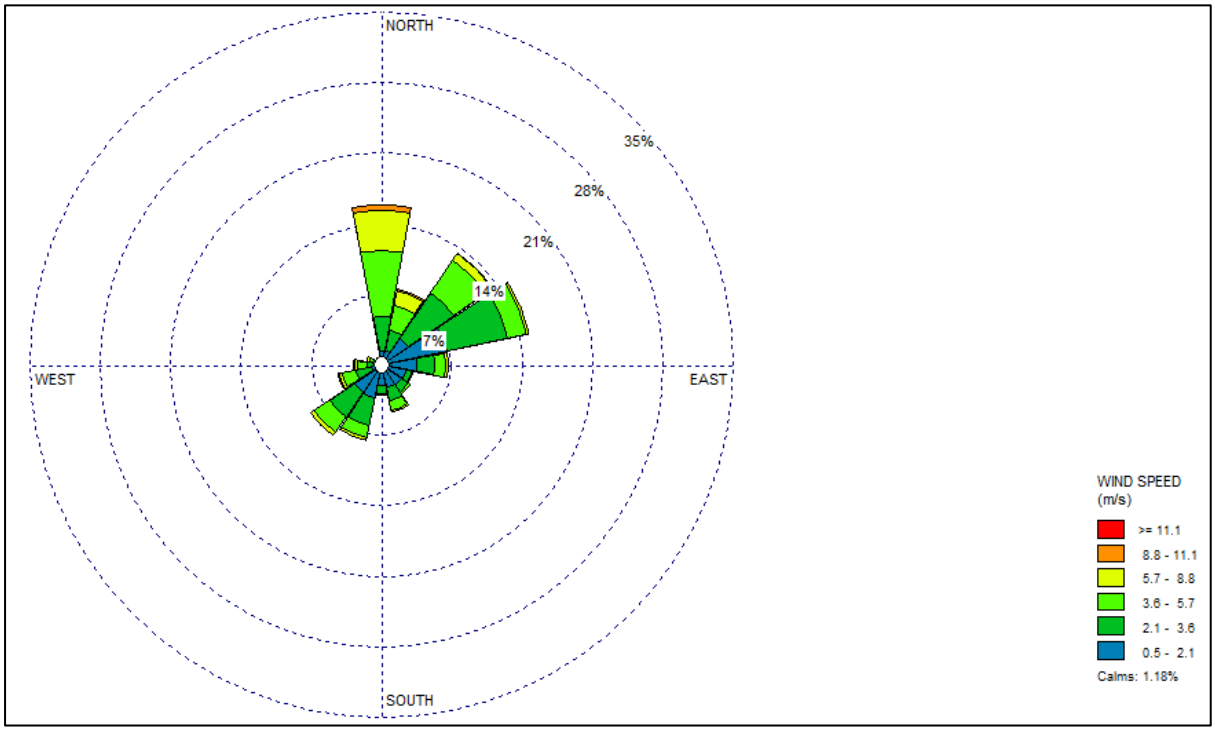

Figure 40: Wind rose for WMU 3 for the period 18 October 2014 to 18 August 2015.

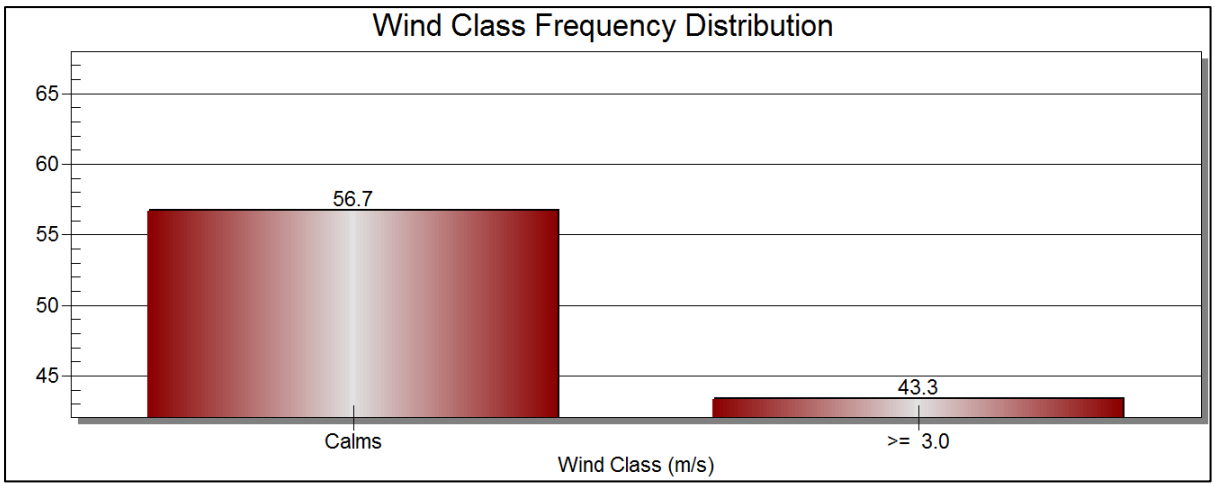

Figure 41: Frequency with which the average wind speed exceeded the tailings material's u_t - value for WMU 3.

4.3.5. Wind profile for WMU 4

Figure 42 is a wind rose of the measured wind velocity profile that was measured by WMU 4 during the research period. This WMU was located approximately at the centre of the W top crest of the facility at an elevation of 1398 m above mean sea level or 33 m above the ground surface.

The wind direction of this monitoring station was dominantly from the N, subordinate wind directions were from the north-northeast to northeast and northwest to southwest. These wind directions all exhibited speeds in excess of 3 $m.s^{-1}$, which would have resulted in wind erosion taking place. The southwest wind component of the WMU 2 and WMU 3 could correspond to the easterly component of WMU 4. This could have been possible due to an easterly wind that is deflected around the northwest corner, resulting in the observed wind directions of WMU 2 and WMU 3.

Figure 43 illustrates the frequency with which the u_t – value of the tailings material was exceeded. The graph shows that the value was exceeded 63.8% of the time during the research period (Figure 43). This value is greater than that of the reference WMU and indicates that the area in which this WMU is located is a higher risk zone for wind erosion.

The average wind speed measured at WMU 4 was 4.1 $m.s^{-1}$, as opposed to 2.9 $m.s^{-1}$ measured at WMU 12. The average wind speed amplification factor was therefore 1.4, with a 23 m elevation difference between these WMUs

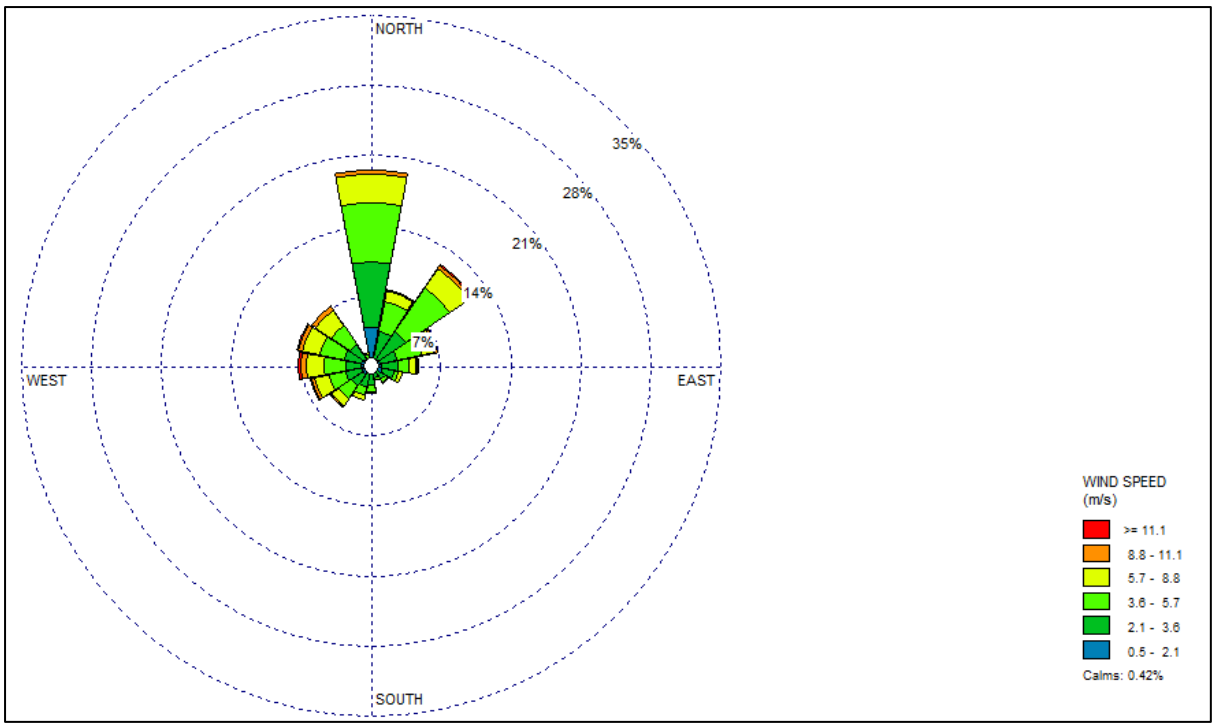

Figure 42: Wind rose for WMU 4 for the period 18 October 2014 to 18 August 2015.

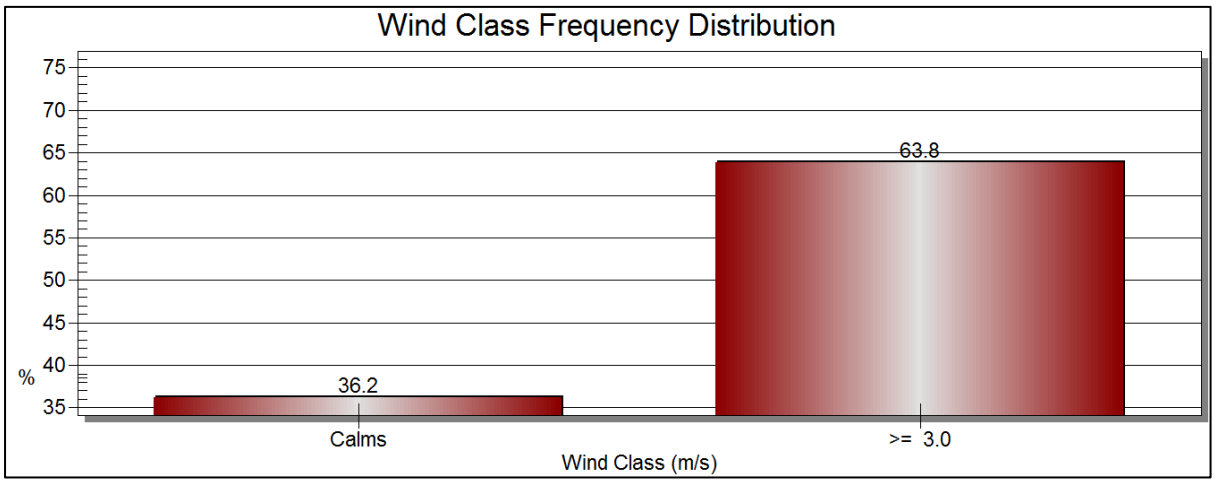

Figure 43: Frequency with which the average wind speed exceeded the tailings material's u_t - value for WMU 4.

4.3.6. Wind profile for WMU 5

Figure 44 is a wind rose of the measured wind velocity profile that was measured by WMU 5 during the research period. This WMU was located approximately at the centre of the S top crest of the facility at an elevation of 1396 m above mean sea level or 31 m above the ground surface.

No clear wind direction pattern is discernible from the data (Figure 44). However, it can be stated that the dominant wind direction was from the north, with a secondary direction from the northwest (which also exhibited the highest wind speeds). These wind directions all exhibited speeds in excess of 3 $m.s^{-1}$, which would have resulted in wind erosion taking place. The high wind speed events recorded by this WMU is likely due to a fluid-compression effect that was caused by air travelling over the beach, pool and inner-crest of the TSF.

Figure 45 illustrates the frequency with which the u_t – value of the tailings material was exceeded. The graph shows that the value was exceeded 73.1% of the time during the research period. This value is greater than that of the reference WMU and indicates that the area in which this WMU is located is a higher risk zone for wind erosion.

The average wind speed measured at WMU 5 was 4.7 $m.s^{-1}$, as opposed to 2.9 $m.s^{-1}$ measured at WMU 12. The average wind speed amplification factor was therefore 1.6, with a 21 m elevation difference between these WMUs

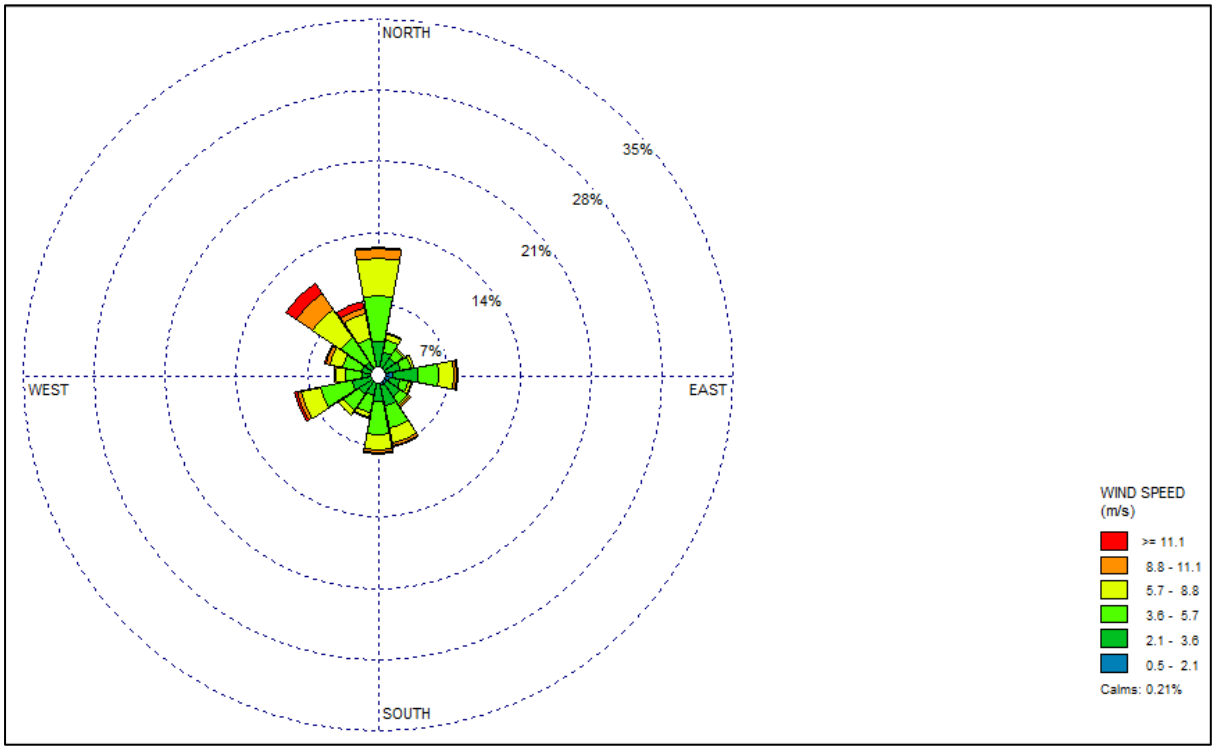

Figure 44: Wind rose for WMU 5 for the period 18 October 2014 to 18 August 2015.

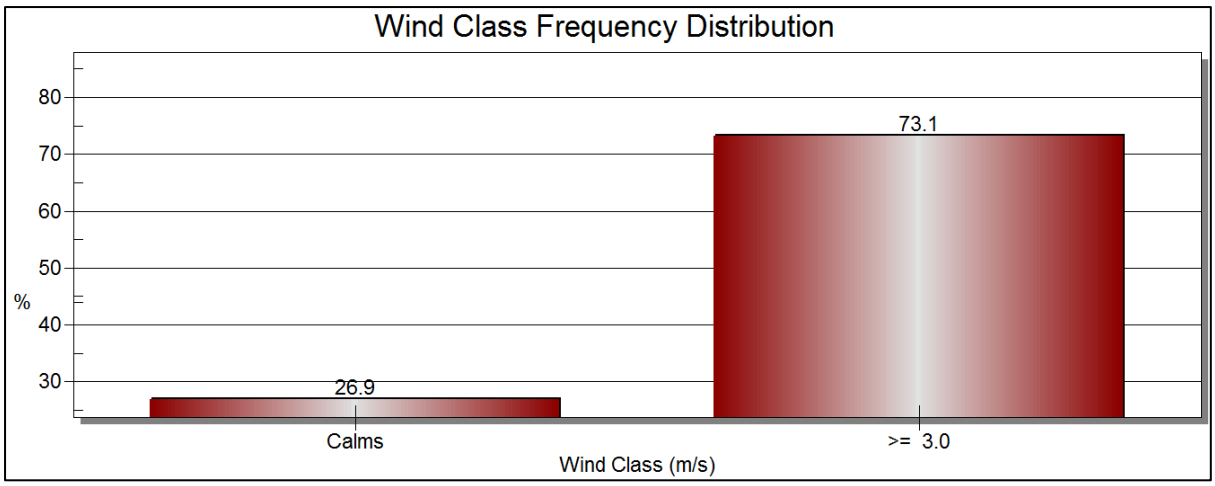

Figure 45: Frequency with which the average wind speed exceeded the tailings material's u_t value for WMU 5.

4.3.7. Wind profile for WMU 6

Figure 46 is a wind rose of the measured wind velocity profile that was measured by WMU 6 during the research period. This WMU was located approximately at the centre of the southern first bench of the facility at an elevation of 1365 m above mean sea level, which is the same elevation as the reference site.

The wind rose (Figure 46) indicates that the major wind directions for the WMU 6 were from the north to east-northeast. However, it can be stated that the dominant wind direction was from the north, with a secondary direction from the southwest. These wind directions all exhibited speeds that were comparatively low in relation to the other WMUs. The portion of wind speed that could have been erosive was comparatively low. The comparatively low wind speed measured at the site is likely due to flow separation that took place. This conclusion is drawn from the location of the WMU 6 that was situated on the first slope of the southern face of the facility. Wind from the N would likely have separated as it left the crest, causing a low wind speed zone where the WMU was located. This corresponds to findings from Blight (2007:103) and others (Blight, 2008:530; Walker, 1999:437; Wiggs *et al.*, 1996:43).

Figure 47 illustrates the frequency with which the u_t – value of the tailings material was exceeded. The graph shows that the value was exceeded 20.9% of the time during the research period. This value is lower than that of the reference WMU 12

and indicates that the area in which this WMU is located is a lower risk zone for wind erosion.

The average wind speed measured at WMU 5 was 2.1 $m.s^{-1}$, as opposed to 2.9 $m.s^{-1}$ measured at WMU 12. The average wind speed amplification factor was therefore 0.72, with a 10 m elevation difference between these WMUs, with the WMU 12 being positioned higher than the WMU 6.

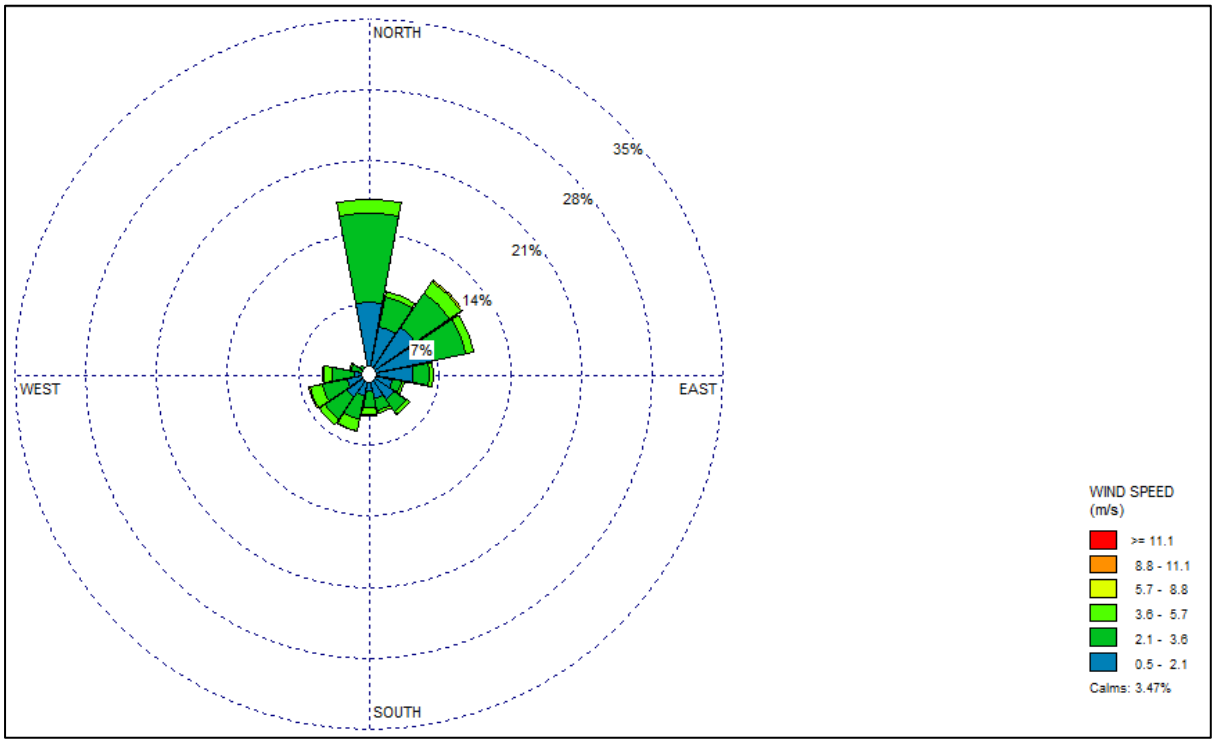

Figure 46: Wind rose for WMU 6 for the period 18 October 2014 to 18 August 2015.

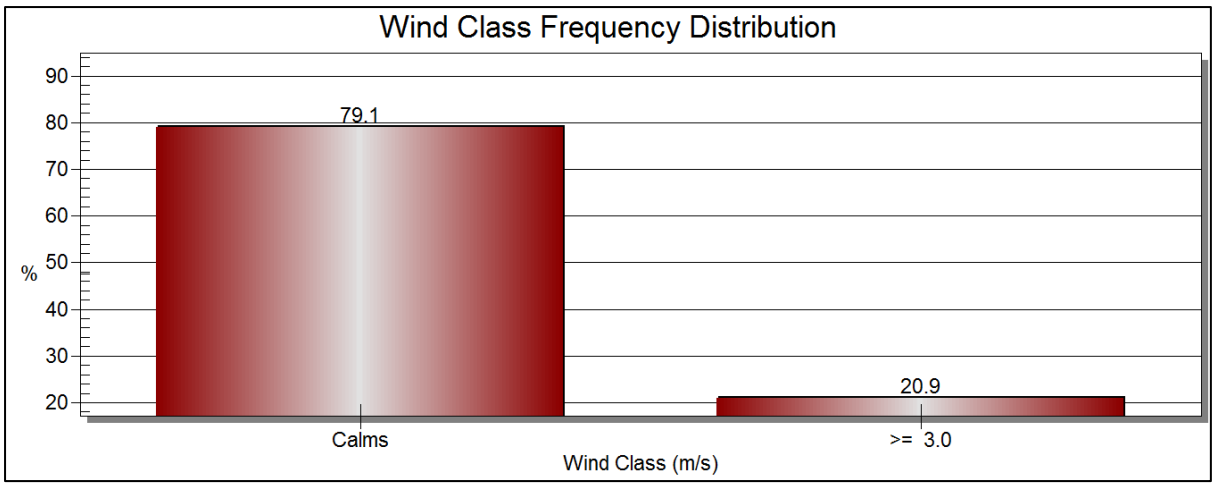

Figure 47: Frequency with which the average wind speed exceeded the tailings material's u_t - value for WMU 6.

4.3.8. Wind profile for WMU 7

Figure 48 is a wind rose of the measured wind velocity profile that was measured by WMU 7 during the research period. This WMU was located approximately at the centre of the eastern the top at an elevation of 1399 m above mean sea level, which is 34 m higher than reference site.

The wind rose (Figure 48) indicates that the major wind directions for the WMU 8 were from the north, with a secondary direction from the southwest. The greatest component of the erosive force was from the northern to eastern quadrant. This wind direction distribution corresponds with measurements from WMUs 12, 6, 3, 2 and 1, which indicates that the geometry of the TSF may have had little influence on redirecting air flow at location point on the TSF.

Figure 49 illustrates the frequency with which the u_t – value of the tailings material was exceeded. The graph shows that the value was exceeded 57.1% of the time during the research period. The amount of times that the u_t value of the tailings material was exceeded (in relation to the reference site), indicates that the wind speed was amplified on the TSF and that the area was at increased risk of being subjected to wind erosion.

The average wind speed measured at WMU 8 was 3.6 $m.s^{-1}$, as opposed to 2.9 $m.s^{-1}$ measured at WMU 12. The average wind speed amplification factor was therefore 1.2, with a 24 m elevation difference between these WMUs.

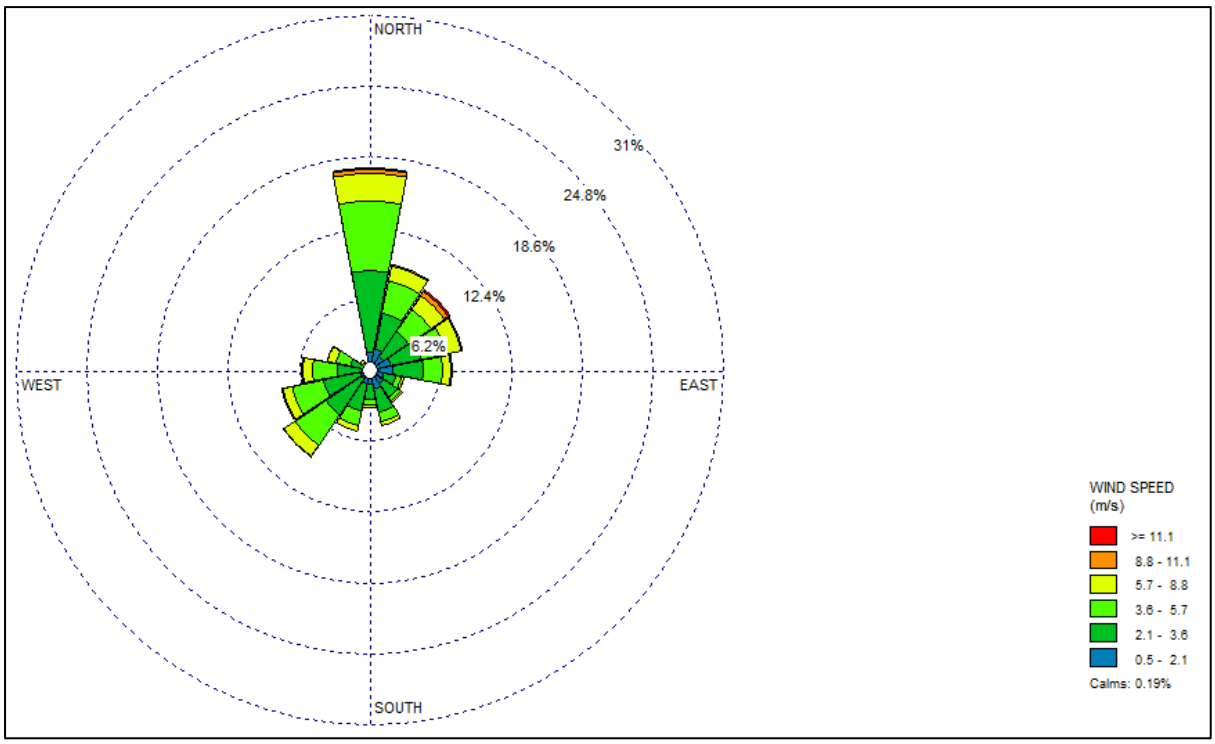

Figure 48: Wind rose for WMU 7 for the period 18 October 2014 to 18 August 2015.

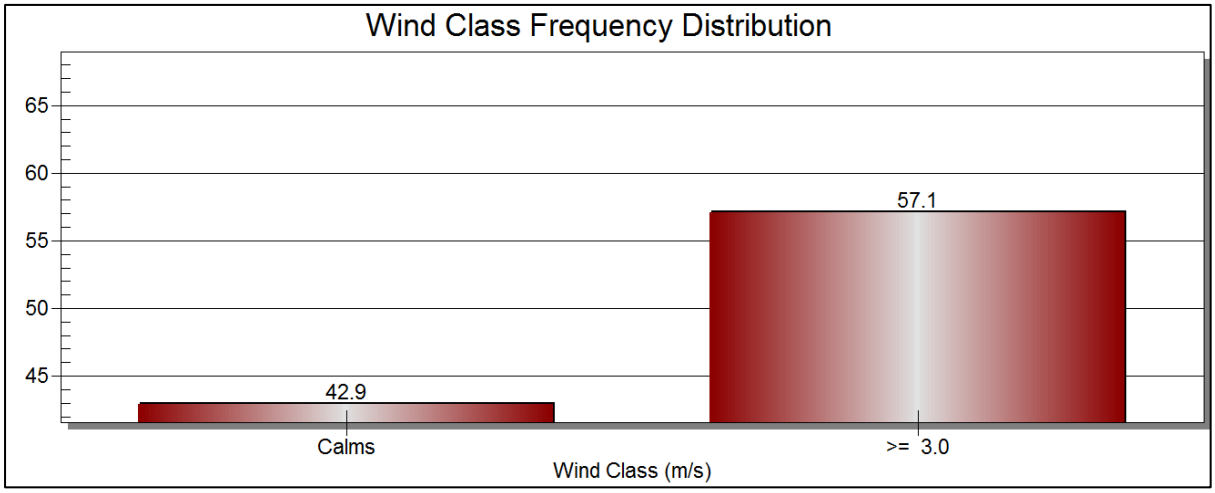

Figure 49: Frequency with which the average wind speed exceeded the tailings material's u_t value for WMU 7.

4.3.9. Wind profile for WMU 8

Figure 50 is a wind rose of the measured wind velocity profile that was measured by WMU 8 during the research period. This WMU was located approximately at the centre of the first bench (from the top) on the eastern side of the TSF at an elevation of 1375 m above mean sea level, which is 10 m higher than the reference site.

The wind rose (Figure 50) indicates that the major wind directions for the WMU 8 were from the N, with a secondary direction from the east. The greatest component of the erosive force was from the north. This recorded wind profile is explainable by the position of WMU 8. This WMU would likely have been sheltered by the eastern top slopes, explaining the small frequency of wind from the east. Air would likely have been forced along the eastern slope, leading to the high frequency of wind from the N.

Figure 51 illustrates frequency with which the u_t – value of the tailings material was exceeded. The graph shows that the value was exceeded 23.2% of the time during the research period. This value is lower than that of the reference WMU 12 and indicates that the area in which this WMU is located is a lower risk zone for wind erosion.

The average wind speed measured at WMU 8 was 2.4 $m.s^{-1}$, as opposed to 2.9 $m.s^{-1}$ measured at WMU 12. The average wind speed amplification factor was therefore 0.83, with a 0 m elevation difference between these WMUs.

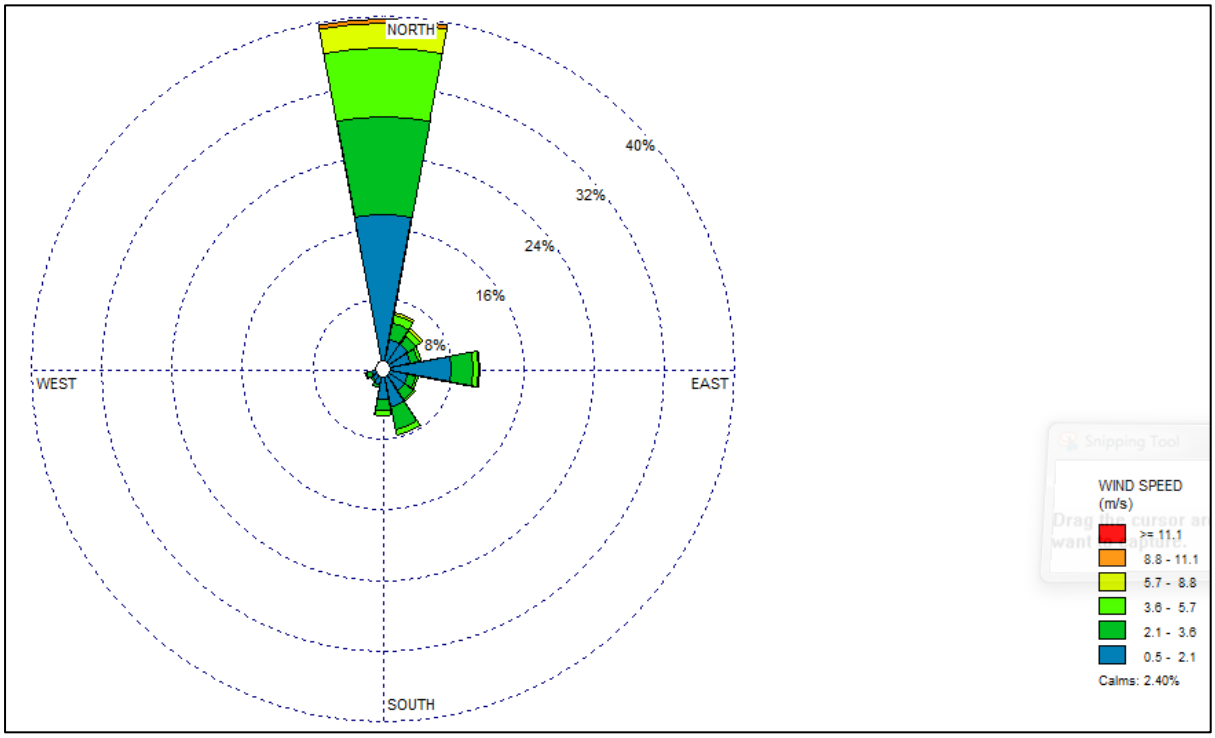

Figure 50: Wind rose for WMU 8 for the period 18 October 2014 to 18 August 2015.

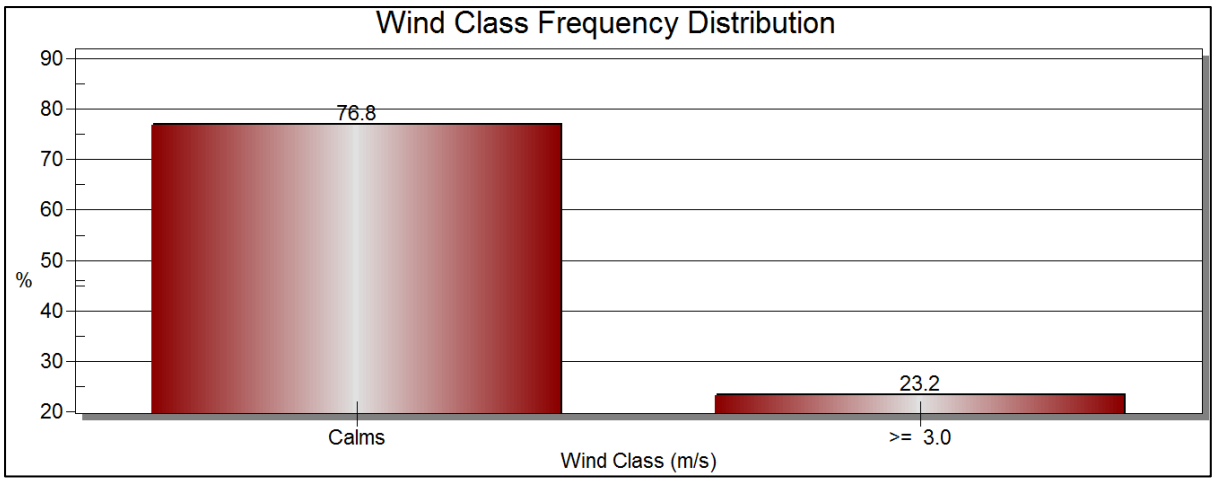

Figure 51: Frequency with which the average wind speed exceeded the tailings material's u_t value for WMU 8.

4.3.10. Wind profile for WMU 9

WMU 9 was located on the natural soil surface on the windward side of the slope, it can therefore be assumed that the friction from the surrounding structures caused the wind speed to be lower than for the other sites. The decrease in wind speed near the earth surface (frictional surface) was reported also by Blight (2012:96) and Neuman *et al.* (1997:1105), which corresponds with the finding of this research.

Figure 52 is a wind rose of the measured wind velocity profile that was measured by WMU 9 during the research period, at an elevation of 1361 m above mean sea level, which is 4 m lower than reference site.

The wind rose (Figure 52) indicates that the major wind directions for the WMU 9 were from the E and ENE, with a secondary direction from the north. The greatest component of the erosive force was from the north. The deviation of the wind direction profile from that of the reference site (WMU 12) was unexpected. The direction classes of the two WMUs in question are similar, however, the frequency of wind measured from the east are greater for WMU 9 than for WMU 12. A possible explanation for the observed differences could be that wind is deflected around the TSF (when from the north), thereby changing the directionality of the incoming wind. This was also depicted in Figure 11 by Greeley and Iverson (1985:205-209). The development of the natural vegetation on the abandoned agricultural field (upwind of the WMU 9) could also have caused anomalies in the wind direction and speed profile for the area.

Figure 53 illustrates the frequency with which the u_t – value of the tailings material was exceeded. The graph shows that the value was exceeded 14.6% of the time during the research period. This value is lower than that of the reference WMU 12 and indicates that the area in which this WMU is located is a lower risk zone for wind erosion and that surface friction was the likely cause of the lower wind speeds.

The average wind speed measured at WMU 9 was 1.6 $m.s^{-1}$, as opposed to 2.9 $m.s^{-1}$ measured at WMU 12. The average wind speed amplification factor was therefore 0.6, with an 14 m elevation difference between these WMUs (WMU 12 had a higher elevation).

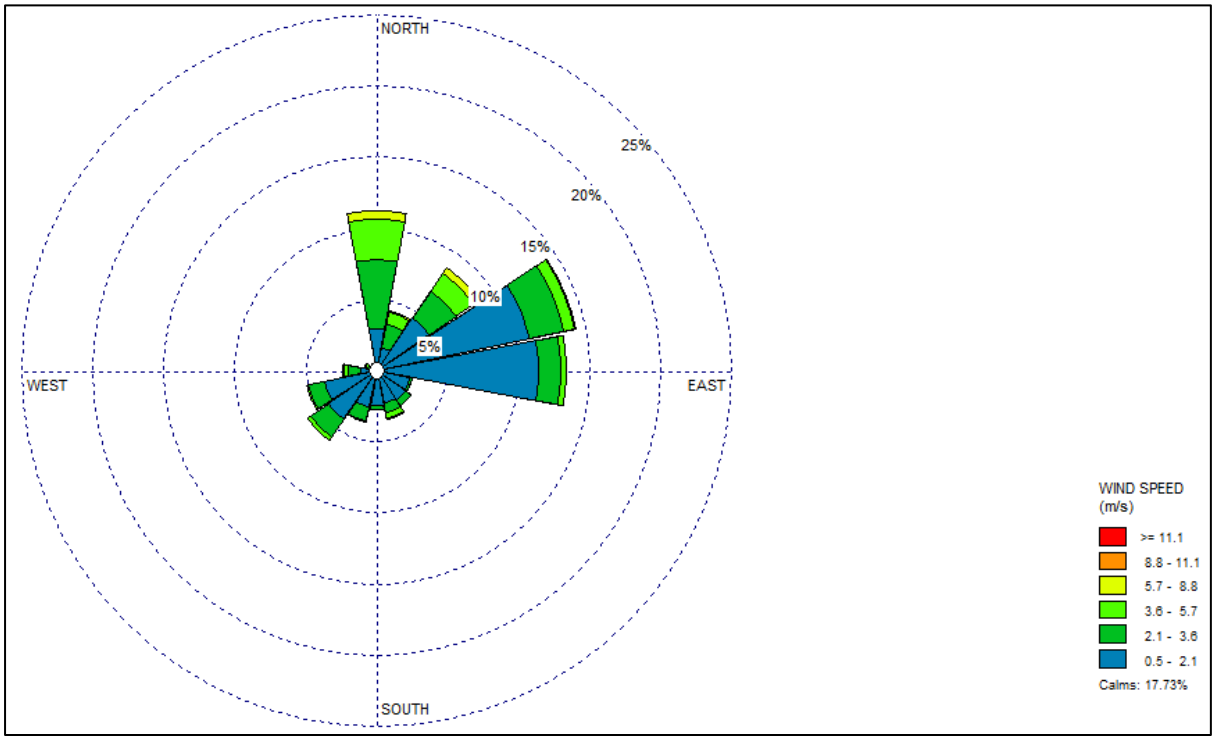

Figure 52: Wind rose for WMU 9 for the period 18 October 2014 to 18 August 2015.

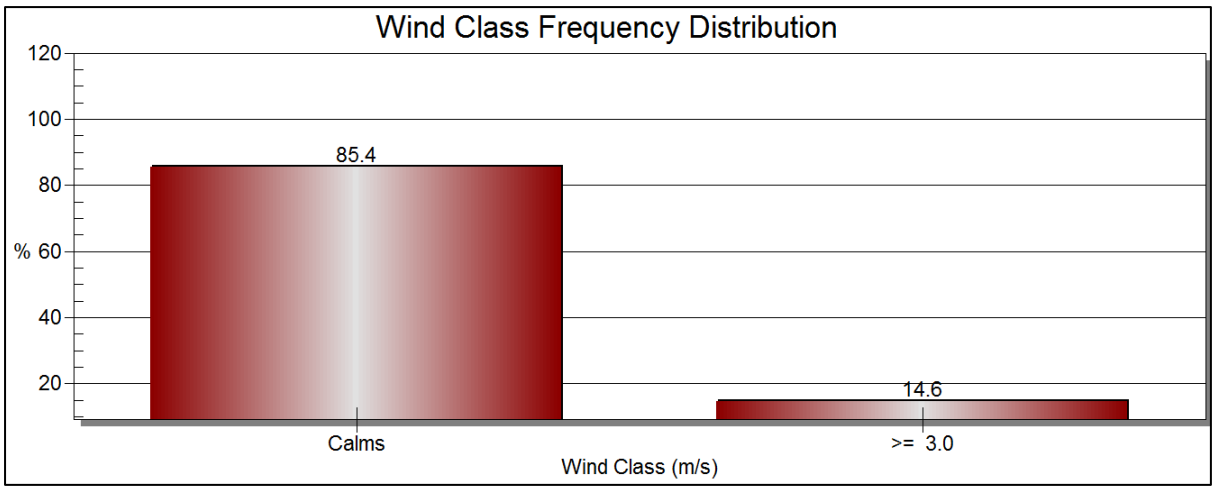

Figure 53: Frequency with which the average wind speed exceeded the tailings material's u_t value for WMU 9.

4.3.11. Wind profile for WMU 10

Figure 54 is a wind rose of the measured wind velocity profile that was measured by WMU 10 during the research period, at an elevation of 1367 m above mean sea level, which is a 2 m higher elevation than reference site.

WMU 10 was located on top of the first slope on the windward side of the TSF. It was, however, somewhat sheltered by vegetation such as grass, shrubs and trees. The reduction of wind speed by vegetation has been recorded by other researchers as well (Ferreira & Lambert, 2011:68; Leenders *et al.*, 2007:1455; Blight, 2012:96; Neuman *et al.*, 1997:1105).

The wind rose (Figure 54) indicates that the major wind directions for the WMU 10 were from the east-northeast, with a secondary direction from the north. The greatest component of the erosive force was from the north. The high frequency with which wind from the east-northeast occurred could possibly be explained by the position of the WMU on the site. Since it was located at the corner of the northwest slope, it is likely that a component of the incoming wind was deflected along the face of the north slope and around the corner on which the WMU was located. Thereby, causing the over representation of the east-northeast wind component.

Figure 55 illustrates the frequency with which the u_t – value of the tailings material was exceeded. The graph shows that the value was exceeded 19.9% of the time during the research period. This is a greater proportion of the time than for WMU 9,

which was located 6 m lower than WMU 10, indicating that wind speed amplification occurred between these areas. The measured erosive component of the wind is lower than that of the reference WMU 12 and indicates that the area in which this WMU is located is a lower risk zone for wind erosion and that surface friction was the likely cause of the lower wind speeds.

The average wind speed measured at WMU 10 was 2.0 $m.s^{-1}$, as opposed to 2.9 $m.s^{-1}$ measured at WMU 12. The average wind speed amplification factor was therefore 0.7, with an 8 m elevation difference between these WMUs (WMU 12 had a higher elevation).

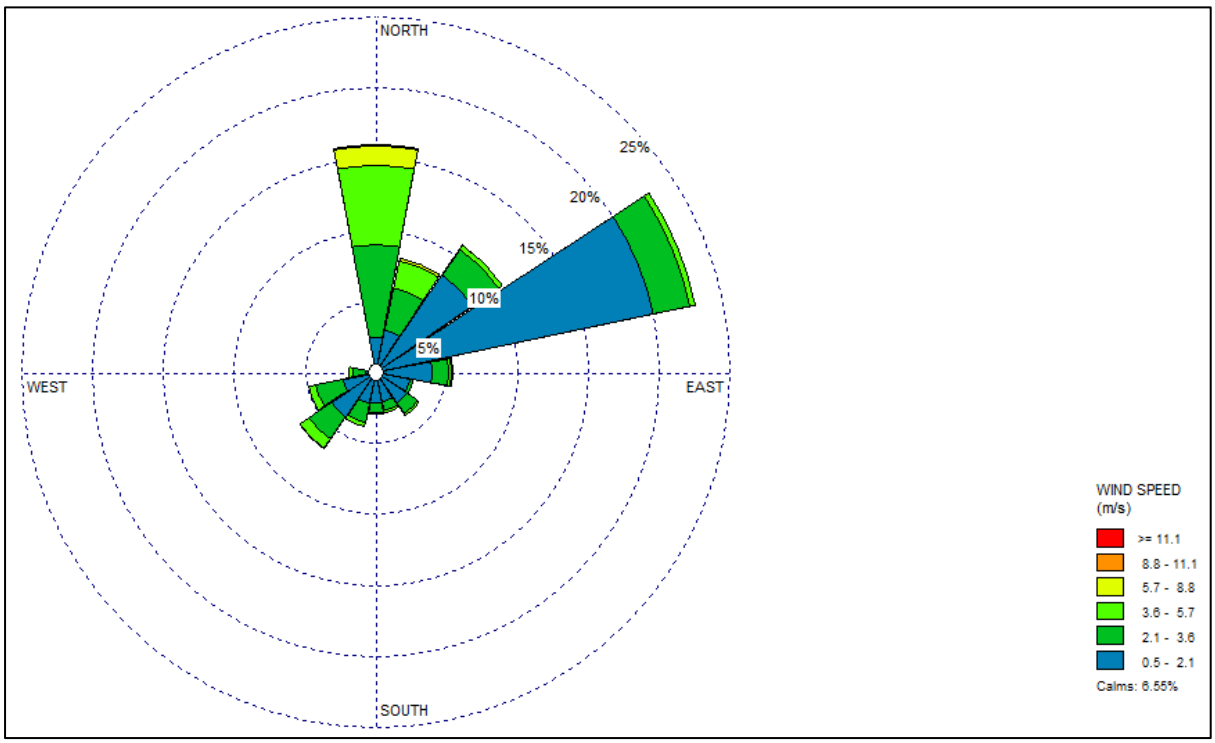

Figure 54: Wind rose for WMU 10 for the period 18 October 2014 to 18 August 2015.

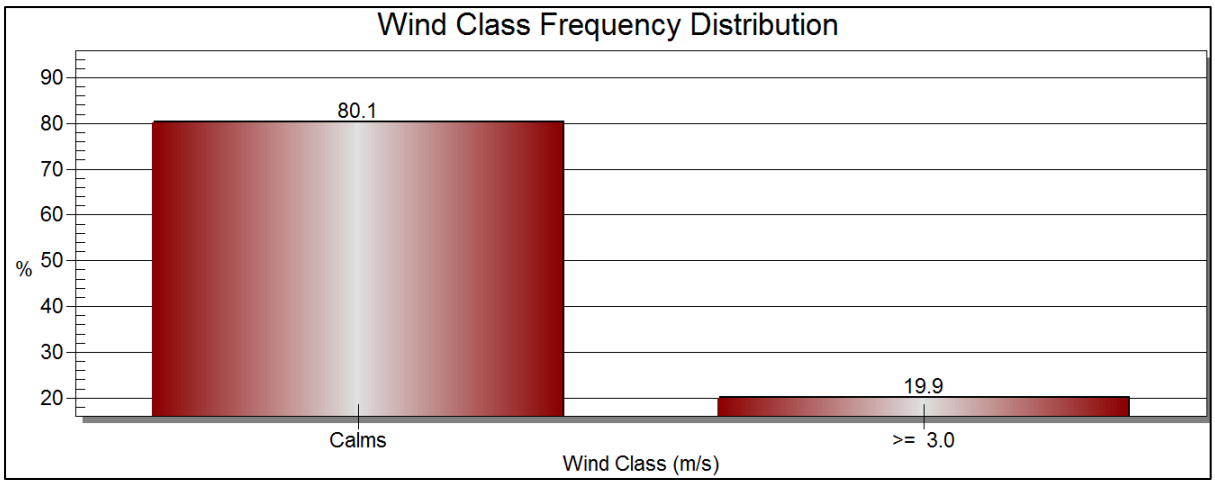

Figure 55: Frequency with which the average wind speed exceeded the tailings material's u_t value for WMU 10.

4.3.12. Wind profile for WMU 11

Figure 56 is a wind rose of the measured wind velocity profile that was measured by WMU 11 during the research period. This WMU was located on the north-facing crest of the facility at an elevation of 1364 m above mean sea level.

The wind direction of this monitoring station was dominantly from the north, with subordinate directions from the east and south-southeast. The wind measured from the north had a greater erosion capacity (based on wind speed and frequency) than the other measured directions. The high frequency of wind from the north is likely due to the position of the WMU. Since it was located on the western slope, a major component of the incoming wind would have been forced along the face of the slope in a north – south direction, resulting in the over representation of the N-component of the incoming wind.

Figure 57 illustrates the frequency with which the u_t – value of the tailings material was exceeded. The graph shows that the value was exceeded 30.8% of the time during the research period. This value is greater than that of the reference WMU and indicates that the area in which this WMU is located is a higher risk zone for wind erosion.

The average wind speed measured at WMU 11 was 2.4 $m.s^{-1}$, as opposed to 2.9 $m.s^{-1}$ measured at WMU 12. The average wind speed amplification factor was

therefore 0.8, with an 11 m elevation difference between these WMUs (the reference site was located at a higher elevation than WMU 11).

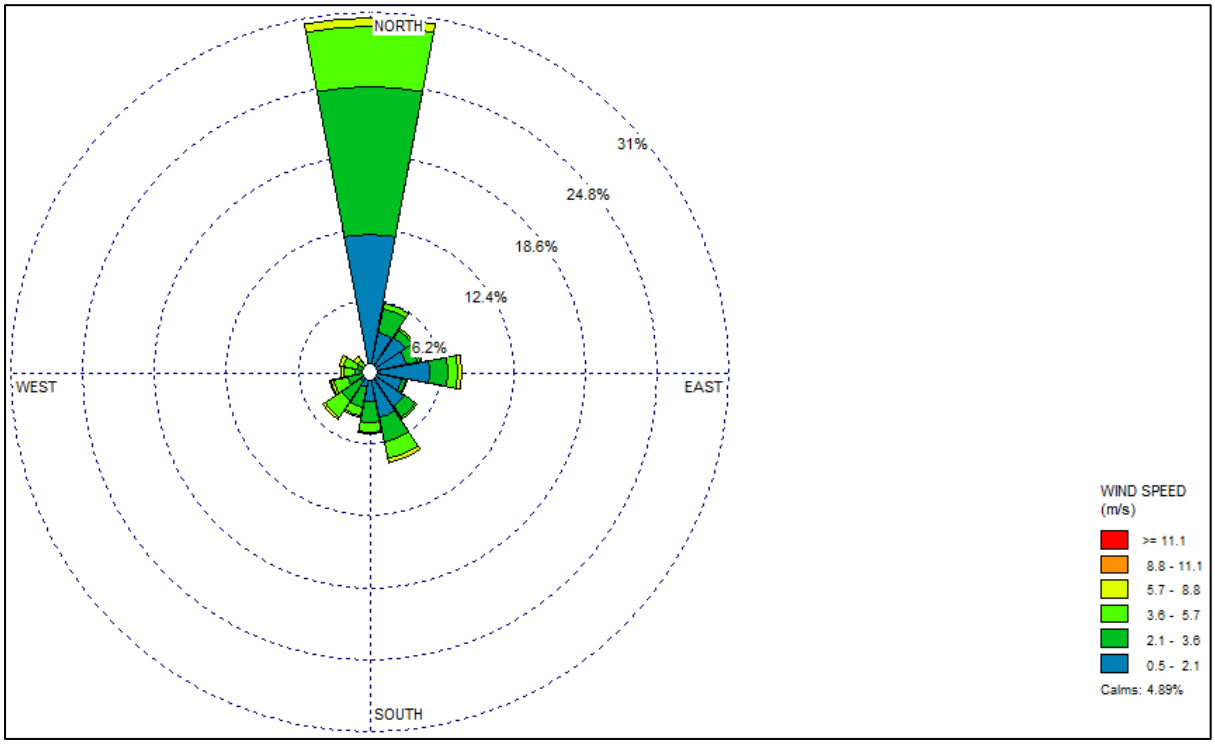

Figure 56: Wind rose for WMU 11 for the period 18 October 2014 to 18 August 2015.

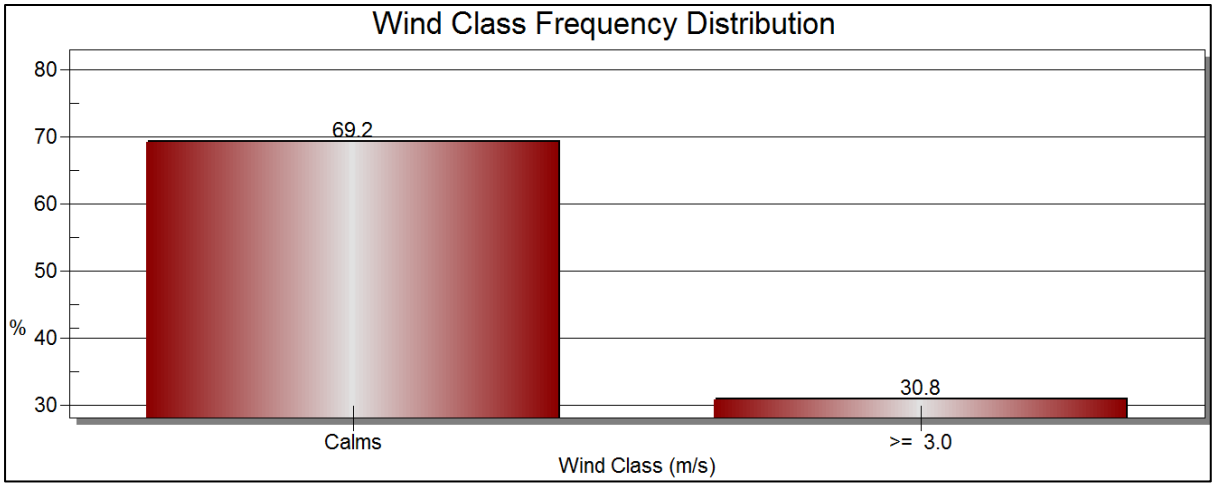

Figure 57: Frequency with which the average wind speed exceeded the tailings material's u_t value for WMU 11.

4.3.13. Wind speed distribution over space

From Figure 58, the average wind speed distribution for the control can be seen, as well as the average wind speed measurements for the remaining WMUs. The data is illustrative of the fact that the wind speed that was measured on the research site was not just a function of elevation, but also a measure of the degree of wind-shelter that the individual WMUs enjoyed. This is evident by the lower wind speed that was recorded by the WMUs 6, 9 and 10, all of which had different degrees of wind shelter (discussed in section 4.3.7, section 4.3.10 and section 4.3.11).

The data further shows a good correlation between relatively high wind speed and elevation. WMUs 1, 2, 4, 5 and 7 had the highest wind speed measurements. These WMUs also had the highest elevations of all the WMUs. Figure 59 illustrates the statistical relationship between the measured mean wind speed and elevation above mean sea level. The graph shows that there is a good correlation for a linear (R^2 – 0.84), logarithmic (R^2 – 0.84) and exponential (R^2 – 0.83) correlation between mean wind speed and elevation. This is an indication that there was a significant relationship between elevation (position on the Chemwest 5 TSF) and mean wind speed. These results correlate well with wind amplification studies by Blight (2012:97) and Neuman *et al.* (1997:1107).

This relationship between elevation and wind speed can be used to determine the mean elevation at which wind speed became erosive on the Chemwest 5 TSF by means of interpolation. When the y-intercept was set to 3.0 $m.s^{-1}$ for the linear and logarithmic equations, the mean elevation was derived at which particle motion could have started to take place. The interpolated elevation is 1377 m above mean sea level. The calculation for the logarithmic equation is displayed in the following equation.

$$y = 81.442 \ln(x) - 585$$

$$\frac{588}{81.422} = \ln(x)$$

$$x = e^{7.228}$$

$$\underline{x = 1377.5\ m}$$

Because the linear and logarithmic correlations were not perfect, i.e. (R^2 – 1.0), the elevation value of 1377.5 m can only serve as an indication. However, the result could still be useful to rehabilitation specialists and managers to prioritise areas on the TSF that require additional dust mitigation measures.

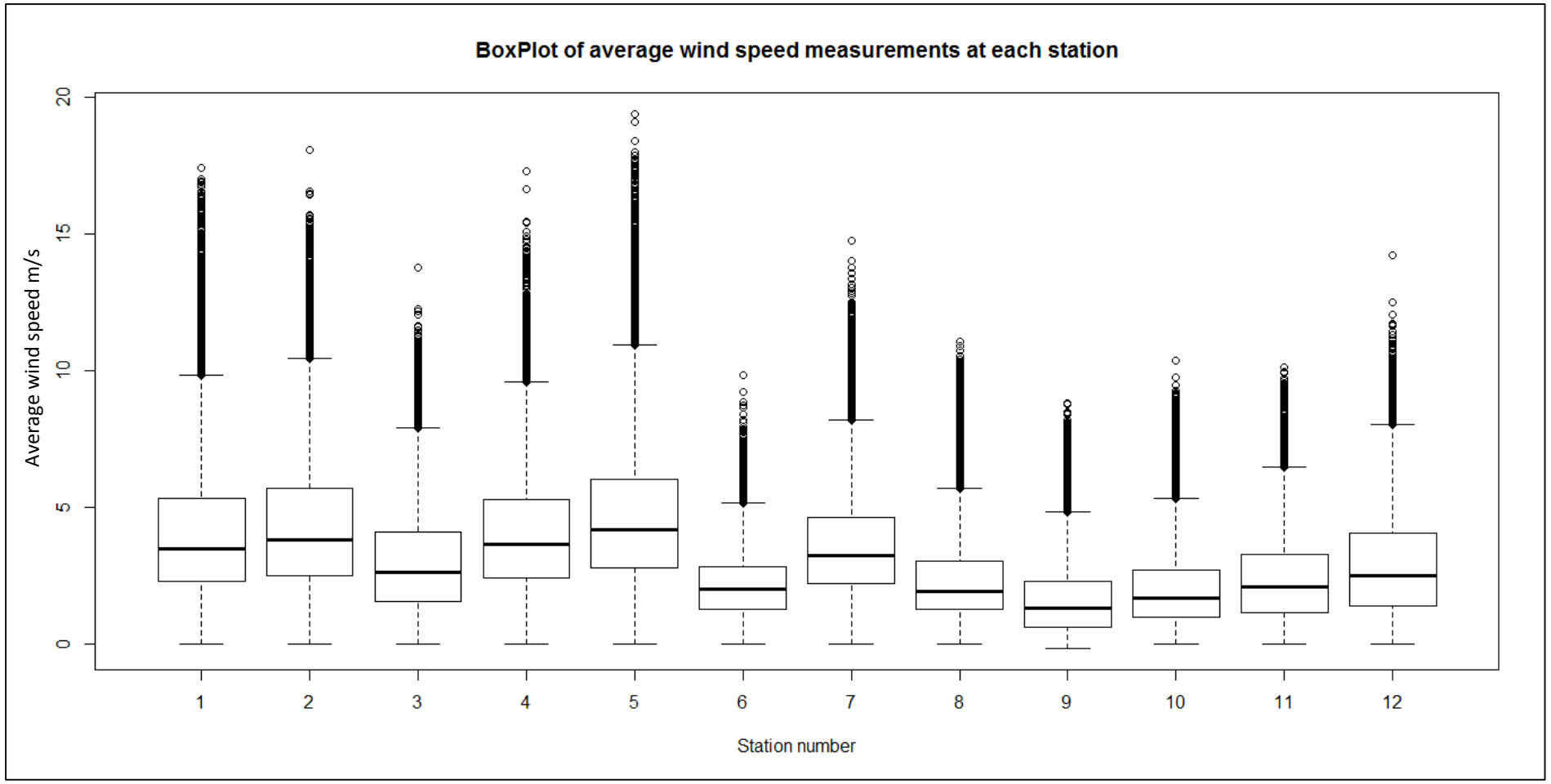

Figure 58: Average wind speed for the different WMUs (WMU 12 is the reference site)

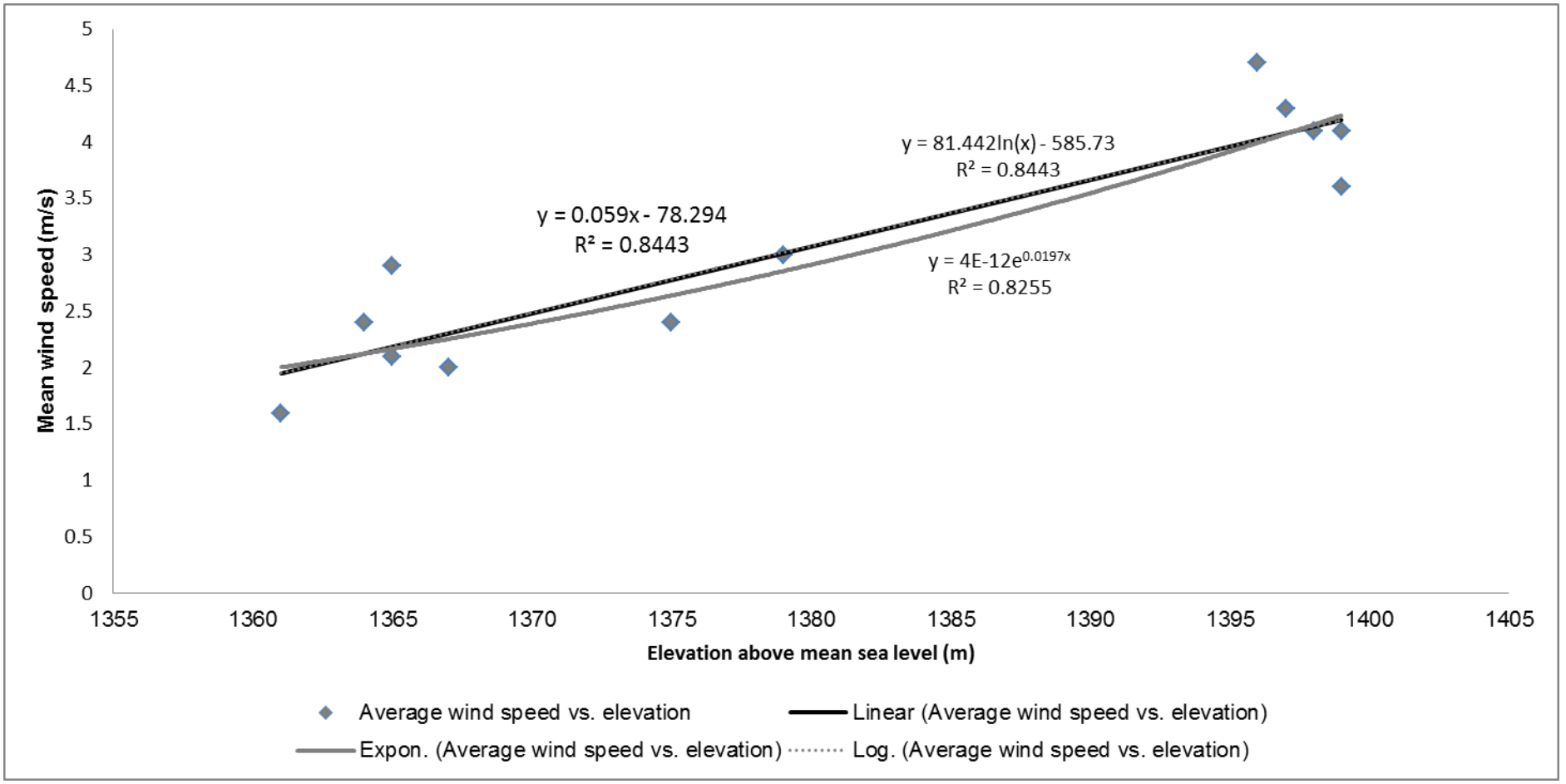

Figure 59: Scatterplot of mean wind speed versus elevation.

4.3.14. Wind speed profile for the Chemwest 5 TSF site during the research period

Figure 60 is illustrative of the wind speed profile over an 11-month period. The data only excludes the data for September, which was lost due to theft of the monitoring equipment. The data does, however, indicate that August (which is generally considered a windy month) had, on average, the second lowest recorded wind speed. The wind speed for October, November and December were the highest recorded.

The observed wind speed profiles over the research period can be linked to the common synoptic scale air circulation over southern Africa. The warmer months of the year (November to February) exhibited the greatest wind speeds. During the height of winter (June to August), the wind speed increased again. It was beyond the scope of this research to link the measured wind speed observations to specific synoptic scale events; however, certain characteristic features of these events provided likely explanations to the observed wind speed profile during the research period. These are referred to in this discussion but are extensively described in the literature review.

The likely cause of the higher wind speed during summer is the greater degree of differential surface heating, brought on by greater insolation (Blight, 2008:526; Greeley & Iverson, 1985:39; Strahler & Strahler, 2005:188). Tropical disturbances in the easterlies are also more common during the summer (Tyson & Preston-Whyte, 2012:194). These take the form of strong upliftments that are associated with surface troughs, which is the result of the boundary that forms between warm, moist air from the northeast and cool, dry air from the southwest and are usually associated with rain (Tyson & Preston-Whyte, 2012:192). Other atmospheric perturbations that could have caused the wind events during the winter months include westerly waves, cut-off lows, southerly meridional flow, ridging anti-cyclones, west coast troughs and cold fronts (Tyson, 1987:131; Tyson & Preston-Whyte, 2012:202). Identification of these events from daily synoptic maps (as provided by the South African Weather Service) could aid in identifying possible high wind-speed events.

4.3.15. Daily wind speed profile for the Chemwest 5 TSF site during the research period

From Figure 61, the average hourly wind profiles for the control (WMU 12) can be seen. The wind speed increased from 07:00 in the morning and decreased from 18:00 in the eventing. This is most probably due to the differential heating and cooling of the land surface that takes place on a daily basis. It can therefore be assumed that the most dust will result during these hours on the TSF.

It can also be seen from Figure 61 that high wind-speed events were recorded during the night. These recorded high wind-speed events that took place during the night on TSFs were previously relatively unknown. This is predominantly due to the lack of activity on these facilities at night. The absence of abundant sunlight also leads to poor visual identification of dust. After review of the data, it can be postulated that dust may also be liberated during the night. This phenomenon will probably not receive much attention in the near future, since dust issues are usually only addresses when it visually becomes problematic.

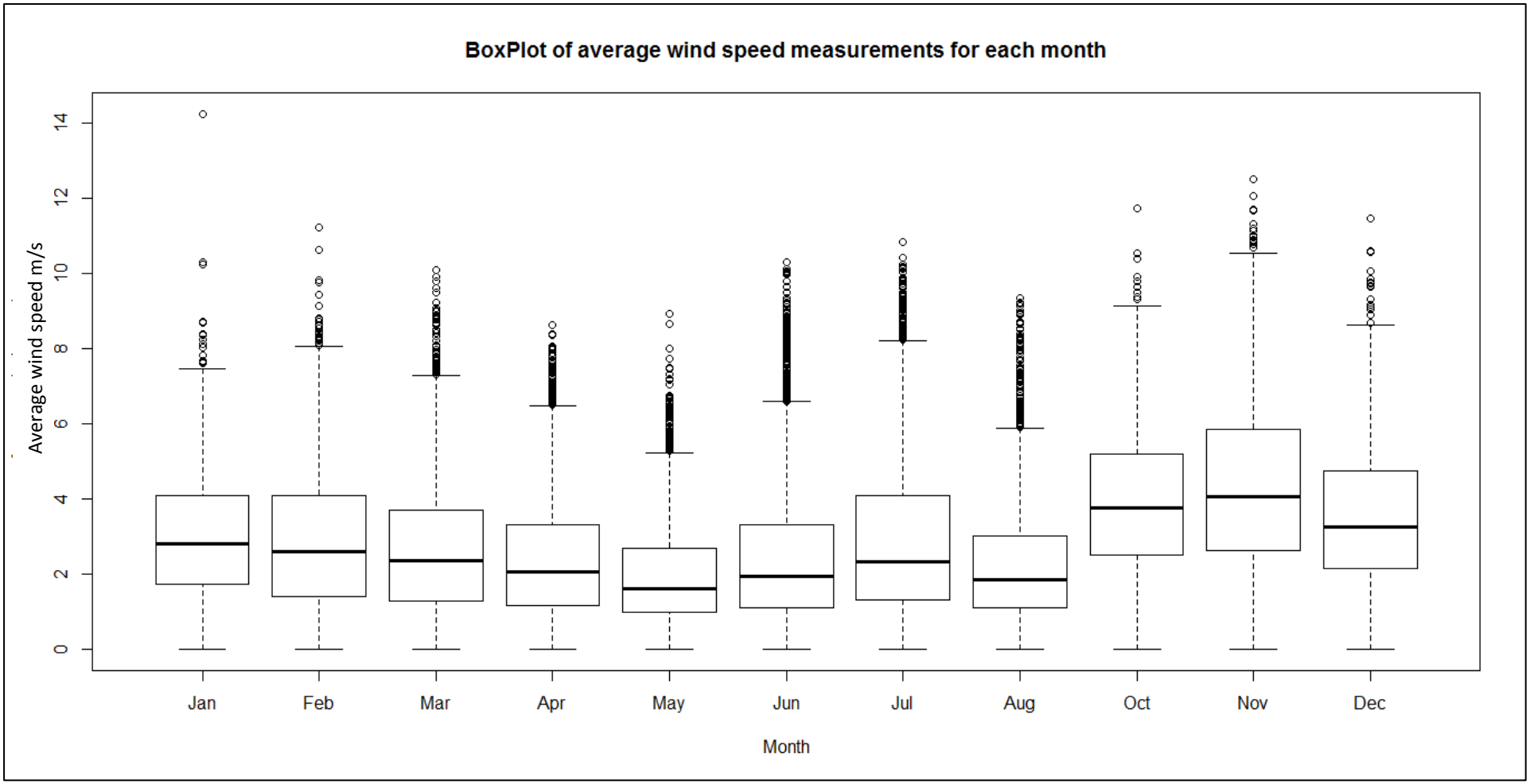

Figure 60: Average wind speed measured for each month at the control WMU

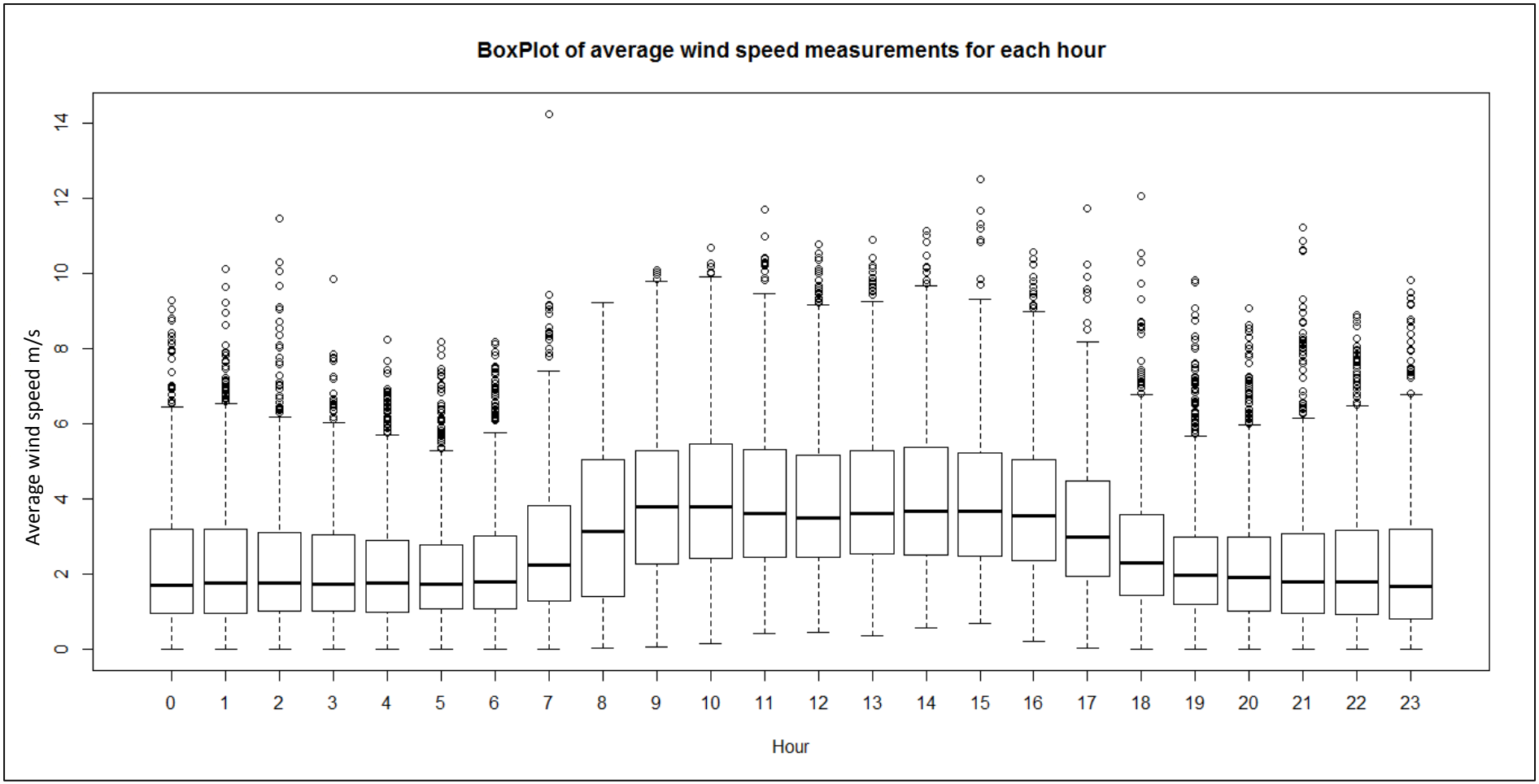

Figure 61: Average wind speed measurement for each hour of the day measured at the control WMU.

4.4. Representativeness of a control WMU for the Chemwest 5 TSF

Figure 63 to Figure 72 are the visual representations of the correlation between the control unit (WMU 12) and the different WMUs placed on the TSF. This analysis was performed in order to see whether a control WMU could be used to quantify the wind dynamics around the TSF.

Table 13 summarises the R-square values and equations for the different WMUs in relation to the control unit. The strength of the linear relationship is also listed in the table by means of the correlation R – value. The R – square values (coefficient of determination) are indicative of the extent to which the linear equation can predict the data.

For the remainder of this section, let the dependant variable Y denote the estimated average wind speed at the WMUs under consideration. Furthermore, let the dependent variable X denote the average wind speed as measured at the control WMU.

Table 13: WMUs R-square, equations and R-values of the different WMU relative to the control

WMU	R-square value	Equation	R - value
Station 1	0.00	Y= 3.96+ 0.06X	0.04
Station 2	0.82	Y= 1.11 + 1.10X	0.91
Station 3	0.84	Y= 0.44 + 0.89X	0.92
Station 4	0.80	Y= 1.13 +1.00X	0.90
Station 5	0.70	Y= 1.36+ 1.14X	0.84
Station 6	0.52	Y= 0.86+0.44X	0.72
Station 7	0.80	Y= 1.06+ 0.88X	0.90
Station 8	0.60	Y= 0.51+0.62X	0.78
Station 9	0.80	Y= -0.15 + 0.61X	0.90
Station 10	0.80	Y= 0.21+ 0.62X	0.90
Station 11	0.72	Y= 0.39+0.68X	0.85

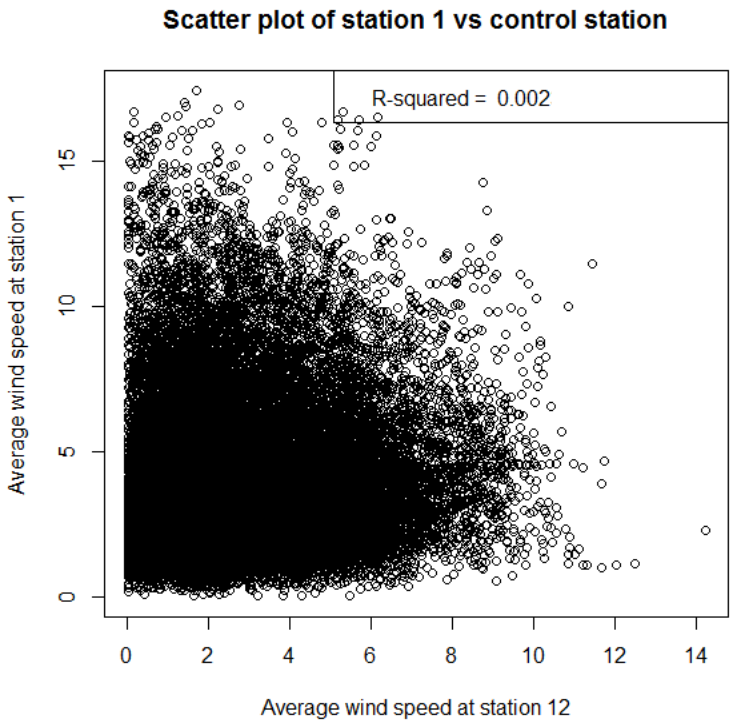

Figure 62: Scatterplot and R - square value for WMU 12 (control) and WMU 1

Figure 62 shows that there is low data predictability between the wind speed measured at the control unit and the wind speed measured at WMU 1. The reasons for the low correlation (0.04) between the aforementioned monitoring stations are unknown. It may be due to the great elevation difference that was present between the units as well as surface roughness factors. It can thus be concluded that the control cannot be used for accurate quantification of the wind speed at the position of WMU 1 on the TSF.

The wind speed can be estimated by using the following equation:

Equation 1: Linear relation equation for WMU 1 vs. the control monitor

$$Y = 3.97 + 0.06X$$

From Figure 63 it can be seen that a good correlation (0.91) exists between the control monitor and WMU 2. The units were both on the windward side of the TSF, but with great elevation and surface roughness differences. These differences took the form of slopes and vegetation dynamics, i.e. height, type, distribution and so

forth. A control unit can thus be used to estimate the wind speed to within reasonable bounds.

Equation 2: Linear relation equation for the WMU 2 vs. the control monitor

Y= 1.11 + 1.10X

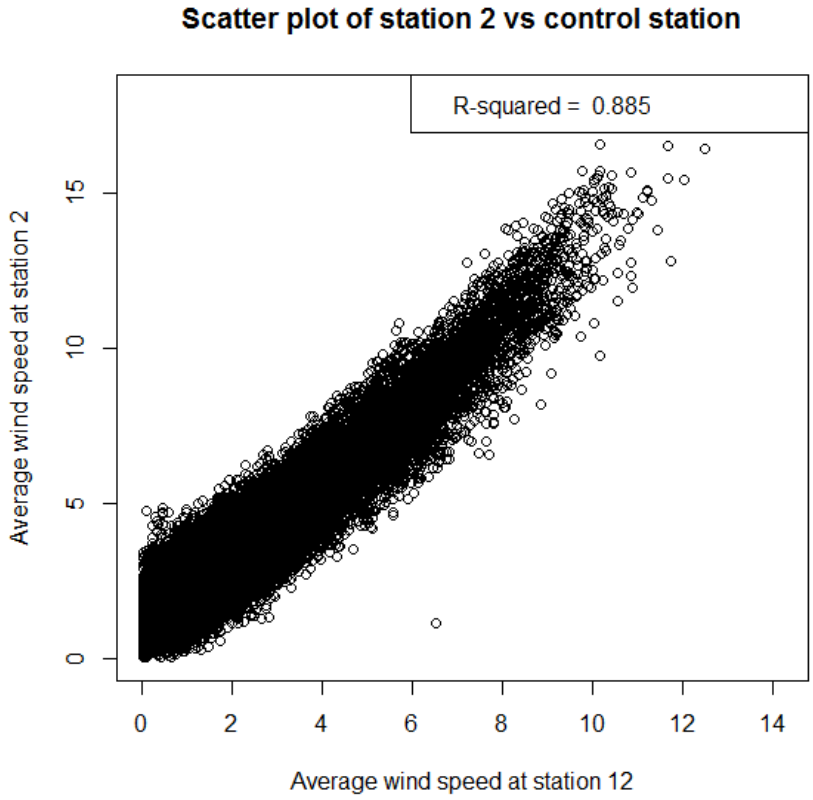

Figure 63: Scatterplot and R - square value for WMU 12 (control) and WMU 2

The control can also be used to estimate the expected wind speed at WMU 3 with reasonable accuracy. As can be seen from Figure 64, the data predictability (R-square) is 0.84, whilst the linear correlation is 0.92. WMU 3 was located on the windward side of the TSF, but at a lower elevation the WMU 2.The following linear equation was obtained for the data:

Equation 3: Linear relation equation for the WMU 3 vs. the control monitor

Y= 0.44 + 0.89X

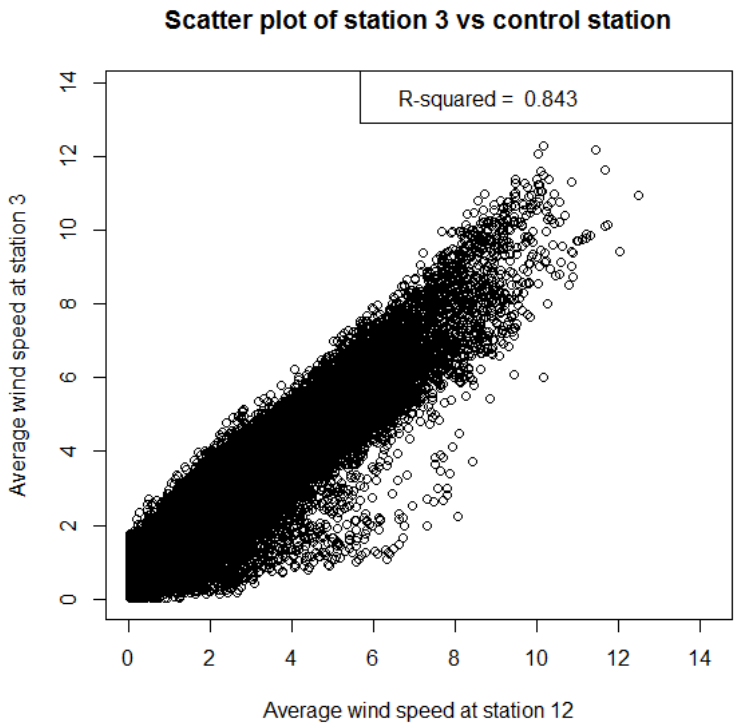

Figure 64: Scatterplot and R - square value for WMU 12 (control) and WMU 3

The data for WMU 4 also has a good correlation with the control. An R-value of 0.90 was determined for the correlation. The degree to which the data is represented by the linear equation is given as 0.80. The WMU in question was stationed on the crest of the TSF but was located approximately in the middle of the western slope (*see* Figure 16). The linear relationship between the two WMU can be mathematically expressed as:

Equation 4: Linear relation equation for the WMU 4 vs. the control monitor

$$Y= 1.129594 +1.001280X$$

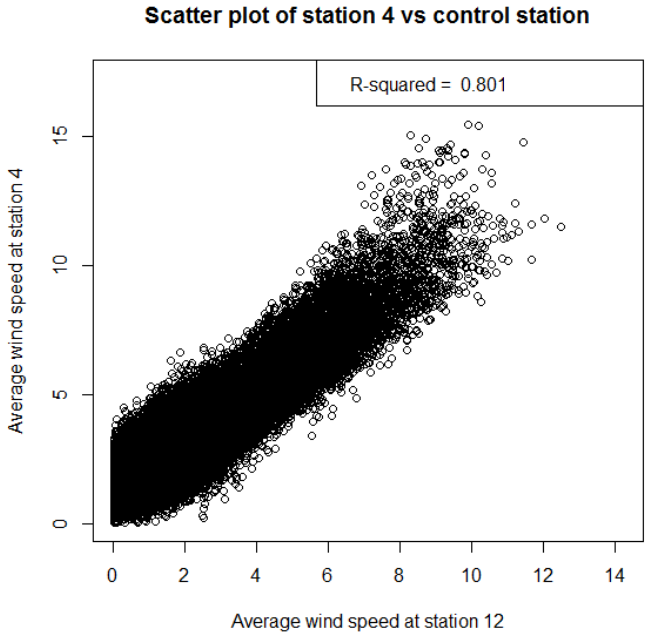

Figure 65: Scatterplot and R - square value for WMU 12 (control) and WMU 4

As can be seen from Figure 66, WMU 5 has a good correlation with the control unit. The correlation is relatively lower than for many of the other monitoring units. The linear relationship between the data has an R-square value of 0.70, whilst the correlation between the monitors in question is given as 0.84. This WMU was located at the crest if the leeward slope of the TSF. Many surface-wind disruptions could thus have influenced the manner in which the wind moved. It should be noted that a fluid compression effect is suspected at the location where this monitor was located. This is due to the somewhat lower linear data correlation between WMU 5 and the control, as well as the fact that this monitor consistently recorded higher wind speed than the other units at approximately the same elevation (*see* Figure 58).

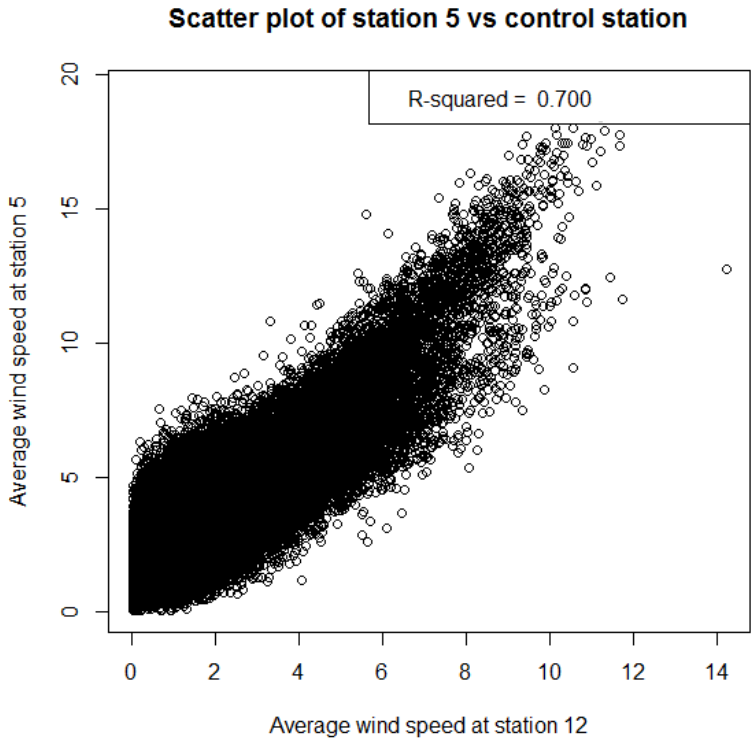

Figure 66: Scatterplot and R - square value for WMU 12 (control) and WMU 5

WMU 6 has the second lowest wind speed predictability (Figure 67). The R – square value for this specific unit is 0.52, whilst the R-value is 0.72. This unit was located on the leeward slope of the TSF and was well sheltered from the dominant wind direction. The type of control used in this research will thus not be able to yield data that can be used to accurately predict wind speed at the location of WMU 6. The linear equation is given by:

Equation 5: Linear relation equation for the WMU 6 vs. the control monitor

$$Y = 0.86 + 0.44X$$

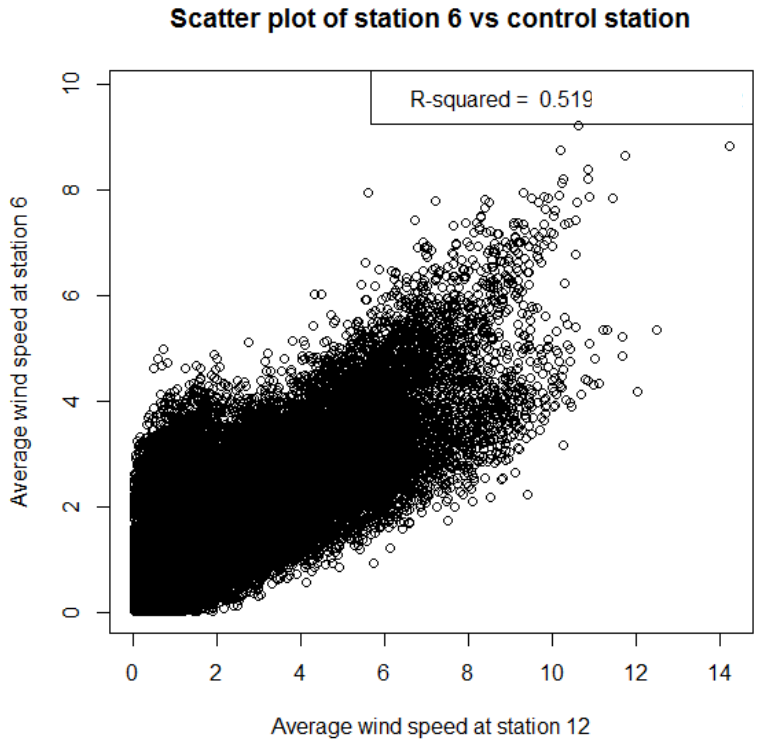

Figure 67: Scatterplot and R - square value for WMU 12 (control) and WMU 6

From Figure 68 it can be seen that there is a linear relationship between WMU 7 and the control. The degree to which the wind speed can be predicted from the control point is R-square of 0.80 and has a correlation of 0.89. This WMU is located in the crest of the eastern slope of the TSF. The linear equation for the data is given as:

Equation 6: Linear relation equation for the WMU 7 vs. the control monitor

$$Y = 1.06 + 0.88X$$

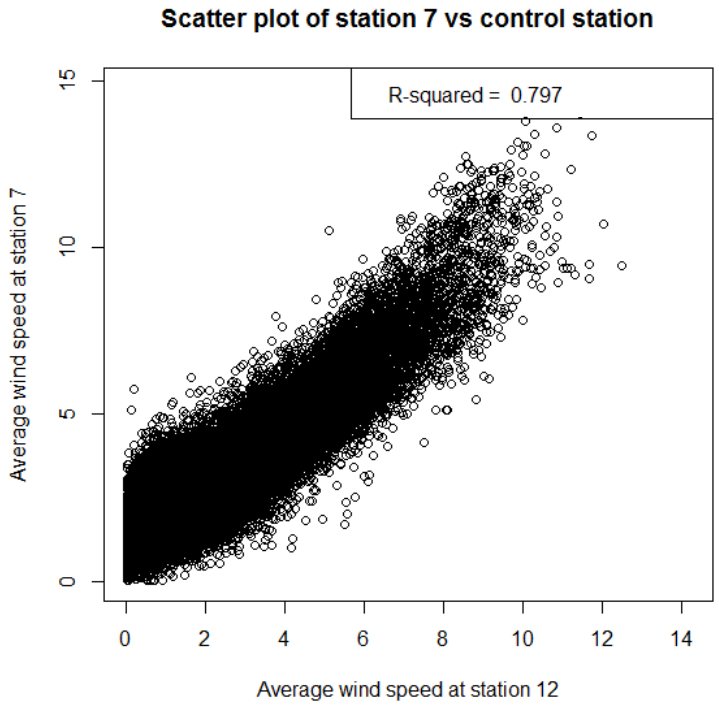

Figure 68: Scatterplot and R - square value for WMU 12 (control) and WMU 7

As can be seen from Figure 69, there is still a good correlation of data between the WMU 8 and the control. The coefficient of determination is somewhat lower at an R-square value of 0.60. This WMU was located on the middle of the eastern slope of the TSF and was not directly exposed to the dominant wind direction. Ample surface roughness factors could also have played a part in decreasing the data correlation between the control and WMU 8. The R-value for the aforementioned data is 0.7776. The linear relationship of the data is given as:

Equation 7: Linear relation equation for the WMU 8 vs. the control monitor

$$Y= 0.51+0.62X$$

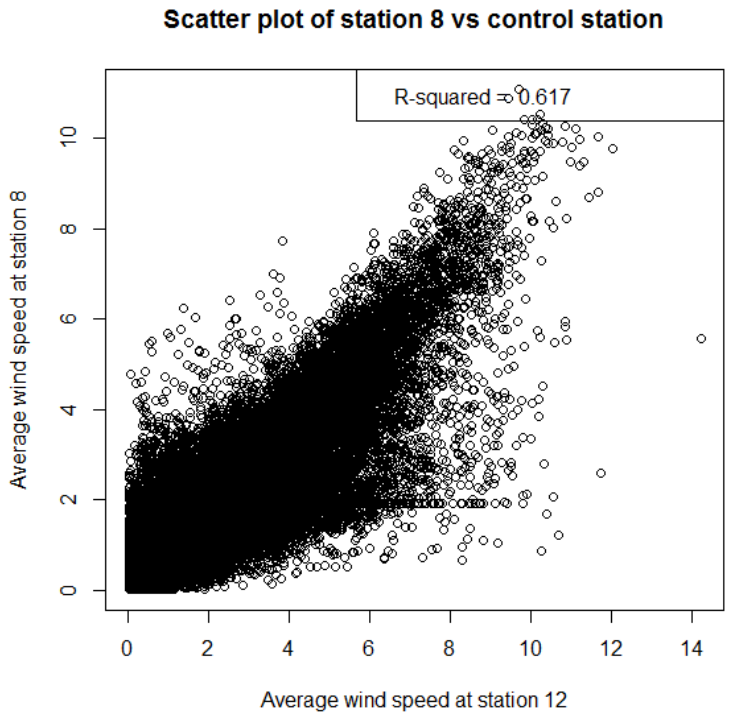

Figure 69: Scatterplot and R-square value for WMU 12 (control) and WMU 8

The control also had a good correlation with WMU 9. The wind monitor in question was located on the windward side of the TSF. It was, however, not located on the facility itself but rather on the natural ground surface at the foot of the TSF. This WMU thus had the lowest elevation and was approximately 8m lower than the control. Surface disturbances to fluid flow could thus have been abundant. The effect of these disturbances of the wind was rather constant, allowing for a coefficient of determination of 0.84 and a correlation value of 0.89. The linear relationship can be expressed as follows:

Equation 8: Linear relation equation for the WMU 9 vs. the control monitor

$$Y = -0.15 + 0.61X$$

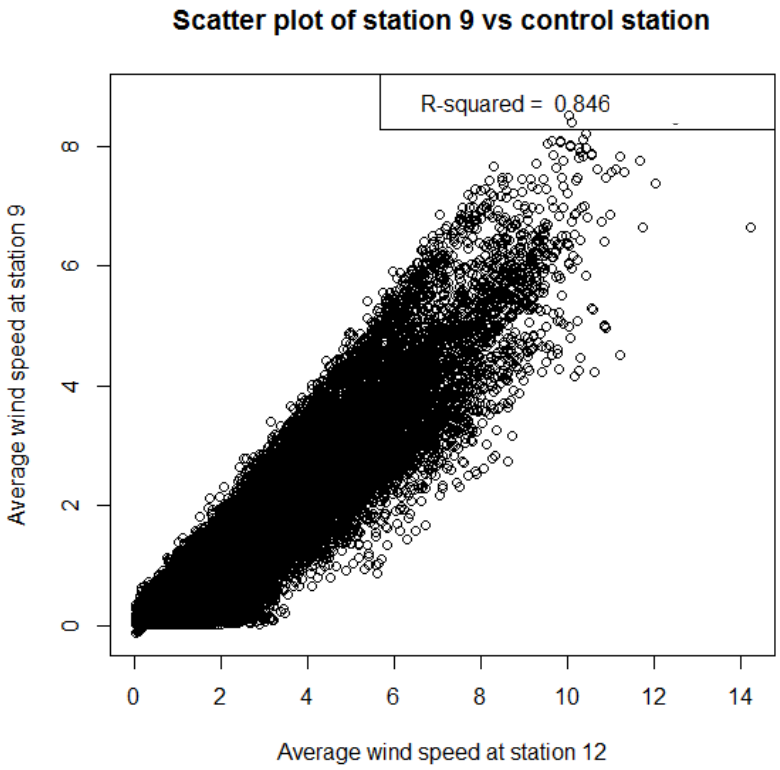

Figure 70: Scatterplot and R - square value for WMU 12 (control) and WMU 9

From Figure 71 it can be seen that the correlation between WMU 10 and the control is good. The R - value for this data is 0.89, whilst the degree to which the data can be estimated is expressed as an R - square value of 0.84. This WMU was located on top of the first slope on the windward side of the TSF and was somewhat sheltered by undulating surface topography and different types of vegetation. The linear relationship of the data is expressed as follows:

Equation 9: Linear relation equation for the WMU 10 vs. the control monitor

$$Y= 0.21+ 0.62X$$

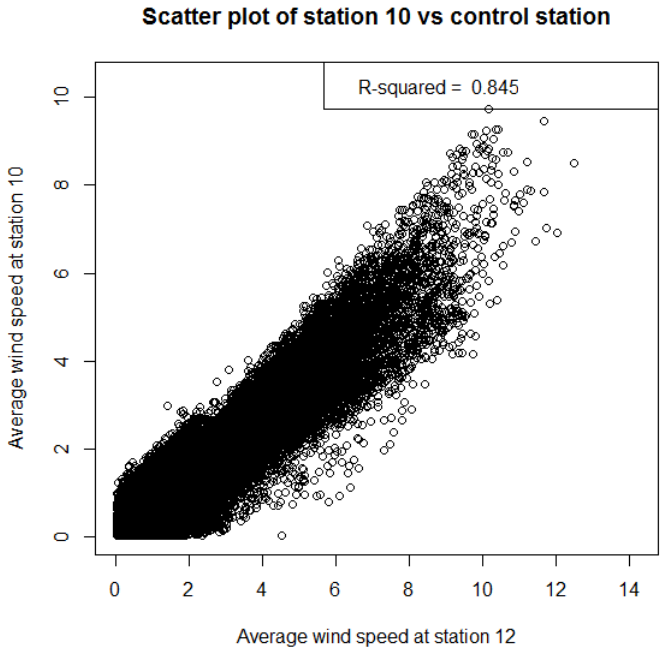

Figure 71: Scatterplot and R – square value for WMU 12 (control) and WMU 10

The WMU 11 was located in the middle of the western slope and was not directly exposed to the dominant wind direction. It was somewhat sheltered by the TSF geometry as well as by the vegetation. From Figure 72 it can be seen that there is a lower correlation between the wind speed data collected from the WMU in question and that of the control. The data correlation is expressed as R = 0.85. The coefficient of determination is presented as 0.72. The linear relationship of the data can be given as follow:

Equation 10: Linear relation equation for the WMU 11 vs. the control monitor

$$Y= 0.39+0.68X$$

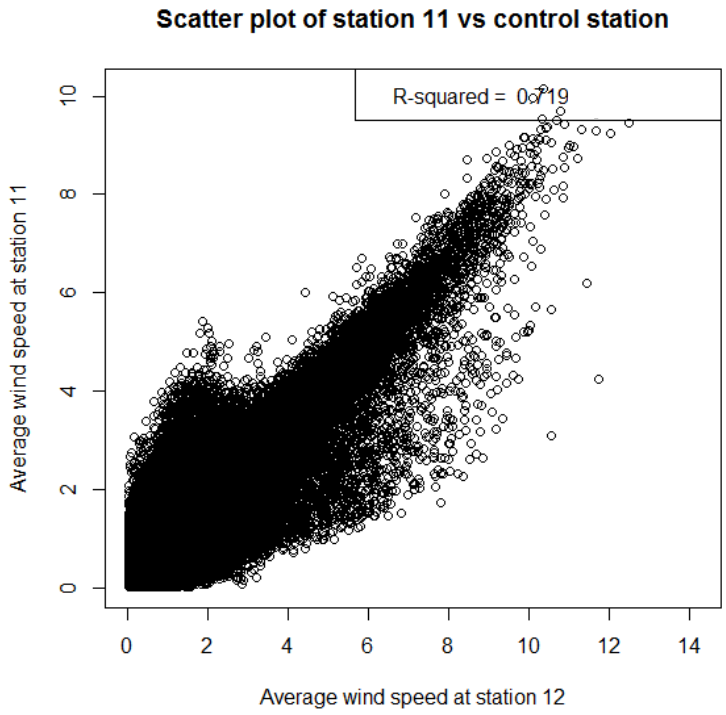

Figure 72: Scatterplot and R - square value for WMU 12 (control) and WMU 11

4.5. Assessment of a control WMU for the quantification of wind-direction dynamics found on the study TSF.

The possible use of a control (WMU 12) to quantify the wind direction dynamics on the research site was also assessed. Assessment took the form of dataset correlations (wind direction) as well as chi-square tests of wind dynamics (direction pairs between the control and other WMUs) observed.

Wind directions that were observed at each of the monitoring sites over time were combined with that of the control WMU. All unique wind dynamic combinations were extracted and used to compile a frequency table of combination occurrences, as can be seen in Annexure 2.

From Table 14 it can be seen that, generally, the dominant wind direction (listed first in the combination) is also dominant on the TSF during the same time (see the second wind direction in the combination). Logically, this is to be expected. What is interesting to note is the occurrence of an E-N combination in the top three categories (out of a possible 256 categories) at some of the WMUs.

It can be deduced from the results that, in general, a north wind at the control WMU will most probably also be from the north on the TSF, however, deviations are possible. Results also show that, at some of the sites, a wind from the east (measured at the control), will influence specific sites on the TSF from the north. It can therefore be assumed that the geometry of the TSF can cause the redirection of airflow and cause shear zones in areas that may not have been suspected to be susceptible to wind.

Table 14: Summary of the three most abundant wind direction combinations measured on the research site

WMU 1*	Frequency	WMU2*	Frequency	WMU3*	Frequency	WMU4*	Frequency
N-N	6024	N-N	5032	N-N	5162	N-N	3595
ENE-N	1441	NE-NE	1538	E-ENE	1766	NE-NE	1474
NNE-N	1273	ENE-ENE	1294	ENE-ENE	1622	ENE-NE	1109
WMU5*	**Frequency**	**WMU6***	**Frequency**	**WMU7***	**Frequency**	**WMU8***	**Frequency**
N-N	6444	N-N	4481	N-N	4314	N-N	5468
ENE-N	3329	ENE-N	1185	NE-NE	1190	ENE-N	1899
E-N	2660	E-N	1121	ENE-N	1091	E-N	1431
WMU9*	**Frequency**	**WMU10***	**Frequency**	**WMU11***	**Frequency**		
N-N	4662	N-N	4404	N-N	4423		
ENE-ENE	1788	ENE-ENE	1853	ENE-N	2350		
NE-NE	1166	E-ENE	1461	NE-N	2118		

Direction combinations reported as WMU 12 – TSF WMUs

Datasets for the different WMUs were also assessed for linear correlation, i.e. which of the datasets are most alike.

Table 15: Wind dynamic correlation between different WMUs

	WMU 1	*WMU 2*	*WMU 3*	*WMU 4*	*WMU 5*	*WMU 6*	*WMU 7*	*WMU 8*	*WMU 9*	*WMU 10*	*WMU 11*
WMU 1	1										
WMU 2	0.9	1									
WMU 3	0.84	0.94	1								
WMU 4	0.82	0.93	0.9	1							
WMU 5	0.81	0.63	0.6	0.57	1						
WMU 6	0.92	0.92	0.91	0.89	0.78	1					
WMU 7	0.87	0.92	0.9	0.95	0.7	0.95	1				
WMU 8	0.91	0.79	0.76	0.72	0.93	0.89	0.82	1			
WMU 9	0.82	0.92	0.94	0.88	0.65	0.92	0.91	0.78	1		
WMU 10	0.81	0.88	0.95	0.84	0.65	0.91	0.87	0.78	0.96	1	
WMU 11	0.91	0.74	0.68	0.73	0.89	0.86	0.82	0.92	0.69	0.7	1

Correlation matrices such as that in Table 15 can be used to identify areas that might not be subjected to the same conditions that are measured at a control site. In this specific research, it can be seen that the wind direction relationship between the control wind monitoring unit and assessment sites that were measured at WMUs 5, 8 and 11 differ to the greatest extent from the other sites. These areas might therefore require different wind mitigation strategies than the rest of the TSF and may also generate dust to a different extent than the other areas.

The wind monitoring units 5, 8 and 11 were all situated on lower slopes and was often in a sheltered position (depending on wind direction). Turbulent airflow, eddies and vortices in the areas of flow separation (where these monitors were located) likely caused the differences in wind direction that were recorded by these monitoring units.

Chi-square tests were also performed in order to determine whether the different WMUs experienced the same wind dynamics over the research period. The aforementioned tests were performed for each of the unique wind direction combinations, with a null hypothesis (H_0) of:

> *H_0 = The wind direction combinations that were measured were independent of the location of the wind monitoring stations.*
>
> *H_1 = The wind direction combinations that were measured were dependant of the location of the wind monitoring stations.*

The results from the test show that the null-hypothesis was rejected in most of the cases. Therefore, the frequencies of wind direction combinations were, in most cases, not the same. Table 30 in Annexure 3 contains the data and chi-square values for all the wind direction combinations that were investigated.

Table 16 shows the scenarios where the null hypothesis was accepted.

Table 16: Acceptance of the null-hypothesis for the wind direction classes

Wind direction class (control vs. site WMU)	Chi-square value
NE-SSW	0.05
NE-SW	0.05
SE-NNW	0.10
SE-NW	0.28
S-NNW	0.05
SSW-NNW	0.13
WNW-ESE	0.10
WNW-NNE	0.06

It is interesting to note that the wind direction combinations that are listed in Table 16 were measured very few times throughout the research period. The combinations of the control wind direction and that monitored on the site are, in some cases, opposite to one another.

The reason for the dependency is unknown. It could be speculated that the atmospheric conditions that give rise to such rare events do not occur often, and when they do occur, causes a change in wind regime throughout the research site. The onset of these atmospheric conditions were possibly due to flow development over a prolong period of time and the subsequent enforcement of flow perturbations such as eddies and vortices at the corners of the TSF.

4.6. High wind-speed event prediction from measured data

Measured wind data presented the opportunity to develop a prediction system for high wind speed events. The purpose of this investigation is to predict possible dust forming events from the Chemwest 5 TSF a day before it takes place. The reason for this is to provide the responsible party the opportunity to deploy dust-suppressing measures before the onset of the dust event. Such predicted data could be useful for landowners or the mine's environmental team. They could prepare in advance for such events and used irrigation systems to mitigate dust. The most applicable dust mitigation measure that could function symbiotically with the Decision-Tree Analysis is irrigation. Irrigation can therefore be applied the day before the predicted dust event and it should effectively prevent any significant amount of wind erosion to take place.

This prediction system was developed by analysing the measured variables from the control monitor at the research site in a Decision-Tree Analysis (DTA) by making use of Statistical Analysis Software (SAS) systems.

The following variables were analysed:

- Maximum air temperature of each day;
- The maximum humidity;
- Average daily wind speed;
- Wind direction (highest frequency for each day).

Data of 321 observations (321 days), of which 197 observations were used to compose the basic statistical model and 49 observations were used for model validation and refining. The model was then verified against 75 recorded observations from the research site.

Decision-tree analyses (DTA) statistically determined the parameters that were associated with windy days, where the mean wind speed was greater than 3 $m.s^{-1}$. Figure 73 shows that the first determining factor of a possible high wind speed day is the mean wind speed of the preceding day. If the wind speed is less than 1.3 $m.s^{-1}$, then there is a 50.0% chance that the wind speed of the following day will not be a windy day. If the wind speed is greater than 1.3 $m.s^{-1}$, then there is a 51.1% chance that the following day will be windy. The next step in the decision tree assesses the maximum recorded temperature for the preceding day. If the maximum temperature is greater than 29.4°C, then there is a 76.9% chance of a windy day. If the wind speed is less than 29.4 $m.s^{-1}$, then the probability that the wind speed will exceed the minimum threshold velocity for the tailings is 40.6%. The last criterion that is assessed in the decision tree is the mean wind speed of the preceding day. If the wind speed is greater than 3.9 $m.s^{-1}$, then there is a 60.0% chance that the wind speed will exceed the minimum wind speed threshold velocity of the material. However, should the mean wind speed be less than 3.9 $m.s^{-1}$, there is only a 31.8% chance that the wind speed of the following day will be significant.

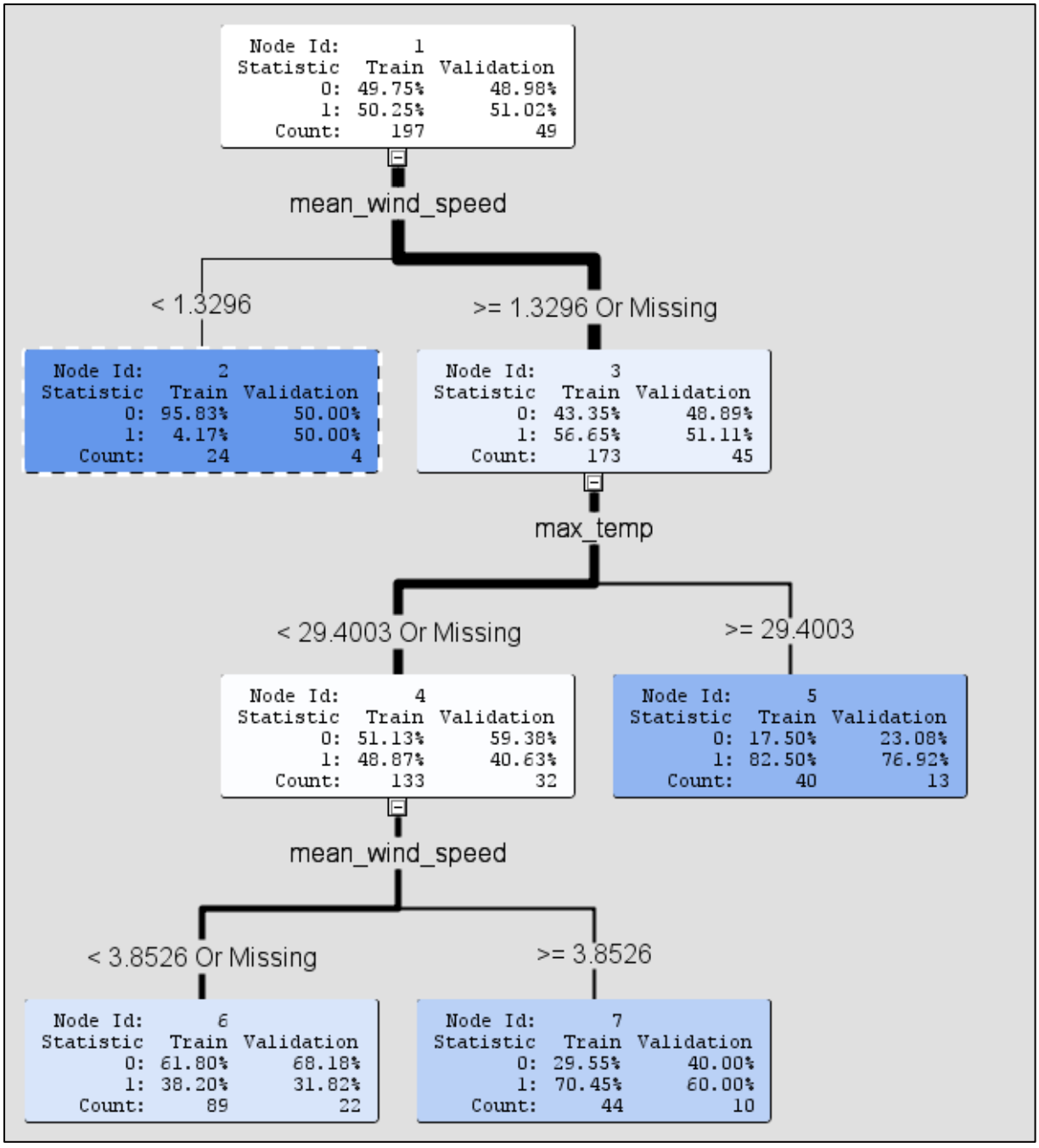

Figure 73: Decision tree for high wind speed events.

Table 17: Misclassification rate - results summary of the decision tree analysis.

Target	Statistics Label	Train	Validation	Test
High-speed	Sum of Frequencies	197	49	75
High-speed	Misclassification Rate	0.28	0.33	0.37

The results show that, when verified against site data, the model was inaccurate for 37% or accurate for 63% of the observations. The result of the analysis does not allow enough certainty to implement the model on the research site. This is because

the implementation of a dust mitigating action, such as irrigation, is a cost-intensive practice and the level of uncertainty present in this analysis will likely make the implementation of this model unfeasible.

It must be stated that this model was developed for the control WMU, which is located on a relatively flat area. Uncertainties in prediction accuracy could further be increased by the intricacies of the airflow over the TSF. The development of a prediction system that can, with a significant of certainty, predict erosive wind speeds on specific locations on a TSF is a subject for a different study, as it exceeds the scope of this research project.

Monitoring additional variables could potentially improve the model's accuracy. Possible variables that can achieve the aforementioned goal are rainfall and solar radiation.

CHAPTER 5: CONCLUSIONS AND RECOMMENDATIONS

This chapter provides the conclusion to the different components of this research. Availability and shortages of literature are highlighted, the success of monitoring wind dynamics on a TSF for nearly a year, the relationship between a reference site and monitoring points (in terms of wind dynamics), the analyses of the tailings crusts and predictive decision-tree analysis are discussed. This chapter is finalised by recommendation for future research.

5.1. Literature survey of the key research in the field of tailings wind erosion

Literature review was of importance for the successful execution of this research and work that was performed by scientists in the past shed light on the research topics of the research. This ranged from the smallest, immeasurable inter-particle forces to global atmospheric circulation patterns to environmental and human health, legislative requirements and airflow characteristics around objects. The literature review thus supplied the principles for the experimental designs and execution thereof.

In the literature review it was found that much work has been done in the field of wind erosion and airflow dynamics. Most of the research was focussed on natural dune systems, with very little research on TSFs. The author is of the opinion that much more research is required on wind dynamics over TSFs to fill the current void in the literature.

Results from past research provided the information required for the sections of this research that could not be investigated in this study. These included human and environmental health impacts of tailings material, relevant legislation pertaining to dust from TSFs as well as sections of the site description. Results from numerous research papers (Blight, 2008:523, Dang, 2013:368; Ojelede, 2012:178; Plumlee and Morman, 2011:399, Nelson, 2013:19520) on the subject of human health and exposure to tailings, indicated that particles from gold TSFs (and others) can affect human health. Environmental pollution issues were briefly reviewed and it was found that dust (from TSFs) could potentially pollute water, soil, air and cause

decreased plant mass yield by blocking solar radiation to plant leaves (Blight, 2008:523).

Legislation that govern dust emissions from TSF are well developed in South Africa. Several general notices and acts govern fugitive dust from mines and are aimed at decreasing the pollution that associated with dust. The basis for all the relevant legislation is accommodated within the Constitution of the Republic of South Africa (Section 24).

Literature resources described the mechanisms and drivers behind certain wind phenomena, which is governed by global circulation patterns that are brought on by the unequal heating of the earth's surface (Strahler & Strahler, 2005:174). This driving mechanism can also take place on smaller scale. Atmospheric circulation over southern Africa, was also investigated. This section greatly leaned on the work of researchers such as Taljaard (1958:32), Taljaard and van Loon (1963:39), Tyson and Preston-Whyte (2012:185), and associated authors. These scientists conducted research in order to characterise the circulation types that influence the weather in South Africa. It was important, for the purpose of this research, to understand the driving mechanisms behind wind erosion. The identification of different weather systems can accordingly give a good indication, qualitatively speaking, of the severity of wind to be expected. This portion of the research also emphasises the fact that wind will most probably persist throughout human existence and that its effects will have to be managed.

5.2. Measuring the wind dynamics (speed and direction) over the Chemwest 5 TSF using purpose designed monitoring units for a period of one year

This section of the research was successfully completed for 11 months. The main focus of the research was to gain a better understanding of the wind dynamics over the Chemwest 5 TSF. The results found that wind speed and direction data from a regional weather station would not have served justice to the intricate airflow over the Chemwest 5 TSF (Figure 62 to Figure 72).

The wind profiles were determined for different locations on the TSF. This was established by creating wind roses for each of the WMUs. The analyses showed that the major wind direction for the area was from the N, with a secondary

component from the ENE. The wind directions and speeds measured on the Chemwest 5 TSF varied from that of the reference WMU. The most significant difference was the measured wind speed on the facility. The monitoring data demonstrated that the wind speed increased with elevation above the ground surface. This was likely caused by a fluid-compression effect that has been reported on for natural dunes and tailings facilities (Blight, 2007:103; Lancaster, *et al.,* 1996:55; Sweet & Kocurek, 1990:1027; Walker & Nickling, 2002:52; Zhang, *et al.,*2000:360).

The results also illustrated an over representation of wind from the north. It is proposed that this is due to the redirection of airflow over the TSF and along the north-south orientated slopes. The area of the slope that was exposed to wind shear is consequently more extensive than expected. This result increases the understanding of airflow on the TSF. The research also found that wind that approaches the TSF is likely diverted around the TSF before it collides with the facility. This corresponds to an illustration by Greeley and Iverson (1985: 205 – 209). The deflection without impact is possible by considering the fluid nature of air and that air is pulled in a direction, allowing a component of the incoming wind to be deflected in the air stream that flowed around the TSF.

A minor component of the monitoring was focussed on the variation of the regional wind profile over a period of time. The results established that the highest wind speed months were recorded to be October, November and December, with August being one of the months with the lowest wind speeds (Figure 60). Diurnal wind-speed profiles were also extracted from the data and can be referred to in Figure 61. The data from the research therefore allows for a better understanding of higher wind shear areas as well as the areas that need to be prioritised with dust suppression efforts.

5.3. Determining whether a reference site can be used to predict surface wind conditions on selected locations on the Chemwest 5 TSF

Linear relationship equations were derived for the wind speed observation of each of the WMUs and can be used to predict wind speed from a control station at different areas of the TSF. Aside from WMU 1, the monitoring units had good correlations with the reference WMU. It can be verified in Figure 58 that each WMU had its own

wind speed profile, indicating that the TSF did not experience uniform wind speed conditions. These unique wind profiles changed over the course of a year and a single annual wind cycle was identified.

Variation in wind direction between the reference WMU and the TSF WMUs were investigated by means of chi-square tests. Findings of the tests revealed that the wind direction differences were statistically significant for only eight of the possible 256 wind direction combinations between the reference WMU and the TSF WMUs. From a statistical perspective, there was little variation between the reference WMU and the wind directions measured on the TSF. The conclusion to this section of the research is that the geometry (and other surface features) of the TSF did not cause major directional disparities in the wind directions measured on the TSF (aside from the direction combination mentioned in Table 16) and that the dominant wind direction is fairly representative of wind direction conditions on the TSF. Redirection of airflow that was observed was as an over representation of wind from the north and was recorded for much of the research site.

5.4. Investigate surface crust structures on the Chemwest 5 TSF by means of electron microscopy

Given that wind erosion on TSFs is dependent on both the tailings and wind characteristics, tailings structures that are not conducive to particle liberation were investigated. These structures occur in a variety of forms and the investigation of all these structures exceed the scope of the research. Due to this reason, only tailings crusts were investigated. Numerous different crusts were identified, these included drying crusts, chemical crusts and erosion crusts. Results from the SEM photographs and analyses showed that the structures were predominantly siliceous based.

Physical crusts exhibited gypsum bonds between the silicate particles. Given the mechanics of wind erosion, it may be assumed that these crusts formed a layer that was resistant to wind erosion, since the particles were not loosely distributed, but assumed a horizontal, tightly packed structure that was reinforced with gypsum precipitate. This preferred orientation and gypsum crystal intergrowths were absent from the chemical and erosion crust. The mechanism by which the chemical crust formed seemed to be by the accumulation of gypsum precipitate on a siliceous

particle bed. Hydraulic settling of the tailings material appeared to have caused the erosion resistant material that gave rise to the erosion crust. All these crust structures should exhibit resistance to wind erosion, but this was beyond the scope of this research to quantify.

Investigation of the crust structures revealed that these structure units, that are readily found on gold TSFs, likely have a positive effect of increasing the resistance of tailings material to wind shear. If these crusts are broken, then the dry, structureless material that underlies it will be exposed to the action of wind, resulting in wind erosion and subsequently dust. Thereby acting as a preferential starting point for dust emissions.

5.5. Determining the minimum wind speed threshold velocity (u_t) of the gold tailings material of the Chemwest 5 TSF by means of wind-tunnel tests

Erodibility of the tailings particles was investigated by the use of a wind tunnel. These tests were conducted on tailings that had no structure and very low moisture contents and therefore represented material that is exceptionally vulnerable to wind erosion. Results of the tests are presented in Table 11 and shows that a relatively low wind speed (3 $m.s^{-1}$) was required for initial particle liberation from a particle bed.

5.6. Determining whether a reference WMU can be used to predict erosive wind-speed days using a decision-tree analysis (DTA).

A DTA system could be used in practice to support dust suppression decisions. The statistical model can predict, to within 62.7% accuracy, whether or not irrigation should be used to suppress dust that may arise due to a wind speed of 3.0 $m.s^{-1}$ or greater.

The verification of this model showed that the accuracy is not sufficient to warrant the implementation of it on the Chemwest 5 TSF. If additional atmospheric variables were to be monitored, then the accuracy of the model will likely improve.

5.7. Recommendations for future research

This research is composed out of several different topics, each of which deserves individual attention in future research. It was, however, beyond the scope of this

dissertation to investigate each of these in depth. From this research, numerous other research questions originated, which includes:

- Effects of tailings physical and chemical crusting on wind erosion;
- Chemical composition of crusts on TSFs and their associated reactions to environmental stimuli;
- Exploring the effects of dust mitigation strategies on the sites where they are implemented;
- Studying the effect that micro-morphology has on the wind speed as well as dust formation or particle liberation.
- Monitoring of additional atmospheric conditions that could improve the accuracy of the decision-tree analysis;
- Health impacts of the tailings material from the TSF in the study area;
- Ambient PM levels around the major dust sources in the area;
- Studying the vertical wind profile around and on the TSFs of the study area;
- Fraction size distribution of windblown dust, and;
- The effects that crusts have on surface stability and the wind speed threshold value of different types of crusts.

REFERENCES

Agassi, M., Morin, J. & Shainberg, I. Division S-6 – Soil and water management and conservation. *Soil Science Society of America journal,* 49:186-190.

Akcil, A. & Koldas, S. 2006. Acid mine drainage (AMD): causes, treatment and case studies. *Journal of cleaner production,* 14:1139-1145.

Al, T.A., Martin, C.J. & Blowes, D.W. 2000. Carbonate-mineral/water interactions in sulphide-rich mine tailings. *Geochimica et cosmochimica acta,* 64(23):3933-3948.

Alfaro, S.C. 2008. Influence of soil texture on the binding energies of fine mineral dust particles potentially released by wind erosion. *Geomorphology,* 93:157-167.

Anhaeusser, C.R. & Maske, S., *eds.* 1986. Mineral deposits of southern Africa Vol I. Johannesburg: The Geological Society of South Africa.

Aucamp, P.J. 2000. Trace element pollution of soils by abandoned gold mine tailings near Potchefstroom, South Africa. Pretoria: UP. (Dissertation – MSc).

Bagnold, R.A. 1965. The physics of blown sand and desert dunes. London: Methuen & Co. Ltd.

Belnap, J. & Gillette, D.A. 1998. Vulnerability of desert biological soil crusts to wind erosion: the influences of crust development, soil texture, and disturbances. *Journal of arid environments,* 39:133-142.

Ben-Hur, M., Shainberg, I., Bakker, D. & Keren, R. 1985. Effect of soil texture and $CaCO_3$ content on water infiltration in crusted soil as related to water salinity. *Irrigation science,* 1985:281-294.

Bini, C. & Gaballo, S. 2006. Pedogenic trends in anthrosols development in sulfidic mine spoils: A case study in the Temperino mine archaelogical area (Campiglia Marittima, Tuscany, Italy). *Quaternary International,* 156-157:70-78.

Blight, G.E. 2007. Wind erosion of tailings dams and the mitigation of the dust nuisance. *The journal of the southern African institute of mining and metallurgy*, 107:99-107.

Blight, G.E. 2008. Wind erosion of waste impoundments in arid climates and the mitigation of dust pollution. *Waste management and research,* 26:523-533.

Blight, G.E. 2012. Long-term research on amelioration of wind and water erosion of mine tailings storages in Southern Africa. *Transactions of the Royal Society of South Africa,* 67(2):91-102.

Bolt, K., Hartman, P., Fleige, H. & Horn, R. 2011. Determination of critical soil water content and matric potential for wind erosion. *Journal of soils and sediments,* 11:209-220.

Campbell Scientific. 2011a. CR200/CR200X Series Dataloggers Revision: 6/11. http:// s.campbellsci.com/documents/us/manuals/cr200.pdf Date of access: 25 Jun. 2013.

Chepil, W.S. 1950a. Properties of soil which influence wind erosion: I. The governing principle of surface roughness. *Soil Science*, 69 (2):149-162.

Chepil, W.S. 1950b. Properties of soil which influence wind erosion: II. Dry aggregate structure as an index of erodibility. *Soil Science*, 69 (5):403:414.

Chepil, W.S. 1951. Properties of soil which influence wind erosion: III. Effect of apparent density on erodibility. *Soil Science*, 71 (2):141-153.

Chepil, W.S. 1958. Soil conditions that influence wind erosion. Washington: United States Department of Agriculture.

Chepil, W.S. & Woodruff, N.P. 1963. The physics of wind erosion and its control. *Advances in agronomy*, 15:253.

Constitution *see* South Africa.

Dang, G.T.T., Barros, N., Higgins, S.A., Langley, R.L. & Lipton, D. 2013. Descriptive review of asbestosis and silicosis hospitalization trends in North Carolina, 2002-2011. *North Carolina medical journal,* 74(5):368-375.

Daniell, A. 2015. Geochemical monitoring of soil pollution from the MWS-5 gold tailngs facility on the Farm Stilfontein. Potchefstroom: NWU. (MSc Dissertation).

Dong, D., Xu, G., Sun, Y. & Hu, P. 1995. Lung cancer among workers exposed to silica dust in Chinese refractory plants. *Scandinavia journal of work, environment & health,* 21:69-72.

Eldridge, D.J. & Leys, J.F. 2003. Exploring some relationships between biological soil crusts, soil aggregation and wind erosion. *Journal of arid environments,* 53:457-466.

Fang, H.Y., Cai, Q.G., Chen, H. & Li, Q.Y. 2007. Mechanism of formation of physical soil crust in desert soils treated with straw checkerboards. *Soil & tillage research,* 93:222-230.

Farres, P.J. 1978. The role of time and aggregate size in the crusting process. *Earth surface processes,* 3:243-254.

Farres, P.J. 1980. Some observations on the stability of soil aggregates to raindrop impact. *Catena*, 7:223-231.

Frank, A.J. & Kocurek, G. Airflow up the stoss slope of sand dunes: limitations of current understanding. *Geomorphology,* 17:47-54.

Ferreira, A.D. & Lambert, R.J. 2011. Numeric and wind tunnel modelling on the windbreak effectiveness to control the aeolian erosion of conical stockpiles. *Environmental fluid mechanics,* 11:61-76.

Gal, M., Arcan, L., Shainberg, I. & Keren, R. 1984. Effect of exchangeable sodium and phosphogypsum on crust structure – scanning electron microscope observations. *Soil Science Society of America Journal*, 48:872-878.

Gicheru, P., Gachene, C., Mbuvi, J. & Mare, E. 2004. Effects of soil management practices and tillage systems on surface soil water conservation and crust formation on a sandy loam in semi-arid Kenya. *Soil & tillage research,* 75:173-184.

Gieré, R., Sidenko, N.V. & Lazareva, E.V. 2003. The role of secondary minerals in controlling the mitigation of arsenic and metals from high-sulfide wastes (Berkul gold mine, Siberia). *Applied geochemistry,* 18:1347-1359.

Google Earth. 2016. https://earth.google.com Date of access: 27/10/2016.

Gong, G., Liu, J., Shao, Q. & Zhai, J. 2014. Sand-fixing function under the change of vegetation coverage in a wind erosion area in northern China. *Journal of resources and ecology,* 5(2):105-114.

Greeley, R. & Iverson, J.D. 1985. Wind as a geological process on Earth, Mars, Venus and Titan. Great Britain: Cambridge University Press.

Greenwood, P.E. and Nikulin, M.S. 1996. A guide to chi-squared testing. Canada: John Wiley and Sons.

Grondklassifikasiewerkgroep. 1991. Grondklassifikasie: ‘n Taksonomiese sisteem vir Suid-Afrika. Pretoria: Departement van Landbou en Ontwikkeling.

Han, Q., Qu, J., Zhang, K., Zu, R., Niu, Q. & Liao, K. 2009. Wind tunnel investigation of the influence of surface moisture content on the entrainment and erosion of beach sand by wind using sands from tropical humid coastal southern China. *Geomorphology,* 104:230-237.

Helalia, A.M., Letley, J. & Graham, R.C. 1988. Crust formation and clay migration effects on infiltration rate. *Soil Science Society of America Journal,* 52: 251-255.

Hnizdo, E., Murrey, J. & Klempman, S. 1997. Lung cancer in relation to exposure to silica dust, silicosis and uranium production in South African gold miners. *Thorax*, 52:271-275.

Hong, S.W., Lee, I.B., Seo, I.H., Kwon, K.S. Kim, T.W., Son, Y.H. & Kim, M. 2014. Measurement and prediction of soil erosion in dry field using portable wind erosion tunnel. *Biosystems engineering,* 118:68-82.

Hupy, J.P. 2004. Influence of vegetation cover and crust type on wind-blown sediment in a semi-arid climate. *Journal of arid environments,* 58:167-179.

Hurry, L. & van Heerden, J. Suider-Afrikaanse weerpatrone: ‘n Gids tot die vertolking van sinoptiese kaarte. Goodwood: Via Afrika Beperk.

Jackson, S.P. & Tyson, P.D. 1971. Aspects of weather and climate over southern Africa. Johannesburg: University of the Witwatersrand. (Occasional Paper No.6).

Jia, R.L., Li, X.R., Liu, L.C., Gao, Y. H. & Zhang, X.T. 2012. Differential wind tolerance of soil crust mosses explains their micro-distribution in nature. *Soil biology & biochemistry,* 45:31-39.

Kneen, M.A., Ojelede, M.E. & Annegarn, H.J. Housing and population sprawl near tailings storage facilities in the Witwatersrand: 1952 to current. *South African journal of science,* 111:1-9.

Lancaster, N., Nickling, W.G., McKenna Neuman, C.K. & Wyatt, V.E. 1996. Sediment flux and airflow on the stoss slope of a barchan dune. *Geomorphology*, 17:55-62.

Langson, G. & McKenna Neuman, C. 2005. An experimental study on the susceptibility of crusted surfaces to wind erosion: A comparison of the strength properties of biotic and salt crusts. *Geomorphology,* 72:40-53.

Leenders, J.K., Boxel, J.H. & Sterk,G. 2007. The effect of single vegetation elements on wind speed and sediment transport in the Sahelian Zone of Burkina Faso. *Earth surface processes and landforms*, 32:1454-1474.

Lu, C.X., Yu, G., Xiao, Y. & Xie, G. 2013. Wind tunnel simulation and evaluation of soil conservation function of alpine grassland in Qinghai-Tibet Plateau. *Ecological economics,* 86:16-20.

Lu, X. & Wang, H. 2012. Microbial oxidation of sulfide tailings and the environmental consequences. *Elements,* 8:119-124.

McCarthy, T. and Rubidge, B. 2005. The story of earth and life. Cape Town: Struik Publishers.

McKenna Neuman, C., Boulton, J.W., Sanderson, S. 2009. Wind tunnel simulation of environmental controls on fugitive dust emissions from mine tailings. *Atmospheric environment*. 43:520-529.

McKenna Neuman, C., Lancaster, N. & Nickling, W.G. 1997. Relations between dune morphology, air flow, and sediment flux on reverse dunes, Silver Peak, Nevada. *Sedimentology,* 44:1103-1113.

McKenna Neuman, N., Lancaster, C. & Nickling, W.G. 2000. The effect of unsteady winds on sediment transport on the stoss slope of a transverse dune, Silver Peak, NV, USA. *Sedimentology,* 47:211-226.

Neels, C., Bril, H., Courtin-Nomade, A. & Dutreuil, J. 2003. Factors affecting natural development of soil on 35-year-old sulphide-rich mine tailings. *Geoderma,* 111:1-20.

Nelson, G. 2013. Occupational respiratory diseases in the South African mining industry. *Global health action,* 6:19520.

Nickling, W.G. 1984. The stabilizing role of bonding agents on the entrainment of sediment by wind. *Sedimentology,* 31:111-117.

Oguntoke, O. & Annegarn, H.J. 2014. Effectiveness of mediation on the resolution of environmental complaints against the activities of gold mining industries in the Witwatersrand region. *The clean air journal*, 24(2):17-23.

Oguntoke, O., Ojelede, M.E. & Annegarn, H.J. 2013. Frequency of mine dust episodes and the influence of meteorological parameters on the Witwatersrand area, South Africa. *International Journal of Atmospheric Sciences*. 2013:1-10.

Ojelede, M.E. 2012. Risk assessment of atmospheric emissions from gold mine tailings on the Witwatersrand. Johannesburg: University of Johannesburg. (PhD Thesis).

Onofiok, O. & Singer, M.J. 1984. Scanning electron microscope studies of surface crusts formed by simulated rainfall. *Soil Science Society of America Journal,* 48:1137-1143.

Plumlee, G.S. & Morman, S.A. 2011. Mine wastes and human health. *Elements,* 7:399-404.

Pagliai, M., Vignozzi, N. & Pellegrini, S. 2004. Soil structure and the effect of management practices. *Soil and tillage research,* 79:131-143.

Qian, G., Dong, Z., Luo, W. & Wang, H. 2009. Variations in horizontal and vertical velocities over two-dimensional transverse dunes: A wind tunnel simulation of the effect of windward slope. *Journal of arid environments,* 73:1109-1116.

R.M. Young Company. 2011. Model 41382VC Relative humidity / temperature probe with Voltage output. http://www.youngusa.com/Manuals/41382VC-90(D).pdf Date of access: 03 Sep. 2013.

R.M. Young Company. 2012. Meteorological Instruments: Instructions Wind Monitor Model 05103. http://www.youngusa.com/Manuals/05103-90(K).pdf Date of access: 25 Jun. 2013

Roth, C.H. 1997. Bulk density of surface crusts: depth functions and relationships to texture. *Catena,* 29:223-237.

Roussel, C., Neel, C. & Bril, H. 2000. Minerals controlling arsenic and lead solubility in an abandoned gold mine tailings. *The science of the total environment,* 263:209-219.

Scalenghe, R. & Ferraris, S. 2009. The first fourth years of a technosol. *Pedosphere,* 19(1):40-52.

Scheifinger, H. & Held, G. 1997. Aerosol behaviour on the South African Highveld. *Atmospheric environment,* 31(21):3497-3509.

Shao, Y. & Lu, H. 2000. A simple expression for wind erosion threshold friction velocity. *Journal of geophysical research,* 105(D17):22437-22443.

Simms, P., Grabinsky, M. & Guosheng, Z. 2007. Modelling evaporation of paste tailings from the Bulyanhulu mine. *Canadian geotechnical journal*, 44:1417-1432.

Sithole, J., Lethlage, D., Mphati, D., Jood, V., Malahlela, Annegarn, H.J. & Mthethwa, D. 2000. A case study in environmental conflict resolution between the community and the Rand Lease Mine tailings dump. *Journal of clean air,* 10(5):3-6.

South Africa. 1996. Constitution of the Republic of South Africa 108 of 1996.

Strahler, A. & Strahler, A. 2005. Physical geography: Science and systems of the human environment, third edition. USA: John Wiley and Sons.

Sweet, M.L. & Kocurek, G. 1990. An empirical model of Aeolian dune lee-face airflow. *Sedimentology*, 37:1023-1038.

Taljaard. J.J. 1958. Cyclogenesis, cyclones and anticyclones in the southern hemisphere during autumn 1958. *Notos,* 13:31-36.

Taljaard, J.J. & van Loon, H. 1963. Cyclogenesis, cyclones and anticyclones in the southern hemisphere during summer 1957 – 1958. *Notos,* 12:37-41.

Taljaard, J.J. 1967. Development, distribution and movement of cyclones and anticyclones in the southern hemisphere during the IGY. *Journal of applied meteorology,* 6(6):973:987.

Taljaard, J.J. 1985. Cut-off lows in the South African region. *South African weather bureau technical paper,* no. 14.

Tan, L., Zhang, W., Liu, B., An, Z. & Li, J. 2013. Simulation of wind velocity reduction effect of gravel beds in a mobile tunnel atop the Mogao Grottoes of Dunhuang, China. *Engineering geology,* 159:67-75.

Thompson, F. 2006. Oxford mathematics study dictionary. Singapore: Oxford University Press.

Tsoar, H., Blumberg, D.G., Stoler, Y. 2004. Elongation and migration of sand dunes. *Geomorphology*, 54:293-302.

Tsoar, H., White, B. & Berman, E. 1996. The effect of slopes on sand transport – numerical modelling. *Landscape and urban planning,* 34:171-181.

Tutu, H., McCarthy, T.S., Cukrowska, E. 2008. The chemical characteristics of acid mine drainage with particular reference to sources, distribution and remediation: The Witwatersrand Basin, South Africa as a case study.

Tyson, P.D. 1969. Atmospheric circulation and precipitation over South Africa. Johannesburg: University of the Witwatersrand. (Occasional Paper No.2).

Tyson, P.D. 1987. Climate change and variability in southern Africa. Cape Town: Oxford University Press.

Tyson, P.D. & Preston-Whyte, R.A. 1993. The atmosphere and weather of southern Africa. Cape Town: Oxford University Press.

Tyson, P.D. & Preston-Whyte, R.A. 2012. The weather and climate of southern Africa: Second edition. Cape Town: Oxford University Press.

Tyson, P.D., Garstang, M. & Swap, R. 1996. Large-scale recirculation of air over southern Africa. *Journal of applied meteorology,* 35:2218-2236.

Van Deventer, P.W. 2014. Chemwest 5 TSF location [personal interview]. 24 Jan., Potchefstroom.

Van Deventer, P.W. 2015. Crust formation and surface compaction by means of hydraulic settling on gold TSFs [30 Nov., Potchefstroom].

Van Wyk, E., Cilliers, S.S. & Bredenkamp, G.J. 1997. Randteveldplantegroei van Klerksdorp, Noordwes Provinsie, Suid-Afrika. *Tydskrif vir natuurwetenskappe en tegnologie*, 16(2):74-85.

Von Gogh, R.G. & Tyson, P.D. 1977. Aspects of wintertime mesoscale temperature structure over Johannesburg. Johannesburg: University of the Witwatersrand. (Occasional Paper No.17).

Walker, I.J. 1999. Secondary airflow and sediment transport in the lee of a reversing dune. *Earth surface processes and landforms, 24: 437-448.*

Walker, I.J. & Nickling, W.G. 2002. Dynamics of secondary airflow and sediment transport over and in the lee of transverse dune. *Progress in physical geography, 26:47-75.*

Weaver, C.M. & Wiggs, G.F.S. 2011. Field measurements of mean and turbulent airflow over a barchan sand dune. *Geomorphology*, 128:32-41.

Wiggs, G.F.S., Livingstone, I. & Warren, A. 1996. The role of streamline curvature in snad dune dynamics: evidence from field and wind tunnel measurements. *Geomorphology*, 17:29-46.

Yan, Y., Wu, L. Xin, Xiaoping, Wang, X. & Yang, G. 2015. How rain-formed soil crust affects wind erosion in a semi-arid steppe in northern China. *Geoderma,* 249-250:79-86.

Youssef, R., Visser, S.M., Karssenberg, D., Erpul, G., Cornelis, W.M. Gabriels, D. & Poortinga, A. The effect of vegetation patterns on wind-blown mass transport at the regional scale: A wind tunnel experiment. *Geomorphology,* 159-160:2012.

Zang, C.L., Zou, X.Y., Gong, J.R., Liu, L.Y. & Liu, Y.Z. 2004. Aerodynamic roughness of cultivated soil and its influences on soil erosion by wind in a wind tunnel. *Soil & tillage research,* 75:53-59.

Zhang, W., Qu, J., Dong, Z., Li, X. & Wang, W. 2000. The airflow field and dynamic processes of pyramid dunes. *Journal of arid environments,* 45:357-368.

Zhang, Y.M., Wang, H.L., Wang, X.Q., Yang, W.K. & Zhang, D.Y. 2006. The microstructure of microbiotic crust and its influence on wind erosion for a sandy soil surface in the Gurbantuggut Desert of Northern China. *Geoderma,* 132:441-449.

Zobeck, T.M. 1991. Soil properties affecting wind erosion. *Journal of sail and water conservation,* 46(2):112-118.

Zobeck, T.M., Baddock, M., Van Pelt, R.S., Tatarko, J. & Ascosta-Martinez, V. 2013. Soil property effects on wind erosion of organic soils. *Aeolian research,* 10:43-51.

ANNEXURE 1: SEM IMAGES OF THE CRUST STRUCTURES.

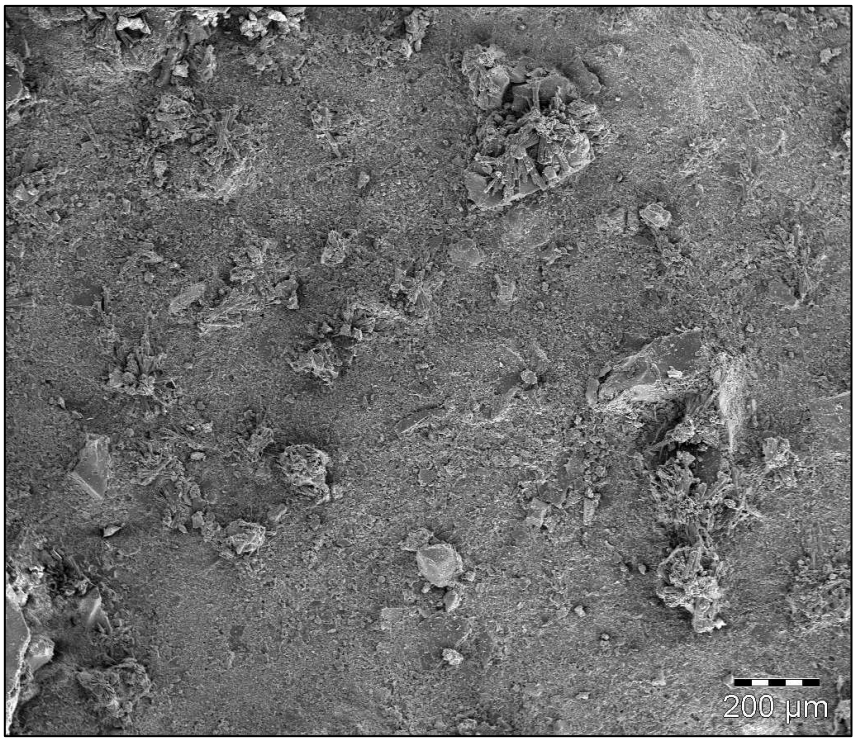

Figure 74: SEM image of the drying crust L1

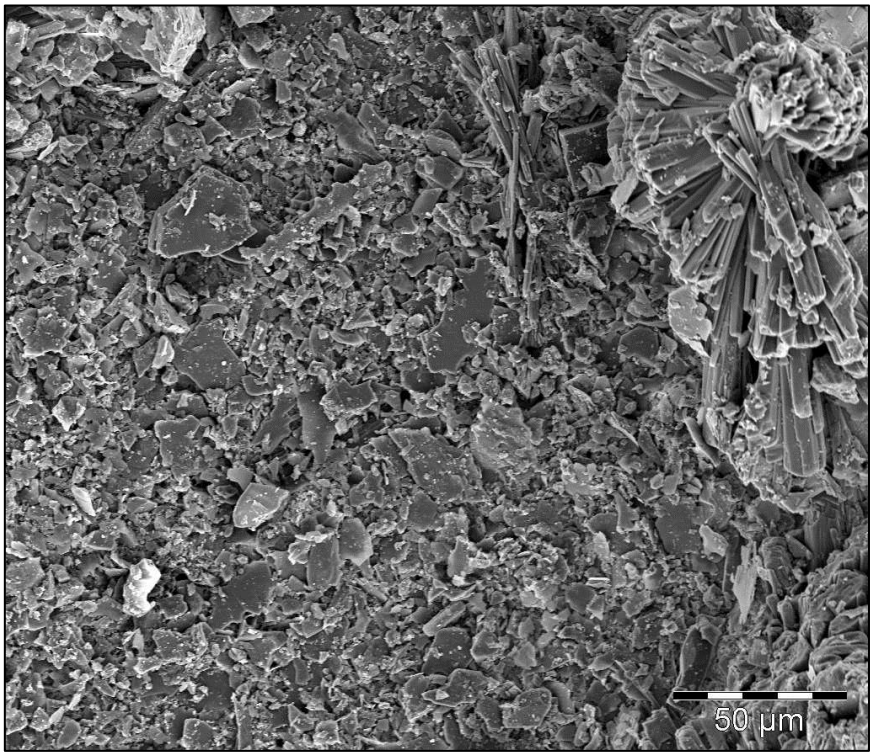

Figure 75: SEM image of the drying crust L1

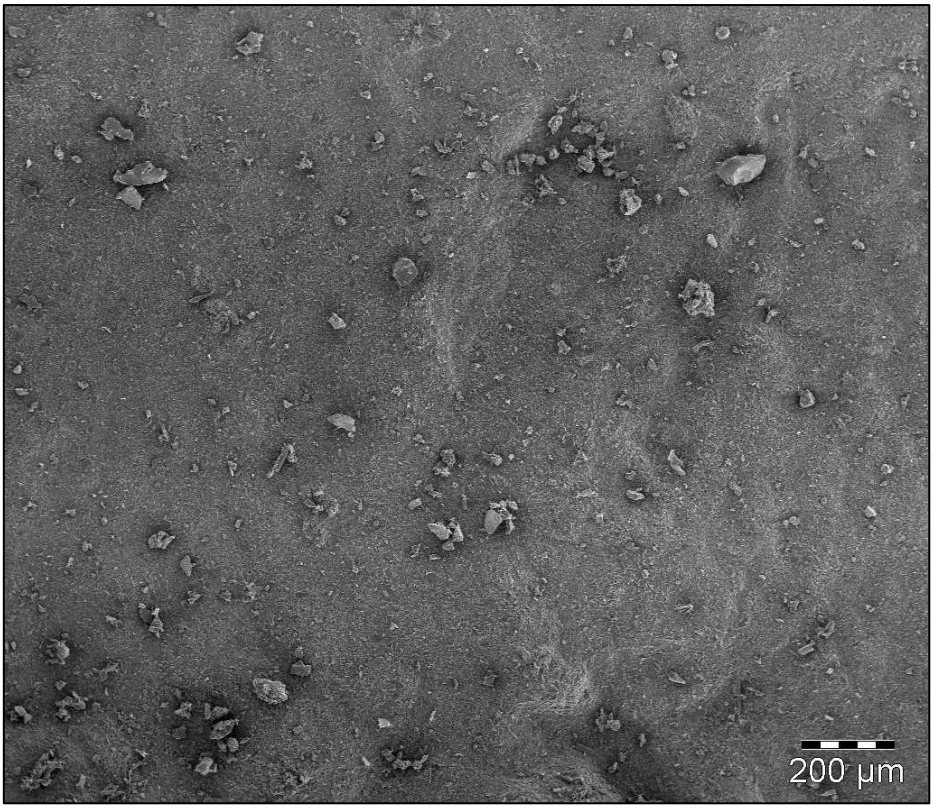

Figure 76: SEM of the drying crust L8 Top

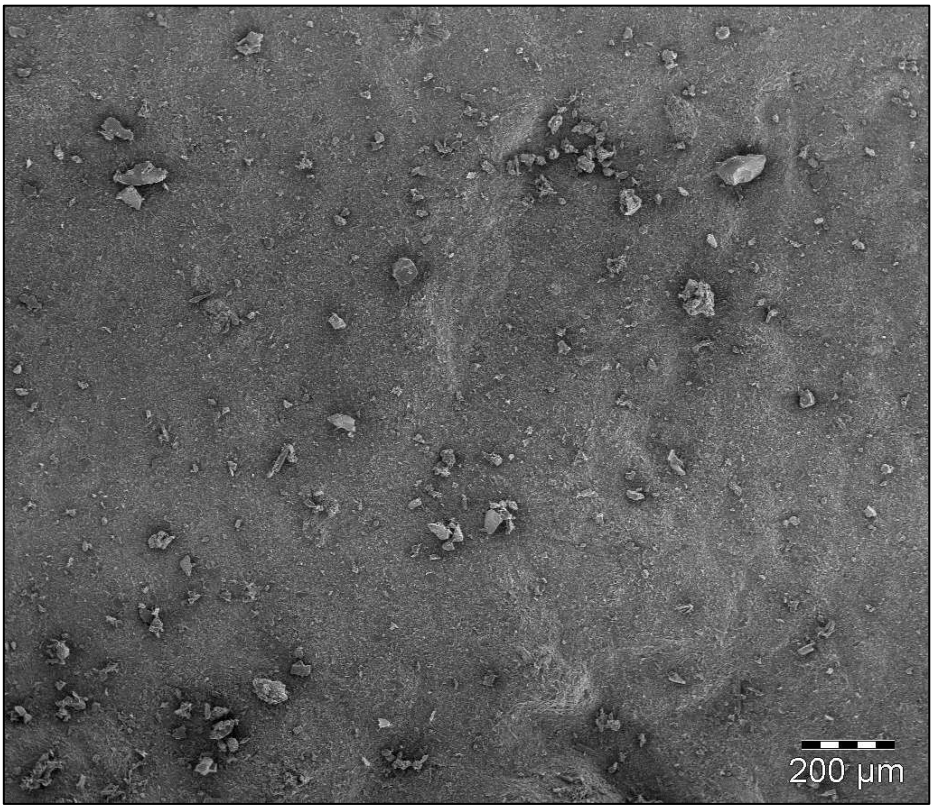

Figure 77: SEM of the drying crust L8 Top

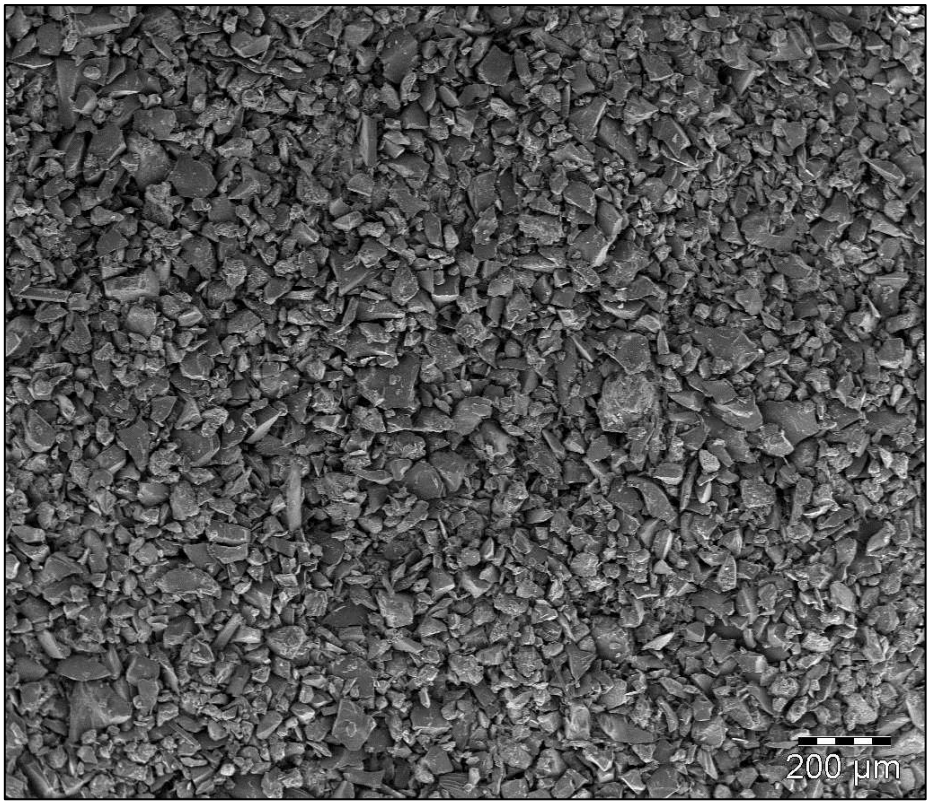

Figure 78: SEM of the drying crust L8 Bottom

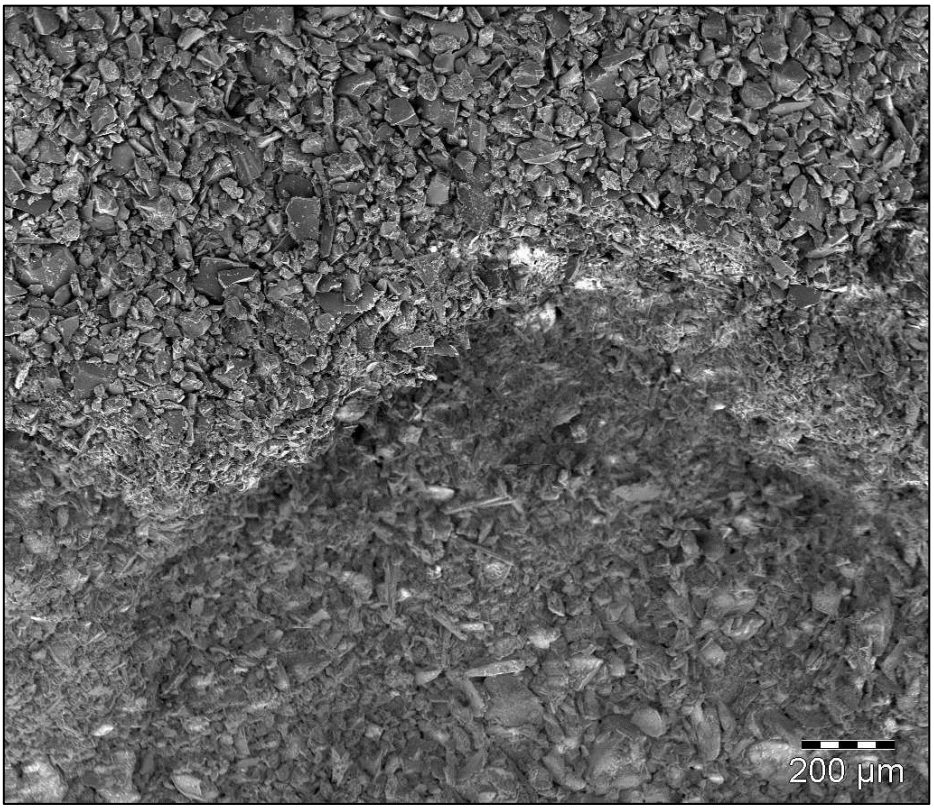

Figure 79: SEM of the drying crust L8 Bottom

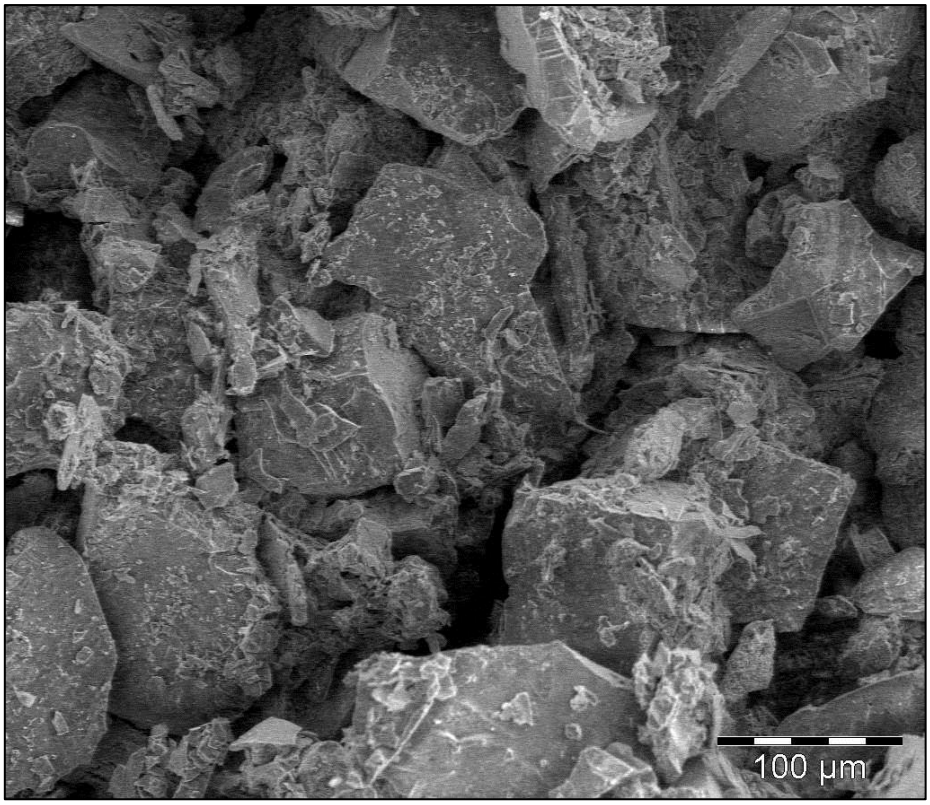

Figure 80: SEM of the chemical crust L1C

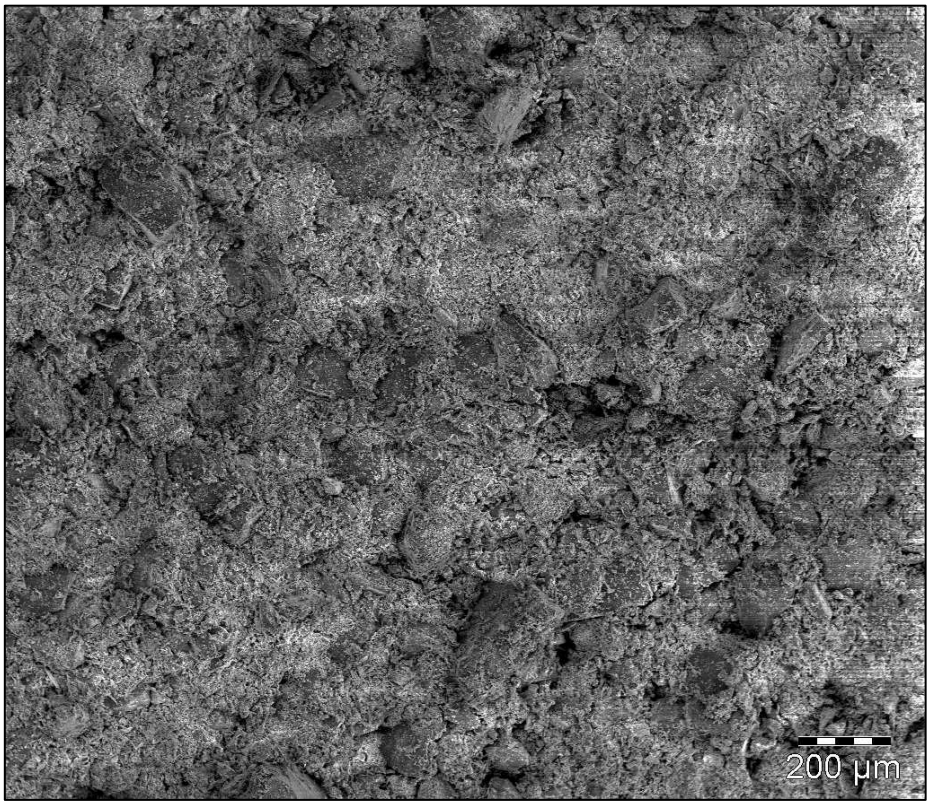

Figure 81: SEM of the erosion crust L2

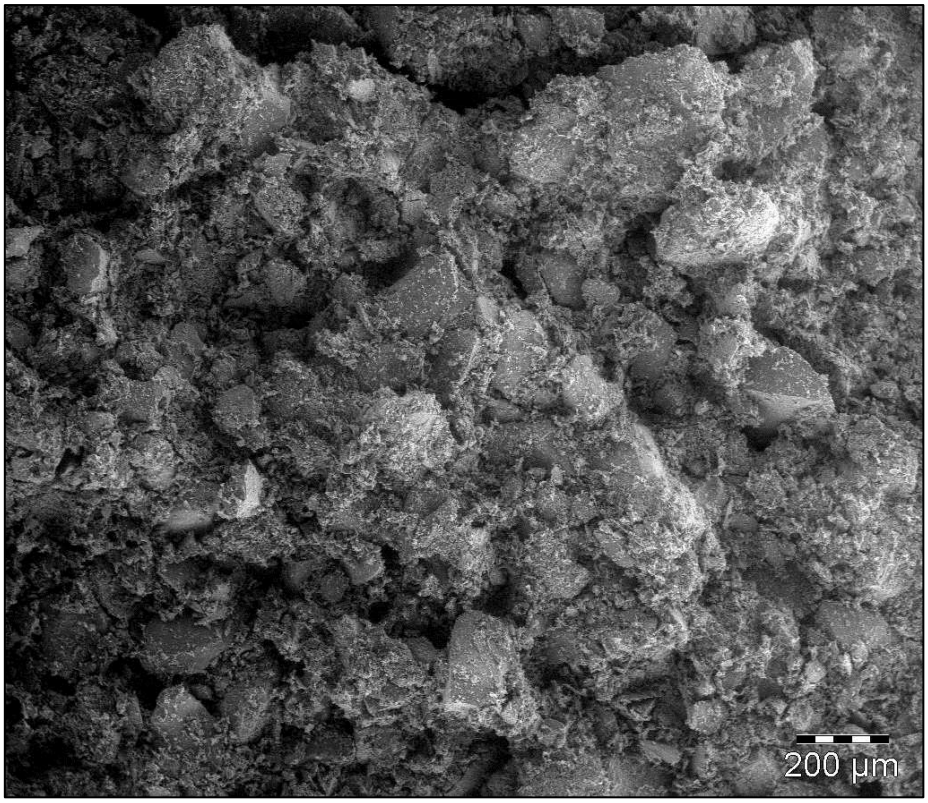

Figure 82: SEM of the erosion crust L2

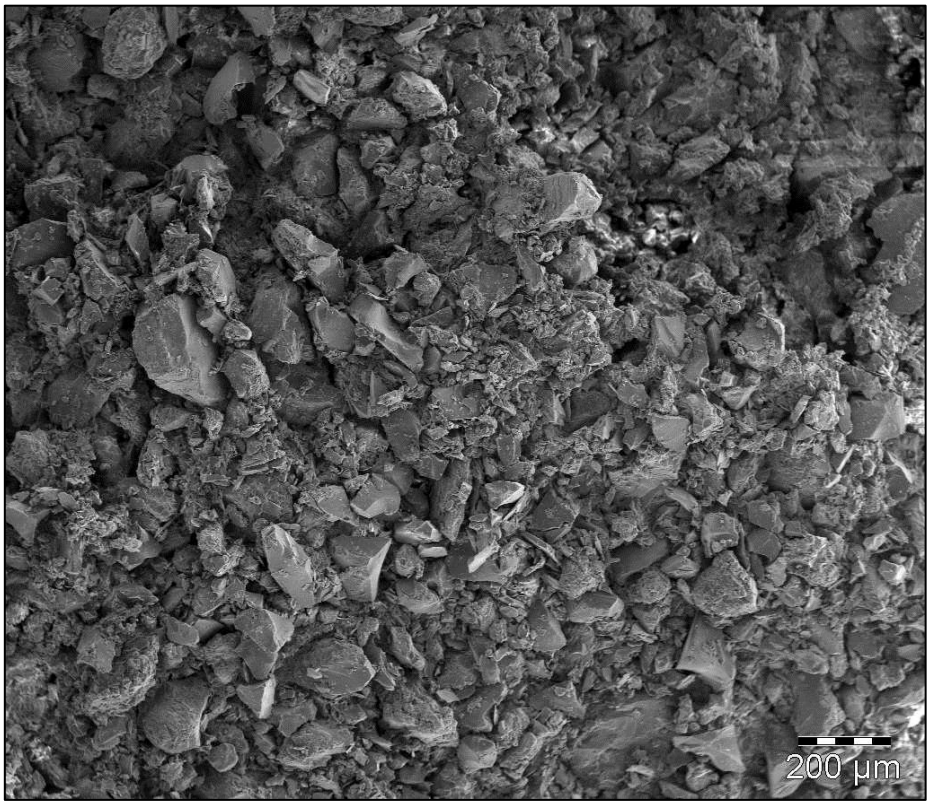

Figure 83: SEM of the drying crust L1C (chemical crust)

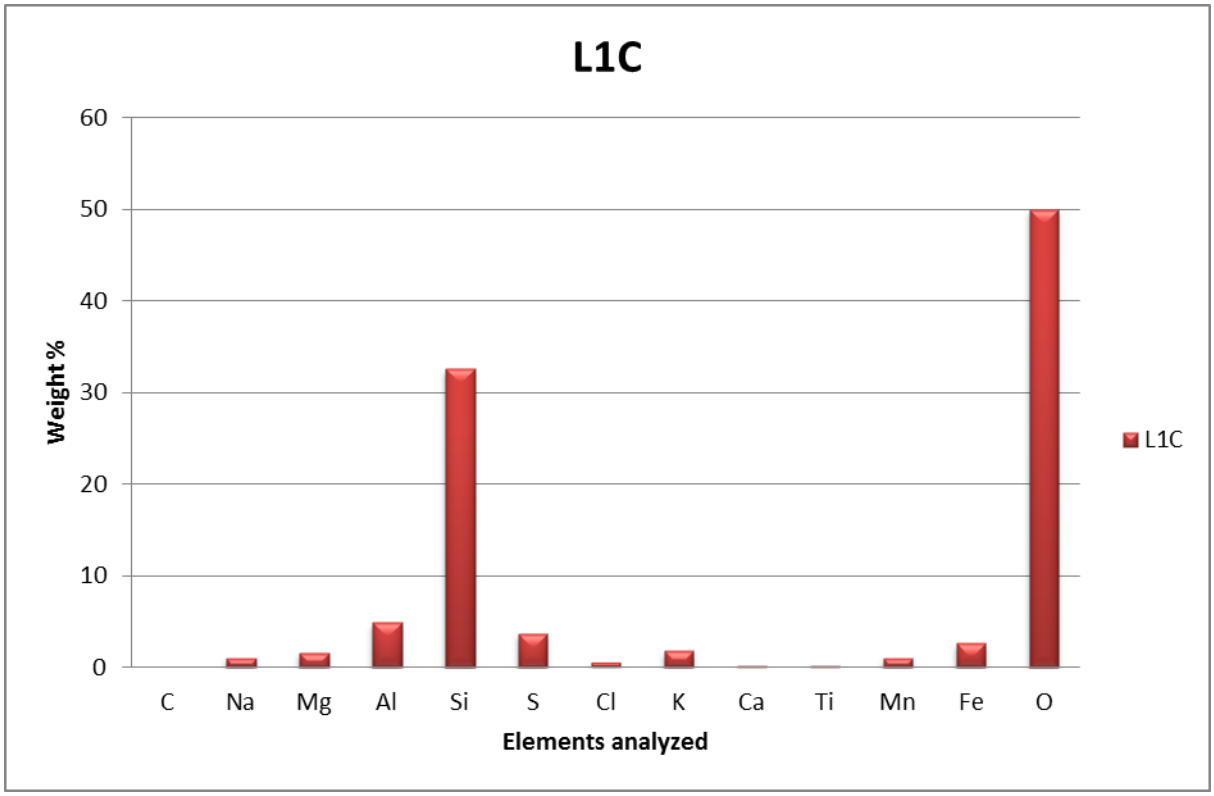

Figure 84: Spectral analysis of the chemical crust.

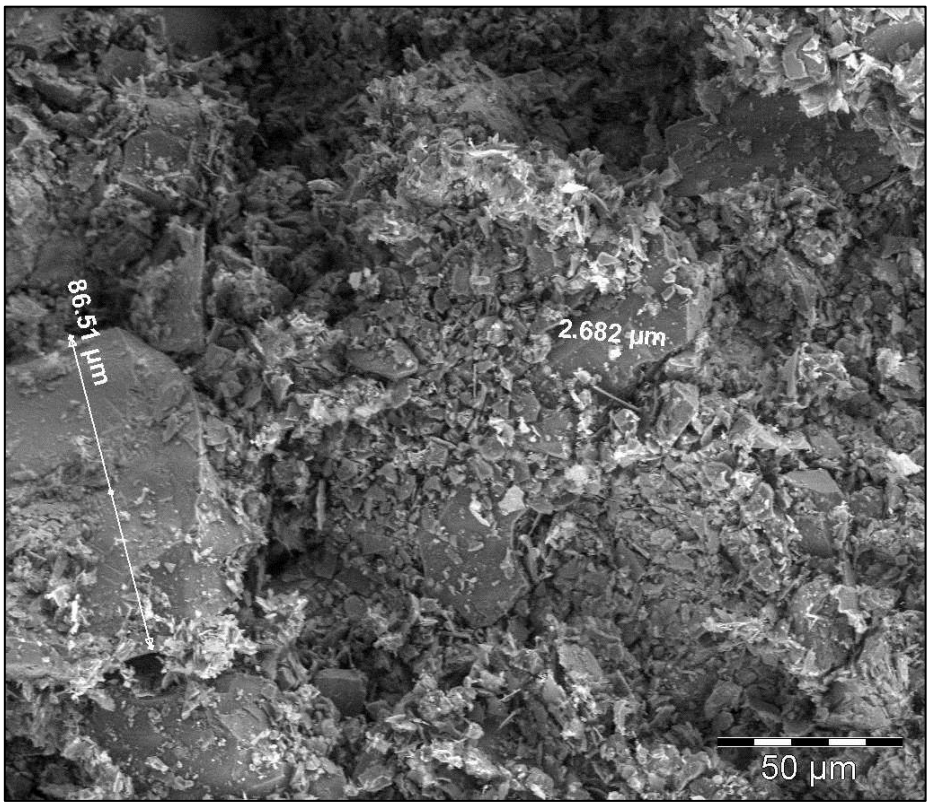

Figure 85: SEM of the erosion crust L2

ANNEXURE 2: DESCRIPTIVE STATISTICS OF THE WMUS

Table 18: WMU 1 descriptive statistics

Average wind speed ($m.s^{-1}$)		***Wind direction (degrees)***		***Wind speed max ($m.s^{-1}$)***		***Air temperature (degrees Celsius)***		***Relative humidity (%)***	
Mean	4.1	Mean	118.8	Mean	6.0	Mean	18.3	Mean	50.9
Standard Error	0.0	Standard Error	0.7	Standard Error	0.0	Standard Error	0.0	Standard Error	0.1
Median	3.5	Median	78.5	Median	5.1	Median	18.4	Median	48.5
Mode	3.3	Mode	0.0	Mode	5.1	Mode	18.4	Mode	48.5
Standard Deviation	2.6	Standard Deviation	118.7	Standard Deviation	3.5	Standard Deviation	6.4	Standard Deviation	23.0
Sample Variance	6.6	Sample Variance	14094.4	Sample Variance	12.2	Sample Variance	41.5	Sample Variance	529.1
Range	17.4	Range	359.8	Range	28.1	Range	37.2	Range	95.5
Minimum	0.0	Minimum	0.0	Minimum	0.0	Minimum	-2.4	Minimum	4.5
Maximum	17.4	Maximum	359.8	Maximum	28.1	Maximum	34.8	Maximum	100.0

Table 19: WMU 2 descriptive statistics

Average wind speed ($m.s^{-1}$)		***Wind direction (degrees)***		***Wind speed max ($m.s^{-1}$)***	
Mean	4.3	Mean	117.7	Mean	6.3
Standard Error	0.0	Standard Error	0.6	Standard Error	0.0
Median	3.8	Median	76.9	Median	5.6

Average wind speed ($m.s^{-1}$)		*Wind direction (degrees)*		*Wind speed max ($m.s^{-1}$)*	
Mode	1.1	Mode	0.0	Mode	5.6
Standard Deviation	2.5	Standard Deviation	109.2	Standard Deviation	3.4
Range	18.0	Range	359.8	Range	30.8
Minimum	0.0	Minimum	0.0	Minimum	0.0
Maximum	18.1	Maximum	359.8	Maximum	30.8

Table 20: WMU 3 descriptive statistics

Average wind speed ($m.s^{-1}$)		*Wind direction (degrees)*		*Wind speed max ($m.s^{-1}$)*		*Air temperature (degrees Celsius)*		*Relative humidity (%)*	
Mean	3.0	Mean	106.7	Mean	4.8	Mean	18.4	Mean	49.9
Standard Error	0.0	Standard Error	0.6	Standard Error	0.0	Standard Error	0.0	Standard Error	0.1
Median	2.6	Median	62.8	Median	4.2	Median	18.5	Median	47.4
Mode	0.0	Mode	0.0	Mode	2.1	Mode	19.6	Mode	41.0
Standard Deviation	1.9	Standard Deviation	104.6	Standard Deviation	2.8	Standard Deviation	6.7	Standard Deviation	23.1
Range	13.8	Range	359.9	Range	22.8	Range	37.7	Range	96.1
Minimum	0.0	Minimum	0.0	Minimum	0.0	Minimum	-2.6	Minimum	3.8
Maximum	13.8	Maximum	359.9	Maximum	22.8	Maximum	35.1	Maximum	100.0

Table 21: WMU 4 descriptive statistics

Average wind speed ($m.s^{-1}$)		***Wind direction (degrees)***		***Wind speed max ($m.s^{-1}$)***	
Mean	4.1	Mean	135.7	Mean	5.9
Standard Error	0.0	Standard Error	0.7	Standard Error	0.0
Median	3.7	Median	95.1	Median	5.4
Mode	2.6	Mode	0.0	Mode	3.8
Standard Deviation	2.2	Standard Deviation	116.9	Standard Deviation	3.2
Range	17.3	Range	359.4	Range	33.1
Minimum	0.0	Minimum	0.0	Minimum	0.0
Maximum	17.3	Maximum	359.4	Maximum	33.1

Table 22: WMU 5 descriptive statistics

Average wind speed ($m.s^{-1}$)		***Wind direction (degrees)***		***Wind speed max ($m.s^{-1}$)***		***Air temperature (degrees Celsius)***		***Relative humidity (%)***	
Mean	4.7	Mean	174.7	Mean	6.6	Mean	18.3	Mean	49.9
Standard Error	0.0	Standard Error	0.8	Standard Error	0.0	Standard Error	0.0	Standard Error	0.1
Median	4.2	Median	186.5	Median	5.9	Median	18.4	Median	47.6
Mode	0.0	Mode	0.0	Mode	4.5	Mode	18.4	Mode	100.0
Standard Deviation	2.7	Standard Deviation	131.5	Standard Deviation	3.7	Standard Deviation	6.4	Standard Deviation	22.8
Range	19.4	Range	360.0	Range	32.6	Range	36.7	Range	95.6

Average wind speed ($m.s^{-1}$)		*Wind direction (degrees)*		*Wind speed max ($m.s^{-1}$)*		*Air temperature (degrees Celsius)*		*Relative humidity (%)*	
Minimum	0.0	Minimum	0.0	Minimum	0.0	Minimum	-2.1	Minimum	4.4
Maximum	19.4	Maximum	360.0	Maximum	32.6	Maximum	34.6	Maximum	100.0

Table 23: WMU 6 descriptive statistics

Average wind speed ($m.s^{-1}$)		*Wind direction (degrees)*		*Wind speed max ($m.s^{-1}$)*		*Air temperature (degrees Celsius)*		*Relative humidity (%)*	
Mean	2.1	Mean	112.5	Mean	3.9	Mean	18.7	Mean	48.8
Standard Error	0.0	Standard Error	0.7	Standard Error	0.0	Standard Error	0.0	Standard Error	0.1
Median	2.0	Median	65.5	Median	3.6	Median	18.8	Median	46.7
Mode	0.0	Mode	0.0	Mode	3.2	Mode	18.8	Mode	0.0
Standard Deviation	1.2	Standard Deviation	111.4	Standard Deviation	2.0	Standard Deviation	6.9	Standard Deviation	23.6
Range	9.9	Range	359.8	Range	21.2	Range	37.9	Range	98.5
Minimum	0.0	Minimum	0.0	Minimum	0.0	Minimum	-2.2	Minimum	0.0
Maximum	9.9	Maximum	359.8	Maximum	21.2	Maximum	35.7	Maximum	98.5

Table 24: WMU 7 descriptive statistics

Average wind speed ($m.s^{-1}$)		***Wind direction (degrees)***		***Wind speed max ($m.s^{-1}$)***		***Air temperature (degrees Celsius)***		***Relative humidity (%)***	
Mean	3.6	Mean	123.1	Mean	5.4	Mean	18.7	Mean	48.9
Standard Error	0.0	Standard Error	0.7	Standard Error	0.0	Standard Error	0.0	Standard Error	0.1
Median	3.2	Median	76.4	Median	4.9	Median	18.7	Median	46.3
Mode	2.0	Mode	0.0	Mode	2.9	Mode	24.5	Mode	28.1
Standard Deviation	2.0	Standard Deviation	115.9	Standard Deviation	2.8	Standard Deviation	6.5	Standard Deviation	23.7
Range	14.8	Range	360.0	Range	27.4	Range	36.5	Range	100.0
Minimum	0.0	Minimum	0.0	Minimum	0.0	Minimum	-1.6	Minimum	0.0
Maximum	14.8	Maximum	360.0	Maximum	27.5	Maximum	34.9	Maximum	100.0

Table 25: WMU 8 descriptive statistics

Average wind speed ($m.s^{-1}$)		***Wind direction (degrees)***		***Wind speed max ($m.s^{-1}$)***	
Mean	2.4	Mean	73.6	Mean	4.0
Standard Error	0.0	Standard Error	0.6	Standard Error	0.0
Median	1.9	Median	0.0	Median	3.4
Mode	1.9	Mode	0.0	Mode	3.4
Standard Deviation	1.6	Standard Deviation	104.6	Standard Deviation	2.3
Range	11.1	Range	359.8	Range	16.5
Minimum	0.0	Minimum	0.0	Minimum	0.0
Maximum	11.1	Maximum	359.8	Maximum	16.5

Table 26: WMU 9 descriptive statistics

Average wind speed ($m.s^{-1}$)		***Wind direction (degrees)***		***Wind speed max ($m.s^{-1}$)***	
Mean	1.6	Mean	116.9	Mean	3.2
Standard Error	0.0	Standard Error	0.6	Standard Error	0.0
Median	1.3	Median	79.4	Median	2.8
Mode	0.0	Mode	0.0	Mode	2.8
Standard Deviation	1.4	Standard Deviation	101.9	Standard Deviation	2.2
Range	9.0	Range	359.7	Range	15.2
Minimum	0.1	Minimum	0.0	Minimum	0.0
Maximum	8.8	Maximum	359.7	Maximum	15.2

Table 27: WMU 10 descriptive statistics

Average wind speed		***Wind direction***		***Wind speed max***	
Mean	2.0	Mean	95.9	Mean	3.8
Standard Error	0.0	Standard Error	0.6	Standard Error	0.0
Median	1.7	Median	65.2	Median	3.3
Mode	0.0	Mode	0.0	Mode	3.3
Standard Deviation	1.4	Standard Deviation	96.3	Standard Deviation	2.3
Range	10.4	Range	359.8	Range	20.1
Minimum	0.0	Minimum	0.0	Minimum	0.0
Maximum	10.4	Maximum	359.8	Maximum	20.1

Table 28: WMU 11 descriptive statistics

Average wind speed ($m.s^{-1}$)		***Wind direction (degrees)***		***Wind speed max ($m.s^{-1}$)***		***Air temperature (degrees Celsius)***		***Relative humidity (%)***	
Mean	2.4	Mean	100.5	Mean	4.2	Mean	18.4	Mean	50.5
Standard Error	0.0	Standard Error	0.7	Standard Error	0.0	Standard Error	0.0	Standard Error	0.1
Median	2.1	Median	28.4	Median	3.8	Median	18.5	Median	48.4
Mode	0.0	Mode	0.0	Mode	4.1	Mode	18.5	Mode	100.0
Standard Deviation	1.6	Standard Deviation	116.4	Standard Deviation	2.5	Standard Deviation	6.9	Standard Deviation	23.0
Range	10.1	Range	360.0	Range	20.4	Range	39.5	Range	95.9
Minimum	0.0	Minimum	0.0	Minimum	0.0	Minimum	-4.0	Minimum	4.1
Maximum	10.1	Maximum	360.0	Maximum	20.4	Maximum	35.5	Maximum	100.0

Table 29: WMU 12 descriptive statistics

Average wind speed ($m.s^{-1}$)		***Wind direction (degrees)***		***Wind speed max ($m.s^{-1}$)***		***Air temperature (degrees Celsius)***		***Relative humidity (%)***	
Mean	2.9	Mean	124.4	Mean	4.7	Mean	17.5	Mean	54.2
Standard Error	0.0	Standard Error	0.6	Standard Error	0.0	Standard Error	0.0	Standard Error	0.1
Median	2.5	Median	82.8	Median	4.1	Median	18.0	Median	53.4
Mode	0.0	Mode	0.0	Mode	1.6	Mode	25.0	Mode	26.8
Standard Deviation	2.0	Standard Deviation	110.2	Standard Deviation	3.0	Standard Deviation	7.7	Standard Deviation	24.0
Range	14.2	Range	359.9	Range	24.4	Range	42.4	Range	95.8
Minimum	0.0	Minimum	0.0	Minimum	0.0	Minimum	-7.1	Minimum	4.1
Maximum	14.2	Maximum	359.9	Maximum	24.4	Maximum	35.3	Maximum	99.9

ANNEXURE 3: CHI-SQUARE TEST RESULTS FOR WIND DIRECTION COMBINATIONS MEASURED ON THE STUDY AREA.

Table 30: Chi-square test results for the observed wind direction classes on the study site.

Wind class	Actual range											Chi-square test
TSF WMU-Reference WMU	WMU 1	WMU 2	WMU 3	WMU 4	WMU 5	WMU 6	WMU 7	WMU 8	WMU 9	WMU 10	WMU 11	
E-E	429	787	450	427	33	288	437	312	662	446	115	9.15E-243
E-ENE	226	440	1766	649	7	515	534	114	1081	1461	175	0.00E+00
E-ESE	290	171	54	43	11	79	46	250	78	72	77	2.80E-158
E-N	980	517	157	458	2660	1121	967	1431	345	265	1431	0.00E+00
E-NE	415	599	234	469	4	344	192	52	292	325	267	5.92E-215
ENE-E	134	184	125	151	2	197	137	177	715	306	68	0.00E+00
ENE-ENE	505	1294	1622	981	17	831	917	390	1788	1853	96	0.00E+00
ENE-ESE	94	80	32	24	8	61	30	56	57	30	40	2.32E-25
ENE-N	1441	436	171	432	3329	1185	1091	1899	371	380	2350	0.00E+00
ENE-NE	836	1120	1455	1109	13	803	642	356	328	742	264	0.00E+00
ENE-NNE	741	254	25	536	120	189	464	118	35	54	461	0.00E+00
ENE-NNW	26	16	4	36	0	32	35	293	20	5	51	0.00E+00
ENE-NW	36	39	2	125	0	35	59	46	8	5	21	3.09E-75
ENE-S	3	1	3	1	0	18	3	29	10	21	36	1.85E-25
ENE-SE	43	22	10	4	2	20	15	38	39	16	20	1.49E-15
ENE-SSE	7	4	7	7	0	16	2	44	20	15	35	1.13E-24
ENE-SSW	2	5	5	3	0	18	3	13	8	24	13	1.84E-10
ENE-SW	4	4	10	4	0	18	2	7	26	22	8	1.11E-12
ENE-W	5	8	3	23	0	29	23	11	13	3	8	4.93E-13
ENE-WNW	27	17	7	46	0	21	57	11	17	2	13	7.49E-29

Wind class	Actual range											Chi-square test
TSF WMU-Reference WMU	WMU 1	WMU 2	WMU 3	WMU 4	WMU 5	WMU 6	WMU 7	WMU 8	WMU 9	WMU 10	WMU 11	
ENE-WSW	9	7	10	9	0	18	11	3	36	13	7	3.47E-13
E-NNE	510	117	27	382	93	87	375	32	65	54	223	0.00E+00
E-NNW	33	16	6	53	0	42	38	356	19	6	78	0.00E+00
E-NW	47	52	6	166	1	39	71	52	11	7	31	7.90E-100
E-S	5	3	8	4	0	21	3	22	22	19	72	3.08E-49
E-SE	50	21	18	8	1	26	11	82	30	23	77	7.60E-44
ESE-E	45	55	142	384	1	146	291	35	344	174	84	2.08E-233
ESE-ENE	9	26	340	50	0	85	30	10	53	226	36	3.67E-306
ESE-ESE	265	445	50	137	7	225	208	177	132	69	88	3.92E-189
ESE-N	160	54	83	43	705	99	88	187	67	106	163	0.00E+00
ESE-NE	14	21	52	21	1	41	16	6	3	35	26	2.72E-21
ESE-NNE	11	6	6	16	18	10	12	3	4	6	7	3.45E-03
ESE-NNW	4	0	3	2	0	10	3	24	4	3	5	2.20E-14
ESE-NW	13	10	2	12	0	5	9	10	7	0	1	3.37E-05
ESE-S	9	6	5	7	0	9	5	17	8	29	37	2.91E-18
ESE-SE	243	87	16	23	7	48	26	187	40	34	168	2.19E-171
ESE-SSE	26	9	11	4	0	15	9	63	19	11	85	1.15E-60
ESE-SSW	1	4	9	2	0	3	6	4	5	18	19	5.61E-10
ESE-SW	1	4	4	6	0	9	4	1	19	9	7	3.91E-07
ESE-W	4	3	5	7	0	13	12	5	9	8	5	1.06E-02
ESE-WNW	9	8	5	21	0	9	15	8	6	6	2	8.67E-06
ESE-WSW	4	1	6	4	0	12	5	2	19	5	6	2.53E-07
E-SSE	11	8	9	3	1	35	3	56	26	32	138	8.58E-111
E-SSW	7	5	7	4	0	36	4	10	17	27	36	5.14E-22
E-SW	4	8	12	7	0	52	5	6	22	27	22	2.70E-27

Wind class	Actual range											Chi-square test
TSF WMU-Reference WMU	WMU 1	WMU 2	WMU 3	WMU 4	WMU 5	WMU 6	WMU 7	WMU 8	WMU 9	WMU 10	WMU 11	
E-W	12	10	16	24	0	28	32	5	44	6	17	8.05E-17
E-WNW	34	33	13	85	0	33	64	10	28	5	20	6.41E-42
E-WSW	8	8	12	13	0	49	11	3	52	19	13	2.39E-32
N-E	36	38	38	92	4	149	71	37	201	119	43	1.24E-94
NE-E	31	41	32	35	0	77	21	27	253	81	16	2.05E-180
NE-ENE	44	135	251	149	0	528	162	59	716	836	29	0.00E+00
NE-ESE	24	19	10	11	5	14	12	9	36	12	10	1.42E-07
NE-N	1205	217	231	262	2408	603	518	1352	214	462	2118	0.00E+00
NE-NE	278	1538	1441	1474	4	1028	1190	500	1166	845	59	0.00E+00
N-ENE	26	32	113	97	1	293	106	47	260	764	29	0.00E+00
NE-NNE	1104	522	517	504	89	175	524	398	17	209	209	0.00E+00
NE-NNW	11	2	3	8	0	13	13	76	5	2	18	7.49E-66
NE-NW	15	9	1	28	0	15	18	25	3	4	22	1.26E-12
NE-S	0	0	2	2	0	5	0	11	7	6	3	1.85E-05
NE-SE	8	6	3	2	0	5	4	6	17	11	4	6.45E-05
N-ESE	32	55	31	57	1	80	39	46	94	34	33	1.84E-25
NE-SSE	5	2	1	2	0	10	3	17	23	8	1	5.82E-14
NE-SSW	1	1	5	2	0	6	2	3	5	8	4	5.49E-02
NE-SW	2	4	5	2	0	9	2	4	8	7	5	5.49E-02
NE-W	6	4	3	6	0	6	13	5	12	4	3	3.74E-03
NE-WNW	7	1	0	13	0	5	20	12	12	4	3	4.09E-09
NE-WSW	2	5	1	6	0	7	4	2	12	7	2	1.75E-03
N-N	6024	5032	5162	3595	6444	4481	4314	5468	4662	4404	4423	8.00E-292
N-NE	43	125	260	137	1	377	197	88	288	315	39	1.13E-193
NNE-E	5	9	9	12	0	34	5	2	74	25	3	4.05E-57

Wind class	Actual range											Chi-square test
TSF WMU-Reference WMU	WMU 1	WMU 2	WMU 3	WMU 4	WMU 5	WMU 6	WMU 7	WMU 8	WMU 9	WMU 10	WMU 11	
NNE-ENE	11	19	65	25	1	218	18	3	180	279	8	1.85E-283
NNE-ESE	5	8	8	7	0	6	3	5	17	8	4	1.61E-03
NNE-N	1273	278	394	394	1305	576	450	1004	224	355	1225	0.00E+00
NNE-NE	14	118	262	164	0	388	178	30	562	272	13	0.00E+00
NNE-NNE	119	866	570	681	21	60	622	198	194	357	44	0.00E+00
NNE-NNW	9	3	4	7	0	11	6	40	7	1	12	2.13E-23
NNE-NW	9	4	1	12	0	7	11	22	0	1	3	1.54E-11
NNE-S	4	5	3	5	0	1	6	9	10	3	2	1.45E-02
NNE-SE	5	6	3	0	0	4	1	2	11	6	0	2.00E-04
NNE-SSE	6	0	1	1	0	0	1	1	9	3	3	7.89E-05
NNE-SSW	1	2	3	1	0	2	3	4	7	7	0	1.48E-02
NNE-SW	1	1	1	4	0	5	0	2	6	2	1	3.36E-02
NNE-W	3	3	0	4	0	4	7	1	10	1	0	1.84E-04
NNE-WNW	4	2	1	8	0	10	13	3	3	0	4	1.17E-05
NNE-WSW	1	3	2	2	0	1	3	1	13	7	5	1.25E-05
N-NNE	68	254	319	270	56	174	353	111	308	368	73	3.90E-140
N-NNW	642	237	100	262	11	88	156	336	96	29	205	0.00E+00
N-NW	376	352	166	1033	11	132	535	138	152	53	854	0.00E+00
NNW-E	7	6	11	8	0	6	8	5	21	17	6	2.13E-05
NNW-ENE	3	6	23	12	0	7	7	1	8	81	3	5.16E-78
NNW-ESE	6	8	3	12	0	8	8	5	35	7	6	6.46E-16
NNW-N	276	199	453	95	616	383	173	386	348	399	300	1.38E-129
NNW-NE	1	10	19	10	0	17	7	6	5	37	8	6.99E-17
NNW-NNE	8	9	8	9	1	14	12	5	3	15	9	1.59E-02
NNW-NNW	275	230	45	45	2	32	17	74	44	5	26	4.33E-245

Wind class	Actual range											Chi-square test
TSF WMU-Reference WMU	WMU 1	WMU 2	WMU 3	WMU 4	WMU 5	WMU 6	WMU 7	WMU 8	WMU 9	WMU 10	WMU 11	
NNW-NW	77	109	20	299	1	49	213	82	27	12	206	1.07E-201
NNW-S	3	0	6	1	0	5	3	12	13	4	3	7.61E-06
NNW-SE	8	7	5	5	0	5	5	2	27	8	4	1.45E-11
NNW-SSE	7	4	4	1	0	6	3	4	22	5	3	5.65E-10
NNW-SSW	8	4	1	3	0	9	4	3	12	5	0	2.79E-04
NNW-SW	5	9	6	6	0	10	7	4	14	8	1	5.51E-03
NNW-W	3	3	6	13	0	16	12	4	20	4	7	2.66E-07
NNW-WNW	13	12	5	91	0	31	133	23	13	7	35	4.99E-106
NNW-WSW	3	4	5	10	0	22	8	4	8	6	3	1.73E-07
N-S	33	21	20	21	0	38	21	69	32	32	45	2.47E-17
N-SE	56	56	19	45	2	54	29	54	60	40	38	3.64E-13
N-SSE	50	22	20	22	1	35	25	53	38	23	49	2.13E-13
N-SSW	24	16	28	24	0	50	42	19	33	53	46	2.86E-14
N-SW	17	30	36	45	0	79	59	9	38	79	55	4.93E-31
N-W	44	83	73	200	2	179	134	12	103	80	133	1.21E-84
NW-E	2	4	7	17	0	5	6	3	13	24	7	4.51E-10
NW-ENE	3	5	20	6	0	9	3	3	3	145	6	6.43E-202
NW-ESE	4	10	13	10	0	4	8	1	7	8	2	1.38E-03
NW-N	463	173	542	88	1380	416	181	1062	493	759	473	0.00E+00
NW-NE	4	11	8	6	0	11	4	2	3	32	5	1.58E-16
NW-NNE	4	3	6	5	3	9	9	5	1	15	12	2.08E-03
NW-NNW	118	25	59	22	1	30	5	48	8	15	24	3.43E-68
NW-NW	911	936	491	254	20	173	152	130	310	114	227	0.00E+00
N-WNW	99	136	103	533	3	222	367	38	120	68	388	0.00E+00
NW-S	9	5	5	4	0	18	5	19	45	8	4	3.83E-26

Wind class	Actual range											Chi-square test
TSF WMU-Reference WMU	WMU 1	WMU 2	WMU 3	WMU 4	WMU 5	WMU 6	WMU 7	WMU 8	WMU 9	WMU 10	WMU 11	
NW-SE	15	10	5	4	0	5	11	5	14	8	4	1.07E-03
NW-SSE	7	6	2	5	1	4	5	11	34	7	4	4.07E-18
NW-SSW	5	3	11	3	0	24	6	9	84	16	5	7.29E-75
NW-SW	4	6	7	8	0	44	11	4	74	49	4	3.59E-62
N-WSW	31	50	51	106	2	108	91	14	54	78	86	6.03E-40
NW-W	16	17	36	103	0	264	185	8	43	59	78	2.90E-193
NW-WNW	102	190	192	859	3	333	810	96	220	96	537	0.00E+00
NW-WSW	1	4	4	14	0	59	7	2	56	53	16	9.94E-57
S-E	2	5	7	17	0	9	7	8	4	18	22	3.30E-08
SE-E	6	9	112	130	0	65	66	15	82	87	67	5.01E-68
SE-ENE	4	5	75	23	0	36	12	2	7	95	12	1.41E-82
SE-ESE	37	94	79	312	1	132	220	51	164	75	112	8.09E-140
SE-N	65	26	128	28	623	64	40	95	80	92	83	0.00E+00
SE-NE	4	4	18	10	0	23	7	2	4	15	8	2.90E-09
S-ENE	1	0	6	3	0	6	8	3	1	78	8	7.18E-100
SE-NNE	0	0	4	2	2	12	4	2	2	3	4	2.52E-04
SE-NNW	2	1	1	1	0	3	2	6	4	2	0	9.96E-02
SE-NW	1	2	4	4	0	5	1	3	4	1	1	2.80E-01
SE-S	19	8	27	12	1	19	24	75	32	76	20	6.29E-41
SE-SE	319	431	84	69	3	204	163	181	126	62	178	4.20E-189
S-ESE	4	9	7	50	0	12	13	9	9	17	44	4.88E-30
SE-SSE	184	38	40	16	3	36	50	176	66	51	141	5.91E-113
SE-SSW	8	2	26	3	1	7	11	17	12	51	4	1.99E-30
SE-SW	0	2	11	5	0	8	11	4	16	14	0	6.24E-08
SE-W	6	6	7	6	0	7	11	0	14	2	0	2.29E-05

Wind class	Actual range											Chi-square test
TSF WMU-Reference WMU	WMU 1	WMU 2	WMU 3	WMU 4	WMU 5	WMU 6	WMU 7	WMU 8	WMU 9	WMU 10	WMU 11	
SE-WNW	7	6	2	11	0	10	5	2	6	3	1	2.69E-03
SE-WSW	2	0	16	2	0	3	7	3	15	5	3	3.79E-09
S-N	96	27	21	23	718	49	23	112	65	49	35	0.00E+00
S-NE	1	1	1	4	0	10	0	0	0	8	2	3.76E-07
S-NNE	1	0	3	2	15	6	1	0	1	2	1	4.15E-10
S-NNW	1	0	0	1	0	4	0	1	0	3	1	5.49E-02
S-NW	1	0	0	3	0	4	1	2	0	10	1	3.29E-06
S-S	407	340	186	180	1	262	241	263	302	114	120	8.39E-123
S-SE	21	43	13	135	1	26	42	23	8	39	129	9.13E-97
SSE-E	7	9	24	50	1	28	25	5	6	32	59	3.64E-30
SSE-ENE	4	5	16	17	0	20	3	7	5	70	15	8.40E-50
SSE-ESE	13	30	47	199	0	51	63	23	30	47	109	5.19E-113
SSE-N	67	25	58	23	597	58	32	79	71	51	61	0.00E+00
SSE-NE	1	5	7	6	0	26	7	1	3	5	7	3.45E-13
SSE-NNE	0	1	1	2	19	6	1	2	0	2	4	3.46E-14
SSE-NNW	1	3	0	2	0	8	1	2	0	0	2	5.09E-04
SSE-NW	5	1	0	1	0	1	2	11	3	2	0	2.99E-06
SSE-S	57	20	147	19	1	58	101	188	131	124	37	3.20E-94
SSE-SE	74	254	70	214	0	138	129	65	87	86	154	3.35E-91
SSE-SSE	407	258	92	61	9	169	162	178	183	73	161	2.14E-150
SSE-SSW	14	5	134	12	0	21	54	53	50	92	11	1.95E-86
SSE-SW	5	2	22	6	0	13	22	4	20	35	1	3.93E-19
SSE-W	3	3	2	4	0	10	10	2	13	1	0	1.20E-06
SSE-WNW	5	1	1	5	0	8	5	1	5	0	2	7.59E-03
SSE-WSW	2	5	6	6	0	12	10	6	20	7	4	9.94E-06

Wind class	Actual range											Chi-square test
TSF WMU-Reference WMU	WMU 1	WMU 2	WMU 3	WMU 4	WMU 5	WMU 6	WMU 7	WMU 8	WMU 9	WMU 10	WMU 11	
S-SSE	220	272	39	244	6	173	72	164	60	54	339	2.39E-168
S-SSW	34	25	418	40	0	92	263	130	197	196	22	9.37E-274
S-SW	11	10	29	21	0	44	50	17	44	100	11	4.56E-50
SSW-E	2	1	3	11	0	5	8	9	1	12	21	2.09E-09
SSW-ENE	1	3	6	3	0	5	5	4	3	156	6	3.94E-254
SSW-ESE	4	4	6	23	0	9	4	8	2	12	33	8.56E-18
SSW-N	170	18	28	25	1224	44	25	162	112	47	58	0.00E+00
SSW-NE	0	3	3	2	0	4	2	2	0	12	7	1.62E-05
SSW-NNE	2	0	0	3	12	1	2	1	2	4	3	1.44E-05
SSW-NNW	1	0	1	3	0	2	3	1	2	6	3	1.32E-01
SSW-NW	8	3	1	8	0	7	2	4	7	39	2	2.13E-29
SSW-S	782	485	81	363	7	357	75	442	41	51	520	0.00E+00
SSW-SE	11	28	10	47	0	9	18	31	4	14	129	2.65E-97
SSW-SSE	68	61	32	91	0	52	32	337	14	21	321	0.00E+00
SSW-SSW	292	566	847	505	6	392	604	167	464	263	100	0.00E+00
SSW-SW	27	52	193	117	1	215	401	61	407	403	32	0.00E+00
SSW-W	6	8	8	12	0	44	9	2	56	39	3	1.22E-42
SSW-WNW	4	9	4	10	0	17	15	6	25	57	1	7.73E-37
SSW-WSW	10	9	27	27	0	87	45	13	110	114	11	1.79E-87
S-W	5	4	3	4	0	10	7	2	29	14	1	3.38E-16
SW-E	3	4	8	7	0	7	6	39	6	20	35	1.32E-25
SW-ENE	3	6	7	6	0	4	6	28	5	187	20	2.94E-251
SW-ESE	2	4	4	16	1	8	5	66	2	8	67	1.35E-74
SW-N	298	36	35	45	1713	61	44	283	160	74	131	0.00E+00
SW-NE	7	3	2	4	0	17	1	17	4	10	13	3.37E-08

Wind class	Actual range											Chi-square test
TSF WMU-Reference WMU	WMU 1	WMU 2	WMU 3	WMU 4	WMU 5	WMU 6	WMU 7	WMU 8	WMU 9	WMU 10	WMU 11	
SW-NNE	3	0	0	1	53	5	3	9	0	6	12	2.19E-54
SW-NNW	1	3	1	3	0	5	0	13	6	9	11	3.85E-06
SW-NW	10	4	2	10	0	16	3	8	12	16	7	6.24E-05
S-WNW	2	0	1	1	0	8	0	1	2	13	2	2.41E-09
SW-S	226	89	55	89	1	74	43	215	26	47	320	2.86E-195
SW-SE	8	15	7	24	0	9	14	184	3	19	164	4.21E-227
SW-SSE	44	24	19	35	1	17	19	528	7	21	291	0.00E+00
SW-SSW	972	660	680	347	3	454	181	152	92	174	557	0.00E+00
SW-SW	334	778	838	872	6	514	1060	136	901	628	104	0.00E+00
S-WSW	4	5	7	13	0	26	13	6	19	26	3	4.54E-12
SW-W	31	22	28	61	1	118	45	21	77	83	13	9.93E-54
SW-WNW	26	25	7	22	0	58	13	11	27	43	5	8.37E-25
SW-WSW	74	106	86	237	0	412	336	69	451	434	29	0.00E+00
W-E	4	3	4	9	0	3	5	21	2	12	15	6.11E-09
W-ENE	1	4	9	6	0	2	4	47	2	180	12	2.13E-245
W-ESE	3	3	7	18	0	3	5	13	5	8	11	1.46E-05
W-N	213	54	76	46	1527	88	48	1041	196	172	313	0.00E+00
W-NE	4	4	4	6	0	10	4	66	1	8	13	1.40E-62
W-NNE	1	2	1	1	31	16	6	61	1	2	13	2.22E-55
W-NNW	4	6	3	6	0	8	0	20	0	6	12	3.04E-09
W-NW	28	26	18	23	0	49	8	26	11	7	31	2.05E-15
WNW-E	2	3	7	6	0	3	3	11	7	13	8	2.07E-03
WNW-ENE	2	4	19	7	0	6	4	3	3	163	9	4.10E-238
WNW-ESE	4	6	3	10	0	4	6	4	6	10	5	1.01E-01
WNW-N	304	119	197	84	1352	181	87	1094	252	395	429	0.00E+00

Wind class	Actual range											Chi-square test
TSF WMU-Reference WMU	WMU 1	WMU 2	WMU 3	WMU 4	WMU 5	WMU 6	WMU 7	WMU 8	WMU 9	WMU 10	WMU 11	
WNW-NE	3	8	7	5	0	6	6	6	5	12	14	1.18E-02
WNW-NNE	4	6	6	8	12	10	3	6	2	11	12	6.16E-02
WNW-NNW	10	8	5	15	0	25	7	33	3	8	23	3.11E-14
WNW-NW	350	138	96	58	16	154	21	57	37	49	78	7.47E-197
WNW-S	13	9	7	6	0	10	6	22	34	12	5	1.10E-12
WNW-SE	4	9	3	11	0	3	5	3	11	7	1	1.73E-03
WNW-SSE	13	8	8	6	0	5	8	11	26	7	9	1.48E-06
WNW-SSW	9	6	17	8	0	17	18	10	52	40	10	1.92E-25
WNW-SW	20	15	31	11	0	43	17	9	127	112	21	8.87E-99
WNW-W	126	266	360	652	1	520	861	27	308	232	413	0.00E+00
WNW-WNW	675	758	540	442	16	238	246	84	377	179	261	0.00E+00
WNW-WSW	24	35	92	69	1	173	100	18	148	148	100	1.20E-82
W-S	18	5	16	7	1	11	15	36	22	19	29	2.88E-10
W-SE	12	19	13	12	0	7	10	20	5	7	21	3.36E-05
W-SSE	29	15	12	11	2	4	10	41	16	9	21	1.29E-13
W-SSW	33	20	29	22	0	22	18	33	50	51	47	2.15E-13
W-SW	118	69	212	67	0	135	92	16	196	297	149	6.01E-130
WSW-E	3	2	2	8	0	3	8	122	4	17	25	2.16E-146
WSW-ENE	1	3	8	7	0	8	12	119	7	206	25	1.81E-252
WSW-ESE	4	4	4	14	0	9	7	123	2	14	39	2.51E-131
WSW-N	218	44	59	57	1667	82	49	620	172	96	283	0.00E+00
WSW-NE	2	5	7	3	0	15	0	46	3	15	21	2.87E-32
WSW-NNE	2	0	5	1	66	9	3	19	0	3	45	3.19E-67
WSW-NNW	6	1	2	4	0	11	4	12	4	8	15	3.02E-05
WSW-NW	24	12	2	17	0	28	8	24	21	11	10	3.42E-09

Wind class	Actual range											Chi-square test
TSF WMU-Reference WMU	WMU 1	WMU 2	WMU 3	WMU 4	WMU 5	WMU 6	WMU 7	WMU 8	WMU 9	WMU 10	WMU 11	
WSW-S	75	20	33	27	3	26	16	101	13	25	127	7.53E-76
WSW-SE	8	15	10	16	0	9	5	104	2	15	64	6.93E-92
WSW-SSE	27	20	11	16	0	11	20	155	7	10	99	4.64E-139
WSW-SSW	257	128	176	93	2	116	62	80	52	129	258	1.29E-107
WSW-SW	618	589	812	314	10	441	405	67	305	435	482	1.10E-279
WSW-W	175	164	81	229	4	237	128	75	200	150	38	2.54E-88
WSW-WNW	56	34	7	64	1	140	24	34	22	32	20	3.80E-73
WSW-WSW	447	719	541	890	7	615	1009	59	946	594	209	0.00E+00
W-W	608	771	512	723	9	481	569	59	609	350	321	1.73E-286
W-WNW	338	139	70	117	5	206	35	51	58	80	72	1.23E-172
W-WSW	320	441	595	507	6	536	752	30	407	373	501	1.10E-259

*Highlighted values indicates the rejection of the null-hypothesis